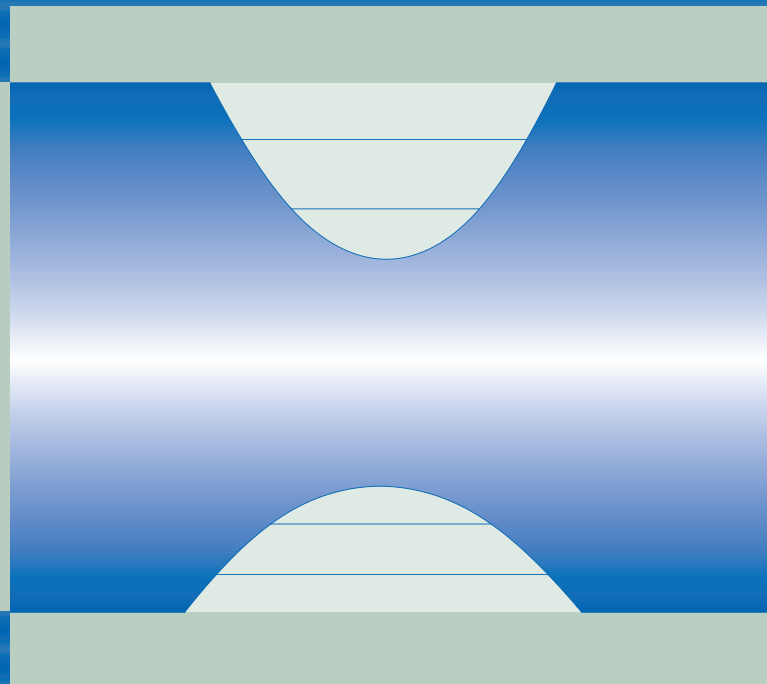Christopher Gies

Theory for Light-Matter Interaction in Semiconductor Quantum Dots

A dissertation submitted
for the degree PhD at
the Universität Bremen

Universität Bremen

A dissertation submitted in application for the degree PhD (Dr. rer. nat.)
with permission of the Institute for Physics and Electrical Engineering,
University of Bremen

Supervisor:
Prof. Dr. Frank Jahnke

First examiner:
Prof. Dr. Frank Jahnke, Universität Bremen

Second examiner:
Prof. Dr. Andreas Knorr, Technische Universität Berlin

Date of submission:
April 21, 2008

Oral Defense:
July 17, 2008

ABSTRACT

A microscopic theory is developed and applied to describe luminescence from semi-conductor quantum dots (QDs). The radiative emission dynamics is studied by the investigation of time-resolved photoluminescence. Special emphasis is placed on the role of carrier correlations and the differences between QDs and atoms. From the most general form of the theory a laser model for QDs in microresonators is developed, which is the central achievement of this thesis. In this model semiconductor effects can be included in a consistent manner. Going beyond the rate equation limit, we calculate the first- and second-order correlation functions to characterize the laser threshold properties, which are, in the classical sense, no longer well defined in current state-of-the-art microcavity lasers with high spontaneous emission coupling into the laser mode. To underline the close connection to applications, all results are presented together with results from recent experiments. To gain a deeper understanding of the derived laser theory and of the difference between QDs and atoms, a detailed comparison with quantum-optical models is performed, namely with the rate equations, a master equation approach and the Liouville/von-Neumann equation for the full density matrix.

Acknowledgements

I am indebted to Frank Jahnke, who has supervised my work and who it has been a pleasure to work with. I am especially grateful that he made it possible for me to go to the plmcn conference in Cuba, which was very enjoyable. At the same time I would like to thank Jan Wiersig, with whom I spent most of my time working together. All the best for your new position in Magdeburg, and stay as relaxed as you are and you will be a good boss...

Many colleagues have made the past three and a half years a colourful experience, first to mention the Bremen-based team: Paul Gartner, Sandra Ritter, Michael Lorke, Jan Seebeck and Frithjof Anders. It has been my pleasure to be able to work together with colleagues in experimental establishments, of whom I would like to mention Sven Ulrich, Thomas Auer, Serkan Ates, Thorsten Berstermann and Manfred Bayer.

When it comes to the subject of physics and the PhD thesis, I believe that my friends and family have not suffered too much under my profession. Nevertheless, I would like to happily thank them here: Linus and Jana, who have made it possible once more for us to spend some time of my graduation period in the same place, Norman and Stefan for good part-time diversion at work and off work, Ivona for many successful evening events, Christian for lots and lots of distraction, Maren for a heaps of fun and some workshop time, as well as Stacey and my family for always being there.

My acknowledgements also to Martin Zech for the design of the thesis cover.

Finally I would like to point out that I am grateful to everybody who does not stop here but reads a bit a bit further.

CONTENTS

Contents

List of Figures

1. Introduction

Whenever the dimensionality of a system is reduced it gives rise to a variety of stunning new effects. To name an example from atomic physics, consider a diluted atomic gas of bosons that can undergo a phase transition and form a Bose-Einstein condensate at finite temperatures [5, 36, 43]. This is true if the gas is not restricted to fewer than three spatial dimensions. A homogeneous Bose gas in two or one dimension, however, is subject to enhanced phase fluctuations that make the formation of one coherent phase impossible, a fact stated in the Mermin-Wagner Hohenberg theorem: Spontaneous symmetry breaking in continuous one- or two-dimensional theories cannot occur at finite temperatures [34, 60, 90, 91]. Also in semiconductor systems lower-dimensional effects play an important role and are an integral part of today's device applications. The discovery of the integer and fractional quantum Hall effect has won Nobel prizes in physics [75, 80, 107], and band engineering relies to a large extent on the modifications the density of states experiences under dimensional reduction.

This reduction is most naturally achieved in nanoscale systems. In fact, the physics of low-dimensional semiconductor nanostructures is a more vivid and rapidly evolving field of research than ever, owing to the advances made in growth technologies and manipulation on such small length scales. In a series of increasing confinement, where quantum wells and quantum wires restrict the propagation of carriers to two and one single dimension, quantum dots define the ultimate limit of no free carrier propagation at all. Quantum dots are zero-dimensional semiconductor structures typically consisting of thousands up to hundreds of thousands of atoms and being tens of nanometers in size. The prominent effect of this reduction in dimensionality manifests itself in the free density of states. The continuous behavior typical for bulk material becomes discrete. In contrast to atoms, however, the level spacing is determined by the size, geometry and composition of the quantum dots, making it possible to tailor the electronic and optical properties. The discrete and tunable optical spectrum is the foundation of quantum dot research and exerts a vast impulse on optoelectronic device applications. With quantum dot emitters one can, in principle, cover the whole visible spectrum and beyond. A flavor of this is given in Figure 1.1, where light emission from colloidal quantum dots is shown. Next to the range of optical fiber telecommunication networks (1300/1550 nm), laser diodes with wavelengths in the blue and green part of the spectrum are of great interest for imaging devices. Laser diodes [8, 31, 95, 104, 138, 144],

Figure 1.1.: Luminescence from colloidal quantum dots of different size and composition. The peak wavelength of the emission can be tuned all the way through the visible range of the optical spectrum and farther into the infrared. Courtesy of Dr. Andrey Rogach [1].

single-photon detectors and field effect transistors [48, 131, 132], and non-classical light sources [3, 15, 94, 96, 105, 112, 119, 126, 134, 158] for fundamental studies and quantum information technology are among the most relevant applications.

In analogy to the three-dimensional carrier confinement in quantum dots, light can be confined in all spatial directions. This is achieved in optical microcavities, see [146] and references therein. As it is possible for quantum dots to tailor their optical properties, the cavity can be brought in line with the emission properties of the gain material by choosing their structure accordingly. These micrometer-scale resonators possess a discrete *photonic* density of states and a large free spectral range due to their small size, which is comparable to the wavelength of the light they confine— an important quality for the achievement of single-mode lasing. The photon confinement is based either on total internal or Bragg reflection. A combination of both confinement mechanisms is employed in the so-called VCSEL (vertical cavity surface emitting laser) structures used for micropillar lasers [151]. Two examples for microcavities are shown in Figure 1.2, a micropillar and a microdisk resonator.

By embedding quantum dots or other kinds of emitters in microresonators we enter the fascinating regime of cavity-quantum electrodynamics (CQED). The coupling of the emitter to a single mode (or more) of the resonator leads to a variety of new effects that can change the emission rate from the gain material, the directionality of the emitted light and the spectral properties. If the coupling is strong, emission into the cavity mode is followed by reabsorption in a reversible cycle of energy exchange between the emitter and the cavity. The strong coupling leads to the formation of polariton quasiparticles [113]. This regime plays a role in fundamental studies of light-matter interaction. A topic fervidly discussed is the possibility of Bose-Einstein condensation of polaritons [39, 68, 133]. From an application point of view, the regime of weak coupling plays a more important role [93, 146]. Photons emitted by
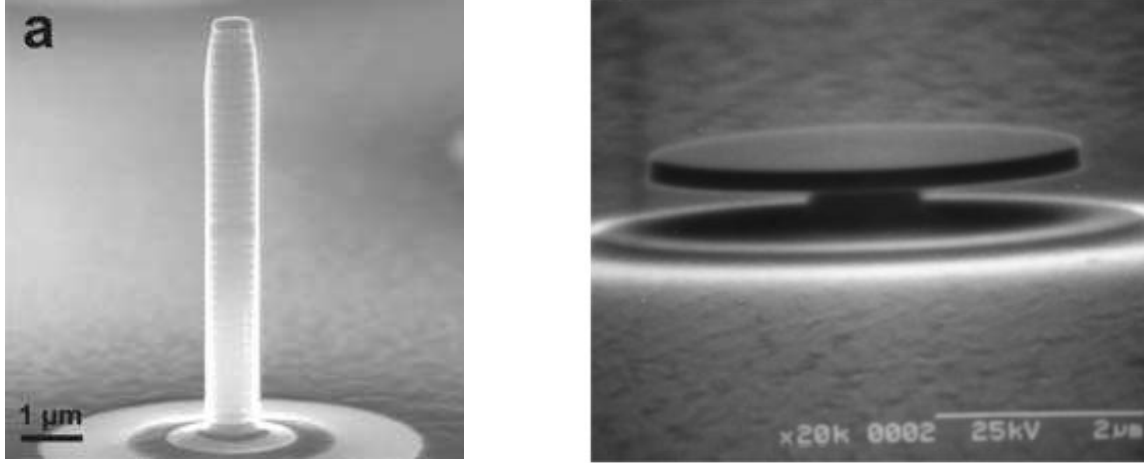
Figure 1.2.: Two examples for microresonators: A VCSEL-pillar (left) and disk (right) microcavity, taken from Refs. [113] and [94], respectively. In the pillar case the light is confined due to total internal reflection at the sidewalls and due to alternating layers of materials with different refractive indices (distributed Bragg reflectors) along the vertical direction. In the maximum of the confined field a layer of quantum dots is placed as the gain medium. In case of the microdisk, long-lived modes are so-called whispering gallery modes that exist close to the perimeter of the disk.

the gain material leave the cavity at a rate determined by the quality factor of the cavity. The spontaneous emission into the cavity, however, is changed due to the modified local density of optical modes inside the resonator, a phenomenon called the Purcell effect [110]. In cavities containing a localized long-lived mode, expressed by a large quality factor Q and a small mode volume V, the spontaneous emission rate becomes increased $\propto Q/V$ by factors of ten and more [82, 124]. This effect is extensively used in the fabrication of efficient low-threshold laser devices, where the spontaneous emission into the laser mode is enhanced over the other non-lasing modes [144]. The important quantity characterizing a laser is the β-factor that determines the fraction of the total spontaneous emission that is channelized into the laser mode. In conventional gas lasers typically only one out of 10^6 photons is emitted into the laser mode. In quantum-dot based semiconductor lasers values of β close to unity have been obtained [31, 104, 134, 138, 144].

Typically, in the input/output power trace of conventional lasers, the laser threshold is developed as a sudden intensity jump over several orders of magnitude. In small lasers with such efficient spontaneous emission coupling, however, the threshold gradually disappears to become a wide smeared-out transition region [118, 152]. Nevertheless, even if the threshold is not visible at all in the intensity output of the laser device, the emitted light changes qualitatively from thermal to coherent as the dominating mechanism changes from spontaneous to stimulated emission. This behavior

is expressed in the photon statistics, which is reflected in the photon second-order correlation function. It serves as an unambiguous identifier for the coherence properties of the emitted light, and a knowledge of the coherence properties is of uttermost relevance for the development of high-β laser diodes.

The view of quantum dots as artificial atoms reflects the historical development in the field, and so does it seem to justify the extensive use of atomic models to explain quantum-dot-related phenomena in the literature. Quantum dots, however, are semiconductor materials and semiconductor effects influence their luminescence properties in several ways atomic models are incapable of accounting for. It is the purpose of the work presented in this thesis to devise new models on which basis luminescence from quantum-dot-based systems can be described. In particular this includes the development of a laser theory for quantum dots in microcavities that allows for a systematic inclusion of semiconductor effects. The calculation of the first- and second-order photon correlation functions is an important part of this thesis and the key to a better understanding of current state-of-the-art laser structures. The theoretical models are presented alongside numerous results from experimental collaborations. This combination yields a consistent picture of the underlying physics.

Outline

This thesis covers three major topics: The fundamental description of photoluminescence from quantum dots together with the introduction of the employed microscopic model and the equation-of-motion technique, the development of a semiconductor laser theory, and an in-depth comparison to various atomic models with different degrees of sophistication.

The description of luminescence from semiconductor quantum dots by means of a microscopic theory is the topic of the first chapter, leading to the introduction of the semiconductor luminescence equations. The theoretical methods used in the remainder of the thesis are explained and results are presented for the spectrally and time-resolved photoluminescence. Special emphasis is placed on the role of semiconductor effects and differences to atomic models.

Based on the theoretical background and insight obtained in the first chapter, a laser theory for quantum dots in microcavities is developed from the semiconductor luminescence equations in the second chapter. By including higher-order correlation functions access is granted to the coherence properties and the threshold characteristics of the laser device. The applicability of the developed theory is demonstrated

in comparison with recent experiments on micropillar quantum-dot lasing. By explicitly considering the time evolution, we point out differences in the output behavior of a laser pumped by pulsed and continuous wave excitation. With respect to frequently used atomic systems, we discuss the well-known relation of the β factor to the threshold in the input/output characteristics. This point is of importance for the interpretation of experimental results, as vital parameters are frequently overestimated due to the inappropriate usage of atomic models.

In the fourth chapter, our theory is extended to the calculation of expectation values that depend on two time arguments. Together with experimental results, the first order coherence properties of semiconductor quantum-dot lasers are analyzed. This includes the two-time first-order correlation function, from which the coherence time of the emitted light can be obtained.

Chapter 5 is a devoted theory chapter, where a 'two-level' version of the semiconductor laser theory is opposed to three different atomic models. Inherent to the many-body problem is the appearance of an infinite hierarchy of coupled equations. To obtain a closed set of equations, this hierarchy must be truncated by an appropriate method. Firstly, we show how the well-established rate equations are obtained from the semiconductor model in the atomic limit. Secondly, by comparing to a birth/death model for the diagonal density matrix, we are able to verify the validity of the employed method used to truncate the infinite hierarchy of equations of motion. Finally, we consider the single-atom laser, a system for which the exact density matrix can be obtained. This particular system does not only offer once more the possibility to test the truncation method, but also provides insight into the role of dephasing and scattering terms— an important step towards the description of the single-quantum-dot laser.

2. LIGHT-MATTER COUPLING IN SEMICONDUCTOR QUANTUM DOTS

Semiconductor quantum dots (QDs) are like atoms in many aspects, but not in all. Most significantly, the band-like energy dispersion of the bulk material is augmented by discrete levels due to the islands of atoms we call QDs. Lying energetically below the states of the bulk material, carriers can be captured in the QD states and recombine at a fixed transition energy, like in an atom. The tunability of this transition energy is one of the biggest advantages in QD-based systems. In principle, optoelectronic devices with a vast range of emission wavelengths can be designed by choosing a particular material system, geometry and surrounding. Applications include lasers and non-classical light sources, as well as fundamental research in the field of cavity-quantum electrodynamics [82, 93].

The foundation of all applications is the understanding of the luminescence behavior of QDs. Due to their discrete level spectrum, QDs are often considered as 'artificial atoms' and treated by means of atomic models. Predictions from these models include an exponential decay behavior of the photoluminescence (PL), which stands in contradiction with many experimental findings [17, 19, 77, 82, 101, 124]. As many-particle physicists, we often use this behavior to stress that QDs are not artificial atoms, but semiconductor systems with a large number of electrons and holes that are subject to many-body effects and correlations. In particular cases this can mean that QDs behave like we expect it from atomic systems, but it is not true in general.

One promising approach for the description of PL is the equation-of-motion technique [70, 71]. The resulting semiconductor luminescence equations (SLE) have previously been used to study PL spectra [65] and exciton formation [62] in quantum-well systems, and the PL-decay dynamics of an ensemble of QDs embedded into a microcavity [124]. It is well-known that the equation-of-motion technique leads to an infinite hierarchy of correlation functions due to the Coulomb and the light-matter interactions. A systematic way to truncate this hierarchy is found in the cluster expansion method that is used throughout this thesis [45, 46, 63].

From an application viewpoint the use of QDs as an active medium in microresonators is of great relevance, creating the possibility to control the spontaneous emission to

a large extent. If emitters are placed inside a cavity, the modified optical density of states can cause an increase or suppression of the spontaneous emission time, an effect first predicted by E. Purcell in the 1940s [110]. While the influence of Coulomb-correlated multi-exciton states on optical spectra of QDs has been investigated by several groups [10, 12, 13, 16, 27, 37, 59], much less is known about the influence of correlations on the spontaneous recombination dynamics. Time-resolved photoluminescence studies provide direct access to the efficiency of carrier scattering processes after optical excitation with short pulses [97] and to the modification of the spontaneous emission lifetime for QDs in optical cavities due to the Purcell effect [77, 82, 101]. The theoretical description is rather challenging, because it requires not only a computation of carrier scattering and correlations, but also a full quantum-mechanical treatment of the light field. The derivation of the semiconductor luminescence equations comprises the quantization of the electromagnetic field. Consequently, spontaneous emission is naturally included and this approach is well suited for the description of the discussed systems.

In this chapter we begin with the derivation of the semiconductor luminescence equations, starting with a description of the model system, the single particle properties and the many-body Hamiltonian in the first section. In Section 2.2 the equation-of-motion technique is explained and a systematic classification- and truncation procedure of operator averages is introduced. In the derivation of the SLE in Section 2.3, special emphasis is placed on the role of carrier correlations introduced by the Coulomb and the light-matter interaction. Correlations between carriers and photons are of key interest in the description of the statistical properties of laser light and are discussed in Chapter 3. Numerical results are presented in Section 2.4, where the stationary spectrum is investigated. The effect of correlations on the time-resolved photoluminescence from QDs is studied in Section 2.5 and limiting cases are discussed. In the framework of the DFG research group "Quantum Optics In Semiconductor Nanostructures" we have collaborated with two experimental groups, so that our theoretical analysis is complemented by joint results: In Section 2.6 the emission into free space from unstructured QD samples is investigated. Comparing the emission from doped and undoped QDs, conclusions are drawn about the influence of electron-hole correlations. Finally, in Section 2.7 we study photoluminescence from QDs embedded in a microcavity. The relevant mechanisms are discussed and modified SLE, that contain feedback and damping terms to account for a photon population in the cavity, are introduced. The theory is compared with results from experiments performed on QD in microresonators. A recapitulation of the main achievements of this chapter can be found in the conclusion.

2.1. System and Hamiltonian

The step required prior to being able to formulate the many-body approach is the choice of the single-particle basis of the non-interacting system. In the formulation of our theoretical model we assume the single-particle problem to be solved. Thus, our formalism is completely independent of the explicit choice of the single particle states. However, they are needed for the calculation of the interaction matrix elements and the free-carrier spectrum that both enter into the Hamiltonian. Before we start with the derivation of the dynamic equations, the choice of the single particle states is explained.

2.1.1. Single-Particle States

The calculation of the single-particle states for a given confinement geometry is all but trivial, and so is the calculation of the bulk band structure. In the following we will give a brief overview that barely scratches the surface of band structure calculations, but gives a general overview of the relevant physics that determine some of the properties of the single particle states.

Due to the three-dimensional carrier confinement QDs possess localized states in contrast to the band structure of the bulk material. Nevertheless, the single-particle states are closely related to the properties of the bulk material, and of course they depend on the QD size and geometry.

First-principle calculations are available for the computation of the electronic structure of small QD systems (200–400 atoms) [111, 120]. Due to the large number of atoms, together with the absence of translational symmetry to greatly simplify bulk calculations, density functional theory-based approaches are computationally too demanding to date. Semi-empirical approaches are used instead, either continuum approaches like the $\mathbf{k} \cdot \mathbf{p}$-model [35] or the effective-mass approach [56, 130, 153] that is used here. Alternatively, methods where the microscopic structure of the lattice enters, like in pseudo-potential [30] or tight-binding models [121–123] can be used. The choice of the effective mass approximation may be understood by looking at the band structure of bulk material, which is basically that of GaAs, shown in the left panel of Figure 2.1. The suitability of Zinc-blende material systems like GaAs, AlAs, InAs, InGaAs, InP, CdSe, and also nitride-based systems grown in the Wurtzite structure for optoelectronic device application lies in the direct band gap, allowing for carrier transitions between the conduction and valence bands by emitting or absorbing photons. Thus, the relevant region of the Brillouin zone is restricted to
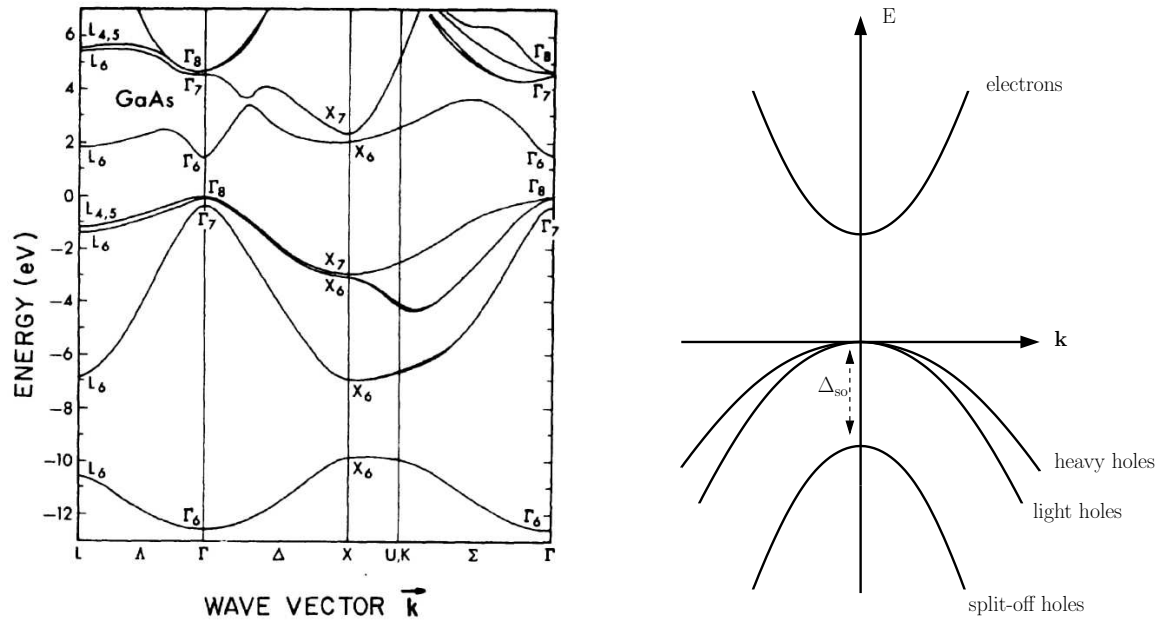
Figure 2.1.: Left: Band structure for GaAs calculated using a pseudo-potential method. The band gap energy is 4.71 eV. The figure is taken from [30]. **Right:** Simplified schematic magnification of the bulk band structure near the Γ point. The valence-band edge is two-times degenerate. Due to the reduced dimensionality in QDs, the degeneracy is lifted as both the light-hold and the split-off bands shift to lower energies.

its center, the so-called Γ-point. A simplified close-up of this region is shown in the right panel of Figure 2.1. Three bands are relevant in the vicinity of the Γ-point: the degenerate heavy- and light-hole band, and the split-off band that occurs due to the spin-orbit coupling. In systems with reduced dimensionality, the separation of the component in growth direction, together with strain-induced energy shifts of the bands, leads to a separation of the split-off band and the light-hole band from the heavy-hole band [141]. The single-particle wave functions are determined by the solution of the Schrödinger equation.

Obvious limitations of continuum methods like the single-band effective mass and the multi-band $\mathbf{k} \cdot \mathbf{p}$ approaches arise, if the atomistic structure and symmetry becomes relevant over the global shape. For Zinc-blende-QDs this is the case if the QD size becomes too small (base diameter $\lesssim 12\,\mathrm{nm}$) [130, 136]. For the work in this thesis, we neglect band mixing effects for the sake of simplicity, so that only one valence band and conduction band is considered. Furthermore, the physics described by an Hamiltonian that is based on a parabolic approximation of the band structure in the center of the Brillouin zone can only be expected to be correct, if the relevant processes involve single-particle states in the vicinity of the Γ-point, which can be assumed for optical processes in semiconductor materials with a direct band gap.
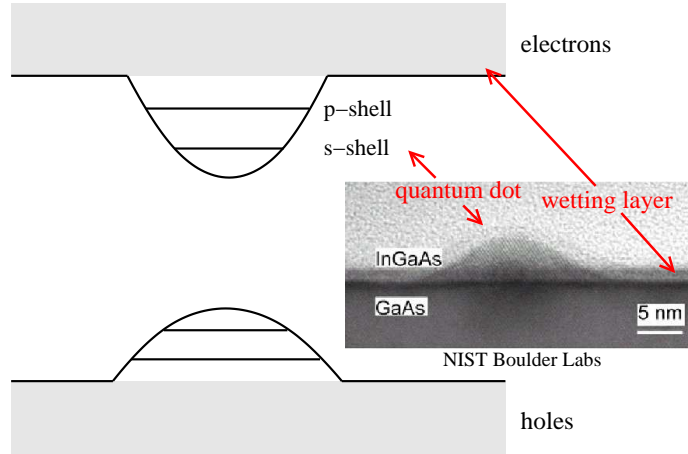
Figure 2.2.: Schematic of the coupled QD-WL system. Two confined shells are considered for both electrons and holes, which lie energetically below a quasi-continuum of delocalized WL states, corresponding to the in-plane motion of carriers in the WL. The transmission electron micrograph image of the InGaAs QD on a GaAs substrate is taken from Ref. [135].

We consider lens-shaped InGaAs/GaAs QDs grown in the Stranski-Krastanow growth mode [137], where lattice-constant mismatch and surface energy minimization induces the self-assembly of islands of atoms. In this process a thin film of a few nanometer thickness called wetting layer is formed between the QDs and the substrate. The QDs and the wetting layer constitute a coupled system with common electronic states. Typical dimensions of the QDs are 25 nm base diameter and less than 10 nm in height, an example can be seen in Figure 2.2. From what we have discussed above, the geometry of this kind of QDs allows for a description within the effective-mass approximation, where a free carrier dispersion with effective masses for electrons and holes is assumed. In fact, it has been shown that in the case of flat, cylindrically symmetric InAs/GaAs QDs, the effective mass approximation yields results very close to those obtained from a $\mathbf{k} \cdot \mathbf{p}$ and a tight-binding model [130]. We separate the wave function into an axial and an in-plane part. The single-particle bound-state wave functions in the plane perpendicular to the growth direction are well approximated by those of a two-dimensional harmonic oscillator [153]. Due to the rotational symmetry around the QD axis, the corresponding angular momentum is a good quantum number. We consider the first two confined shells of such a system, which are denoted by s and p according to their in-plane symmetry. The s-shell is only spin-degenerate, while the p-shell has an additional angular-momentum two-fold degeneracy. To account for the strong confinement in growth direction both for the QDs and the wetting layer, we use an infinite potential well to model the corresponding finite extension of the wave-function. The spectrum of the potential well introduces a splitting into subbands with a spacing that depends on the strength of the axial confinement, although the

term subband is somewhat misleading for the QD case, as these posses only a discrete spectrum due to the additional in-plane confinement. For an infinite potential well, the spacing between the first two energy levels is given by $\Delta E = 3h^2/8m_{\text{eff}}L^2$, where L is the width of the well and m_{eff} is the effective mass of electrons or holes. We study structures of only a few nanometers thickness, corresponding to a large energy spacing for the electrons of roughly 1eV for $L = 4\,\text{nm}$. For this reason, only the energetically lowest subband is considered.

The discrete states are located energetically below a quasi-continuum of delocalized states, corresponding to the two-dimensional motion of carriers in a wetting layer. At this point it is worth mentioning that the actual number of discrete QD states is limited by the height of the confinement potential and the distance in energy to the wetting layer states. Localized states exist only below the quasi-continuum states of the wetting layer. In the wetting layer, the in-plane momentum $\mathbf{k}$ is a good quantum number if the effect of the localized states on the continuum is neglected. Thus, in the most simple approximation the quasi-continuum of the wetting layer states can be modeled by using plane waves with wave vector $\mathbf{k}$. In Figure 2.2 a schematic of the energy levels of the coupled QD-wetting layer system is shown. Further details of the QD model are discussed in Ref. [100]. Strictly speaking, the localized states and the wetting layer states are solutions of the single-particle problem for one common confinement potential and must, therefore, form an orthogonal basis. By performing a separate ansatz for the QDs and the wetting layer, this orthogonality is not ensured and can be enforced, for example by an orthogonalization procedure of the continuum states. The obtained so-called orthogonal plane waves (OPWs) represent a more correct description of the wetting layer states. For details we refer to Ref. [100].

2.1.2. Many-Body Hamiltonian

To investigate the optical properties of QDs, the system may be off-resonantly excited by an optical pulse. The excitation creates carriers in the barrier-, wetting layer-, or higher QD-states. The possibility of this non-resonant kind of excitation is a feature of self-assembled QDs and is not found in colloidal QDs where the wetting layer is missing, or even in atomic systems where only an excitation of localized states is possible. In the case of barrier excitation, there are plenty of scattering channels between the two quasi-continua, so that relaxation into the wetting layer states is fast. Fast scattering (relaxation) into the lower QD states is facilitated by scattering with LO-phonons and, especially at high carrier densities, carrier-carrier scattering [100, 128]. Both mechanisms provide efficient scattering channels both for transitions between localized states and between localized states and the wetting layer. Figure 2.3
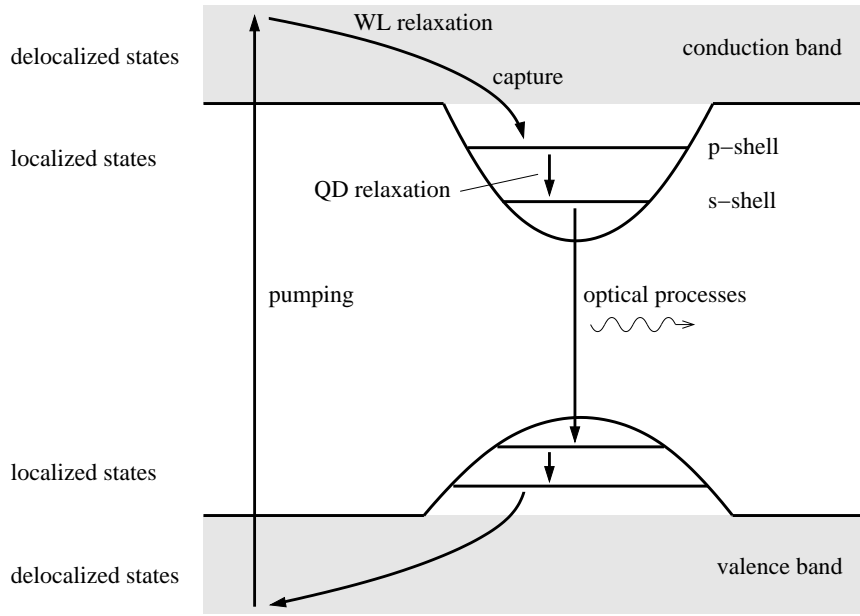
Figure 2.3.: Schematic of the relevant processes in the QD-WL system. Off-resonant excitation creates carriers in higher excited localized states or in the WL, followed by relaxation processes due to carrier-carrier and carrier-phonon scattering. Carrier recombination via photon emission takes place between the localized states.

schematically displays the relevant processes in the system for exemplary excitation into the wetting layer.

At low temperatures and low to moderate densities, the carriers solely populate the QD states. In this case the wetting layer states are mainly important for carrier-scattering processes if the system is excited in the continuum states. For the recombination dynamics due to carrier-photon interaction, the unpopulated wetting layer states are of negligible importance. Furthermore, if the wetting layer states are mainly unpopulated, Coulomb correlations between the discrete QD states and the energetically displaced quasi-continuum of the wetting layer are much weaker than those between QD states. Calculations presented in this thesis are performed at low temperatures, mostly at $4\,\mathrm{K}$. For this reason, the wetting layer is not included in our calculations.

The driving process for photoluminescence is the spontaneous recombination of carriers in the valence and conduction band. Spontaneous emission is a quantum-electrodynamical process that is caused by field fluctuations. Thus we treat both the electromagnetic field and the carrier system in the formalism of field quantization.[1]

---

[1]It is, however, possible to describe spontaneous emission with a classical light field in the formalism of quantum mechanics or quantum statistics by considering external fluctuations, e.g., using the Langevin theory [29].

The total Hamiltonian for the system has the following contributions:

$$H = H_{\text{carr}}^0 + H_{\text{Coul}} + H_{\text{ph}}^0 + H_{\text{D}} \ . \tag{2.1}$$

The Coulomb Hamiltonian which describes the interacting system of valence- and conduction-band electrons has the two parts

$$H_{\text{carr}}^0 = \sum_\nu \varepsilon_\nu^c \, c_\nu^\dagger c_\nu + \sum_\nu \varepsilon_\nu^v \, v_\nu^\dagger v_\nu \ , \tag{2.2}$$

$$H_{\text{Coul}} = \frac{1}{2} \sum_{\alpha'\nu\nu'\alpha} \left[V_{\alpha'\nu,\nu'\alpha}^{cc} \, c_{\alpha'}^\dagger c_\nu^\dagger c_{\nu'} c_\alpha + V_{\alpha'\nu,\nu'\alpha}^{vv} \, v_{\alpha'}^\dagger v_\nu^\dagger v_{\nu'} v_\alpha \right]$$

$$+ \sum_{\alpha'\nu\nu'\alpha} V_{\alpha'\nu,\nu'\alpha}^{cv} \, c_{\alpha'}^\dagger v_\nu^\dagger v_{\nu'} c_\alpha \ . \tag{2.3}$$

The free Hamiltonian H_{carr}^0 contains information about the single-particle spectrum $\varepsilon_\nu^{c,v}$ and describes a system of non-interacting charge carriers. The Coulomb interaction between the carriers is accounted for in H_{Coul}. For details we refer to Refs. [10, 58]. The operators c_ν ($c_\nu^\dagger$) annihilate (create) electrons in the one-particle states $|\nu\rangle$ of energy ε_ν^c. The corresponding operators and single-particle energies for valence-band electrons are v_ν ($v_\nu^\dagger$) and ε_ν^v, respectively. The explicit form of the single-particle wave function $\langle \mathbf{r}|\nu, \lambda \rangle = \psi_\nu^\lambda(\mathbf{r})$ enters the description via the Coulomb matrix elements [10]

$$V_{\alpha'\nu,\nu'\alpha}^{\lambda\lambda'} = \int \mathrm{d}^3r \int \mathrm{d}^3r' \ \psi_{\alpha'}^{\lambda*}(\mathbf{r}) \psi_\nu^{\lambda'*}(\mathbf{r}') V(\mathbf{r} - \mathbf{r}') \psi_{\nu'}^{\lambda'}(\mathbf{r}') \psi_\alpha^\lambda(\mathbf{r}) \tag{2.4}$$

with the band index $\lambda = c, v$ and the Coulomb potential $V(\mathbf{r}) = e^2/4\pi\epsilon_0\epsilon r$, and via the light-matter interaction (see below). The dielectric constants of the vacuum and the background material are given by ϵ_0 and ϵ, respectively.

To obtain the expressions for the quantized Hamiltonian involving the electromagnetic field, the transverse electric field[2] $\mathbf{E}_T$ and the magnetic field $\mathbf{B}$ are expanded into modes, where each mode ξ is associated with a quantum mechanical harmonic oscillator with the mode energy $\hbar\omega_\xi$. In the usual fashion, operators are introduced that create or destroy a photon in the mode ξ, denoted as $b_\xi^\dagger$ and b_ξ, respectively. For details we refer to [64, 87, 89]. The total energy of the free electromagnetic field is given by the Hamiltonian [92]

$$H_{\text{ph}}^0 = \sum_\xi \hbar\omega_\xi \left(b_\xi^\dagger b_\xi + \frac{1}{2} \right) \ . \tag{2.5}$$

---

[2]For the quantization of the electromagnetic field, the Coulomb gauge is usually used. In the Coulomb gauge, the electric field decouples into transversal and longitudinal parts, such that the longitudinal part vanishes in the absence of sources in the system. The transversal part is determined by the dynamics of the vector potential, thus describing electromagnetic waves.

In free space, the mode label ξ contains the wave vector $\mathbf{q}$ and the polarization vector of the electromagnetic field $\mathbf{e}_{\mathrm{p}}(\mathbf{q})$, with the index $\mathrm{p} = \pm$. The mode frequencies are then given by $\omega_\xi = c|\mathbf{q}|$, with c being the speed of light, and the explicit form of the modes is $\mathbf{U}_\xi(\mathbf{r}) = \mathbf{e}_{\mathrm{p}}(\mathbf{q})e^{i\sqrt{\epsilon}\,\mathbf{q}\mathbf{r}}$ [87].

The light-matter interaction Hamiltonian in dipole approximation reads [6, 33, 70]

$$H_{\mathrm{D}} = -i \sum_{\xi,\,\alpha\nu} \left(g_{\xi\alpha\nu}\, c_\alpha^\dagger v_\nu b_\xi + g_{\xi\alpha\nu}\, v_\alpha^\dagger c_\nu b_\xi \right) - \mathrm{h.c.} \tag{2.6}$$

The resonant elementary process associated with this Hamiltonian is the transition of an electron from the valence into the conduction band (or vice versa) by absorption (emission) of a photon. The non-resonant terms contained in Eq. (2.6) are neglected in the rotating wave approximation[3] (RWA) [58]. As an example for a non-resonant process, consider the absorption of a photon while a transition from the conduction to the valence band takes place (in Eq. (2.6) the second term), and vice versa. The matrix elements $g_{\xi\alpha\nu}$ describe the coupling between the mode ξ of the electromagnetic field and the carrier transition between states $|\alpha\rangle$ and $|\nu\rangle$ and are given by

$$g_{\xi\alpha\nu} = E_\xi \int d^3r \; \psi_\alpha^{c*}(\mathbf{r})e\mathbf{r}\mathbf{U}_\xi(\mathbf{r})\psi_\nu^v(\mathbf{r}) \;, \tag{2.7}$$

where $E_\xi = \sqrt{\hbar\omega_\xi/2\epsilon\epsilon_0 V}$ is the vacuum field amplitude [92] and V is the normalization volume. Using the envelope-function approximation [58] the wave-function $\psi_\alpha^c(\mathbf{r})$ and $\psi_\nu^v(\mathbf{r})$ can now be decomposed into an envelope part, which varies only slightly over a unit cell, and the rapidly oscillating Bloch-factor $u_{\mathbf{k}\approx 0}(\mathbf{r})$. Taking into account that the electromagnetic field is approximately constant over the extent of a QD and considering for simplicity equal envelopes for the conduction- and valence-band electrons (equal-envelope approximation [58]), one finds

$$g_{\xi\alpha\nu} = E_\xi\mathbf{d}_{cv}\mathbf{U}_\xi(\mathbf{r}_0)\delta_{\alpha\nu} \equiv g_\xi\delta_{\alpha\nu} \;. \tag{2.8}$$

Here, $\mathbf{d}_{cv}$ are the interband matrix elements and $\mathbf{r}_0$ is the position of the QD. In this form, the band indices occur only in the interband matrix elements, which are the same for identical QDs. Thus, the light-matter coupling constant depends only on the mode of the electromagnetic field. If *different* QDs were considered, the index ν must be kept with the coupling matrix element to account for the varying coupling strengths in the ensemble, as it contains both the single-particle state and the QD position. From Eq. (2.8) it follows that, within the envelope-function approximation, optical transitions occur only between the s-shells or the $p_\pm$-shells of electrons and holes.

---

[3]The rotating wave approximation is commonly applied in quantum-optical problems. In the RWA, off-resonant terms occurring in the equations of motion are dropped. For simplicity, this may already be done in the Hamiltonian. These terms posses a phase factor causing a oscillation rapid in comparison to the dynamics caused by the optical processes close to resonance.

2.2. The Hierarchy Problem and Truncation of Correlations (Cluster Expansion Method)

The time evolution of the single carrier and photon operators is obtained by using Heisenberg's equations of motion together with the Hamiltonian of the interacting system. For an operator a it is given by

$$i\hbar\frac{\mathrm{d}}{\mathrm{d}t}\,a = [a, H] \; . \tag{2.9}$$

From this we derive coupled equations for operator averages, like the carrier population or photon number in a cavity mode or in a continuum mode of free space. The many-body problem, and in particular the equation-of-motion approach inherently bears a hierarchy problem, caused by the interaction parts of the Hamiltonian. In order to achieve a consistent formulation of this problem, the classification and truncation of correlation functions will be addressed before the semiconductor luminescence equations are introduced.

The appearing operator averages are classified into singlets, doublets, triplets, quadruplets, etc., according to the number of particles they involve. Considering interband transitions, it must be borne in mind that the excitation of one electron is described as the destruction of a valence band carrier and the creation of a conduction band carrier. For the corresponding interaction processes, a photon operator is connected to *two* carrier operators [11, 69]. Formally, this can be seen from integrating the time evolution of a photon operator, readily obtained from Eq. (2.9),

$$i\hbar\frac{\mathrm{d}}{\mathrm{d}t}\,b_\xi^\dagger(t) = -\hbar\omega_\xi b_\xi^\dagger(t) + i\sum_\nu g_\xi c_\nu^\dagger(t)v_\nu(t) \; , \tag{2.10}$$

which yields

$$b_\xi^\dagger(t) = b_\xi^\dagger(0)e^{i\omega_\xi t} + \frac{1}{\hbar}\sum_\nu \int_0^t \mathrm{d}t'\, g_\xi c_\nu^\dagger(t')v_\nu(t')e^{i\omega_\xi(t-t')} \; . \tag{2.11}$$

This fact is used to classify mixed expectation values with photon and carrier operators. For example, the electron population $f_\nu^e = \langle c_\nu^\dagger c_\nu\rangle$ is a singlet contribution, the source term of spontaneous emission $\langle c_\alpha^\dagger v_\alpha v_\nu^\dagger c_\nu\rangle$ and the photon-assisted polarization $\langle b_\xi^\dagger v_\nu^\dagger c_\nu\rangle$ are doublet terms.

In the following, N-particle averages, schematically denoted as $\langle N\rangle$ and containing $2N$ carrier operators or an equivalent replacement by photon operators, are factorized into all possible combinations of averages involving one up to $N-1$ particle averages. For

the difference between the full operator average and this factorization, we introduce a correlation function of order N, denoted as $\delta\langle N\rangle$. Schematically the factorization of singlets, doublets, triplets, and quadruplets is given by

$$\langle 1\rangle = \delta\langle 1\rangle \ , \tag{2.12a}$$

$$\langle 2\rangle = \langle 1\rangle\langle 1\rangle + \delta\langle 2\rangle \ , \tag{2.12b}$$

$$\langle 3\rangle = \langle 1\rangle\langle 1\rangle\langle 1\rangle + \langle 1\rangle\delta\langle 2\rangle + \delta\langle 3\rangle \ , \tag{2.12c}$$

$$\langle 4\rangle = \langle 1\rangle\langle 1\rangle\langle 1\rangle\langle 1\rangle + \langle 1\rangle\langle 1\rangle\delta\langle 2\rangle$$
$$+ \langle 1\rangle\delta\langle 3\rangle + \delta\langle 2\rangle\delta\langle 2\rangle + \delta\langle 4\rangle \ . \tag{2.12d}$$

Looking at the last equation, the first four terms on the right hand side represent all possible combinations of singlets, singlets and doublets, singlets and triplets, and doublets, respectively. The last term is the remaining quadruplet correlation function. Continuing the series (2.12a)–(2.12d) leads to quintuplet terms and so on. Note that singlets cannot be factorized any further.

The essential idea of what has become known as the *cluster expansion method* [45, 46, 63] is to replace all occurring operator expectation values $\langle N\rangle$ according to the Eqs. (2.12) so that equations of motion for the corresponding correlation functions $\delta\langle N\rangle$ are obtained. Then the hierarchy of correlation functions is truncated rather than the hierarchy of expectation values itself. This allows the consistent inclusion of correlations up to a certain order in all of the appearing operator expectation values. Noting that terms of increasing order in the cluster expansion describe *correlated events* between more and more particles justifies a truncation, as these events are the less probable the more particles are involved. The described truncation procedure has previously been used to describe the luminescence dynamics of quantum wells [62, 70] and recently also of QDs [11, 44, 124]. If the hierarchy is truncated at the level of two-particle correlation functions, the so-called semiconductor luminescence equations for the coupled carrier and photon populations emerge, which consistently include carrier-carrier correlations up to the doublet level. When we discuss the photon statistics in Chapter 3, correlations up to the quadruplet level must be included, as the photon second-order correlation function $g^{(2)}(0) \propto \langle b^\dagger b^\dagger bb\rangle$ is of this order itself.

It is worth pointing out that the choice of a truncation method is not unique. Furthermore, a truncation at a consistent level in the number of involved particles does not necessarily introduce physical effects consistently. One example is the screening of the Coulomb potential occurring in the equations of motion for singlets. There, the screening is introduced by electron-hole correlations, which are doublet quantities. However, the screening of the Coulomb potential in the equations of motion for doublet quantities is introduced on the triplet level, so that a truncation on doublet level

leaves the Coulomb potential relevant for interaction processes between correlated carriers unscreened. Thus, if screening of carrier-carrier correlations was required, the consistency must either be violated to include only the screening terms of the triplet level, or the triplet level must be included all together. Then the problem carries over to the next higher level, where screening of triplet quantities is introduced on the quadruplet level. This stands in contrast to the diagrammatic Green's function approach, where physical processes are always considered for all occurring quantities via the choice of an appropriate self energy. The introduced renormalizations or screening effects are then considered up to infinite order due to the recursive structure of the Dyson equation. However, by the choice of certain diagrams for the self energy or the polarization function in the case of Coulomb screening, the theory is then restricted to certain classes of interaction processes.

The correlation functions defined according to Eq. (2.12) show peculiarities when algebraic manipulations are performed on them. This is illustrated in the following example, where we consider the operator identity

$$c_\nu^\dagger c_\nu c_\nu^\dagger c_\nu = c_\nu^\dagger c_\nu \ . \tag{2.13}$$

For a correlation function, however,

$$\delta\langle c_\nu^\dagger c_\nu c_\nu^\dagger c_\nu \rangle \neq \delta\langle c_\nu^\dagger c_\nu \rangle \ , \tag{2.14}$$

as can be seen by expanding the left and right hand sides of this equation according to Eqs. (2.12b) and (2.12a), respectively, i.e.

$$\langle c_\nu^\dagger c_\nu c_\nu^\dagger c_\nu \rangle - \langle c_\nu^\dagger c_\nu \rangle^2 + \langle c_\nu^\dagger c_\nu \rangle \langle c_\nu c_\nu^\dagger \rangle \neq \langle c_\nu^\dagger c_\nu \rangle \ . \tag{2.15}$$

This implies that algebraic operations *inside the δ-symbol* of the correlation function are not permitted. Otherwise using an identity like Eq. (2.13) could be used to change the order of correlations, e.g.

$$\delta\langle c_\nu^\dagger c_\nu c_\nu^\dagger c_\nu \rangle \overset{\substack{\text{use Eq. (2.13)}\\ \text{inside } \delta\langle...\rangle}}{=} \delta\langle c_\nu^\dagger c_\nu \rangle \ , \tag{2.16}$$

which stands in contradiction to Eq.(2.14).

Examples for the factorization of operator averages are given in Appendix A with the intention to clarify the application of the cluster expansion method to the reader.

2.3. Equations of Motion

With the classification and truncation method at hand, we now derive the so-called semiconductor luminescence equations that contain operator averages consistently

up to the doublet level. This includes carrier-carrier correlations that arise from the source term of the spontaneous emission. Amongst these are excitonic populations that play an important role in the understanding of the decay behavior of the photoluminescence, and we go into detail about this in Section 2.5. With the theory on this level we describe both the spectrum and time-resolved photoluminescence.

We assume in the whole of this thesis that the luminescence takes place in the incoherent regime where the influence of a coherent polarization can be neglected. Exemplary situations include incoherent carrier excitations or coherent excitation of higher states (barrier, wetting layer or higher localized states) with rapid dephasing and carrier relaxation, leading to a quasi-equilibrium distribution of the carriers at the lattice temperature. The absence of a coherent external field is expressed in the vanishing expectation values of the field operator $\langle b_\xi \rangle = 0$ and the coherent polarization $\langle v_\nu^\dagger c_\nu \rangle = 0$. True at the initial time $t = 0$, it can be shown to be preserved also during the time evolution: Taking the operator average of Eq. (2.11) we see that the evolution of the field operator is driven by the coherent polarization. Vice versa, the coherent polarization remains zero at all times without a driving coherent field [70]. However, for situations where a coherent polarization is present, like resonance fluorescence [2, 70–72], these additional terms must be considered in all equations of motion.

Operator averages are kept within the rotating wave approximation, implying that terms with a rapidly oscillating phase are neglected.

2.3.1. QD Semiconductor Luminescence Equations

Photon and carrier numbers. Writing down Heisenberg's equation of motion for the photon number, we find

$$i\hbar \frac{\mathrm{d}}{\mathrm{d}t} \langle b_\xi^\dagger b_\xi \rangle = 2i \operatorname{Re} \sum_\nu g_\xi^* \langle b_\xi^\dagger v_\nu^\dagger c_\nu \rangle \ , \tag{2.17}$$

which couples to the photon-assisted polarization amplitude $\langle b_\xi^\dagger v_\nu^\dagger c_\nu \rangle$.[4] The corresponding equation of motion is given by

$$
\begin{aligned}
i\hbar \frac{\mathrm{d}}{\mathrm{d}t} \langle b_\xi^\dagger v_\nu^\dagger c_\nu \rangle = {} & (\tilde{\varepsilon}_\nu^c - \tilde{\varepsilon}_\nu^v - \hbar\omega_\xi - i\Gamma) \langle b_\xi^\dagger v_\nu^\dagger c_\nu \rangle \\
& + (f_\nu^c - f_\nu^v) \sum_\alpha V_{\nu\alpha\nu\alpha} \langle b_\xi^\dagger v_\alpha^\dagger c_\alpha \rangle \\
& + i\, g_\xi f_\nu^c (1 - f_\nu^v) + i \sum_\alpha g_\xi C_{\alpha\nu\nu\alpha}^{\mathrm{x}} \ .
\end{aligned}
\tag{2.18}
$$

---

[4]In the incoherent regime $\langle b_\xi^\dagger \rangle = 0$ and thus, according to Eq. (2.12b), $\langle b_\xi^\dagger v_\nu^\dagger c_\nu \rangle \equiv \delta\langle b_\xi^\dagger v_\nu^\dagger c_\nu \rangle$.

2. Light-Matter Coupling in Semiconductor Quantum Dots

The evolution is determined by the Coulomb-renormalized energies

$$\tilde{\varepsilon}_\nu^c = \varepsilon_\nu^c - \sum_\alpha V_{\nu\alpha\nu\alpha} f_\alpha^c \,,$$

$$\tilde{\varepsilon}_\nu^v = \varepsilon_\nu^v - \sum_\alpha V_{\nu\alpha\nu\alpha} f_\alpha^v \,, \tag{2.19}$$

the resonance frequency ω_ξ of the optical mode ξ, and a phenomenological dephasing Γ causing a broadening of the spectral lines. The relevant mechanism for dephasing in semiconductor systems is Coulomb scattering and scattering with acoustic or optical phonons. This could be included on a microscopic level by adding a Hamiltonian analogous to Eq. (2.6) for the carrier-phonon interaction [62, 127, 128]. Predominantly interested in the luminescence and effects introduced by the Coulomb and light-matter interaction, we restrict ourselves to a phenomenological dephasing constant in association with carrier interband transitions. For further discussion, see Section 5.3.5. The term in the second line is analogous to the quantum well case, where it gives rise to the excitonic photoluminescence below the band gap [71]. Here it introduces the corresponding excitonic resonances for the QD states due to the interband Coulomb exchange interaction. The source term of spontaneous emission $\langle c_\alpha^\dagger v_\alpha v_\nu^\dagger c_\nu \rangle$ enters the theory naturally due to the quantization of the light field. In its factorized form it appears in the last line of Eq. (2.18), with the electron-hole correlation function $C_{\alpha'\nu\nu'\alpha}^{\mathrm{x}} = \delta \langle c_{\alpha'}^\dagger v_\nu^\dagger c_{\nu'} v_\alpha \rangle$. The spontaneous emission source term is of particular interest, as it deviates from the source term obtained in atomic models. While for atoms only the number of electrons contributes, here a two-particle average containing electron- and hole operators occurs. We have omitted the term representing stimulated emission/absorption, which contributes for example if an external field is resonant with the considered transitions or if a resonator provides feedback due to the emitted photons [124]. This feedback term is of extreme relevance when considering QDs in microcavities and will be discussed in Section 2.7, where the theory is presented for open-cavity systems. Before evaluating the correlation term in the last line of Eq. (2.18), we give the time evolution of the carrier population

$$i\hbar\frac{\mathrm{d}}{\mathrm{d}t} f_\nu^c = -2i \,\mathrm{Re} \sum_\xi g_\xi^* \langle b_\xi^\dagger v_\nu^\dagger c_\nu \rangle \tag{2.20}$$

$$+ 2i \,\mathrm{Im} \sum_{\alpha\alpha'\nu'} V_{\nu\alpha'\alpha\nu'} \left(C_{\nu\alpha'\alpha\nu'}^c - C_{\alpha'\nu\alpha\nu'}^{\mathrm{x}} \right) \,,$$

$$i\hbar\frac{\mathrm{d}}{\mathrm{d}t} f_\nu^v = 2i \,\mathrm{Re} \sum_\xi g_\xi^* \langle b_\xi^\dagger v_\nu^\dagger c_\nu \rangle \tag{2.21}$$

$$- 2i \,\mathrm{Im} \sum_{\alpha\alpha'\nu'} V_{\nu\alpha'\alpha\nu'} \left(C_{\nu\alpha'\alpha\nu'}^v - C_{\alpha'\nu\alpha\nu'}^{\mathrm{x}} \right) \,.$$

Here additional intraband correlation functions $C^c_{\alpha'\nu\nu'\alpha} = \delta\langle c^\dagger_{\alpha'} c^\dagger_\nu c_{\nu'} c_\alpha\rangle$ and $C^v_{\alpha'\nu\nu'\alpha} = \delta\langle v^\dagger_{\alpha'} v^\dagger_\nu \, v_{\nu'} v_\alpha\rangle$ appear. Restricting ourselves to s- and p-shells for the localized states, we consider only s-states with zero angular momentum and p-states with angular momentum of ±1, which, as we now explain, allows us to take $\langle a^\dagger_\nu a_{\nu'}\rangle = f^a_\nu \, \delta_{\nu\nu'}$. Initially all expectation values but for the population in the s- and p-shells are set to zero. The rotational symmetry of the system and the resulting conservation of angular momentum ensures that all off-diagonal terms $\langle a^\dagger_\nu a_{\nu'}\rangle$ with $\nu \neq \nu'$ describe forbidden transitions and remain zero during the time evolution. Therefore, in all equations expectation values of two carrier operators are restricted to populations, i.e. averages of valence- or conduction-band-carrier creator and annihilator with equal indices. An inclusion of higher angular momentum states is straightforward, but unnecessary at low temperatures and left out for transparency. Also remember that polarization-like averages of the form $\langle v^\dagger_\nu c_\nu\rangle$ vanish in the incoherent regime, as is explained in the beginning of this section.

Carrier correlations. We now turn to the interband, or electron-hole correlations that occur in Eqs. (2.18), (2.20) and (2.21), namely

$$
\begin{aligned}
C^{\mathrm{x}}_{\alpha'\nu\nu'\alpha} &= \delta\langle c^\dagger_{\alpha'} v^\dagger_\nu c_{\nu'} v_\alpha\rangle \\
&= \langle c^\dagger_{\alpha'} v^\dagger_\nu c_{\nu'} v_\alpha\rangle - \langle c^\dagger_{\alpha'} v^\dagger_\nu c_{\nu'} v_\alpha\rangle_{\mathrm{S}} \\
&= \langle c^\dagger_{\alpha'} v^\dagger_\nu c_{\nu'} v_\alpha\rangle + f^c_{\nu'} f^v_\nu \, \delta_{\nu\alpha}\delta_{\nu'\alpha'}
\end{aligned}
\tag{2.22}
$$

according to the general definition of a two-particle correlation function in Eq. (2.12b). Here, the factorization into singlets is equivalent to the Hartree-Fock approximation.

With the following discussion we offer an intuitive interpretation of the interband correlations $C^{\mathrm{x}}_{\alpha'\nu\nu'\alpha}$. They describe a process where a conduction-band-carrier transition from a state ν' to a state α' is accompanied by a valence-band-carrier transition from a state α to a state ν. It is important to understand that these transitions are *correlated* and do not coincidentally occur at the same time, reflected by the fact that the uncorrelated part of the operator average $\langle c^\dagger_{\alpha'} v^\dagger_\nu c_{\nu'} v_\alpha\rangle$ has already been subtracted in the definition of C^{x} in Eq. (2.22).

A special role inhere the matrix elements $C^{\mathrm{x}}_{\alpha\nu\nu\alpha}$, as they also contain contributions corresponding to excitonic population. This can be inferred from the spontaneous-emission contribution in Eq. (2.18). The term $\propto f^c_\nu(1 - f^v_\nu)$ is the factorized part $\langle c^\dagger_\alpha v^\dagger_\nu c_\nu v_\alpha\rangle_{\mathrm{S}}$ and describes an uncorrelated electron-hole plasma for the state ν. The correlated part is given by the sum over the matrix elements $C^{\mathrm{x}}_{\alpha\nu\nu\alpha}$. If the matrix elements are non-zero, correlations between electrons and holes are introduced into the electron-hole system. The correlation function with four identical indices may

be interpreted as excitonic carrier occupations, but also off-diagonal correlations contribute towards the luminescence. The formation of excitonic populations has been studied in quantum wells in Ref. [62].

Note that a generalization of the source term of spontaneous emission in Eq. (2.18) to QDs at different positions can be formulated to account for coupling of carrier transitions in *different* dots. In that case, the state indices are understood to include the position indices of each dot, and the sum runs over all QD positions. Then, in addition to the electron-hole correlation (2.22) within one QD, $R_1 = R_2$, one obtains correlation functions of the type $\delta\langle c^\dagger_{\alpha,R_1} v^\dagger_{\nu,R_2} c_{\nu,R_2} v_{\alpha,R_1}\rangle$ with R_1 and R_2 referring to the spatial positions of two different QDs. It can be shown that the Coulomb interaction cancels for QDs at different positions $R_1 \neq R_2$, leaving only the light-matter interaction as the driving mechanism for these correlations. A straightforward interpretation lies in the radiative, or more precisely, superfluorescent coupling. This effect refers to the collective emission of radiation after an incoherent excitation. In contrast to stimulated emission, however, this effect is not mediated by a photonic population in a resonator, but is caused by a direct radiative coupling between the emitters. While superfluorescense and superradiance is intensely studied in the literature [22–24, 40, 103, 139, 140, 147, 148], we do not consider this effect within this thesis under the assumption that it is small in an ensemble of self-organized QDs. The coupling can only be effective if the emitters couple constructively. This is either the case for very few emitters, or for an array with a regular spacing of half of the emission wavelength between single emitters. In an irregular array of self-assembled QDs, the effect is expected to average to zero.

The time evolution of the interband correlations is given by the equation of motion

$$
\begin{aligned}
i\hbar\frac{\mathrm{d}}{\mathrm{d}t}C^{\mathrm{x}}_{\alpha'\nu\nu'\alpha} = &-\big(\varepsilon^c_{\alpha'} + \varepsilon^v_\nu - \varepsilon^c_{\nu'} - \varepsilon^v_\alpha\big)\langle c^\dagger_{\alpha'} v^\dagger_\nu c_{\nu'} v_\alpha\rangle \\
&- \sum_{\nu_2\nu_3\nu_4}\Big[V_{\nu_1\nu_2\nu_3\alpha'}\langle c^\dagger_{\nu_4}(c^\dagger_{\nu_2}c_{\nu_3} + v^\dagger_{\nu_2}v_{\nu_3})v^\dagger_\nu c_{\nu'} v_\alpha\rangle \\
&\qquad + V_{\nu_4\nu_2\nu_3\nu}\langle c^\dagger_{\alpha'} v^\dagger_{\nu_4}(c^\dagger_{\nu_2}c_{\nu_3} + v^\dagger_{\nu_2}v_{\nu_3})c_{\nu'} v_\alpha\rangle \\
&\qquad - V_{\nu'\nu_2\nu_3\nu_4}\langle c^\dagger_{\alpha'} v^\dagger_\nu(c^\dagger_{\nu_2}c_{\nu_3} + v^\dagger_{\nu_2}v_{\nu_3})c_{\nu_4} v_\alpha\rangle \\
&\qquad - V_{\alpha\nu_2\nu_3\nu_4}\langle c^\dagger_{\alpha'} v^\dagger_\nu c_{\nu'}(c^\dagger_{\nu_2}c_{\nu_3} + v^\dagger_{\nu_2}v_{\nu_3})v_{\nu_4} v_{\nu_4}\rangle \Big] \\
&- i\sum_\xi \Big[g^*_\xi \langle b^\dagger_\xi v^\dagger_{\alpha'} v^\dagger_\nu c_{\nu'} v_\alpha\rangle - g^*_\xi \langle b^\dagger_\xi c^\dagger_{\alpha'} v^\dagger_\nu c_{\nu'} c_\alpha\rangle \\
&\qquad + g_\xi \langle b_\xi c^\dagger_{\alpha'} v^\dagger_\nu v_{\nu'} v_\alpha\rangle - g_\xi \langle b_\xi c^\dagger_{\alpha'} c^\dagger_\nu c_{\nu'} v_\alpha\rangle \Big] \\
&- i\hbar\frac{\mathrm{d}}{\mathrm{d}t}\langle c^\dagger_{\alpha'} v^\dagger_\nu c_{\nu'} v_\alpha\rangle_{\mathrm{S}} \,.
\end{aligned}
\tag{2.23}
$$

Here, the first line is due to the free carrier Hamiltonian (2.2), the first sum due to the carrier Coulomb interaction (2.3), and the second sum due to the light-matter interaction (2.6) containing triplet terms. Note that the time derivative of the singlet factorization must be subtracted in order to obtain the pure four-operator correlation, which can be seen by taking the time derivative of Eq. (2.12b), i.e.

$$\frac{\mathrm{d}}{\mathrm{d}t}\,\delta\langle 2\rangle = \frac{\mathrm{d}}{\mathrm{d}t}\,\langle 2\rangle - \frac{\mathrm{d}}{\mathrm{d}t}\,\langle 1\rangle\langle 1\rangle\;. \tag{2.24}$$

Evaluating Eq. (2.23) on the doublet level, i.e., neglecting triplet level and higher order correlations, leads to

$$
\begin{aligned}
i\hbar\frac{\mathrm{d}}{\mathrm{d}t}\,C^{\mathrm{x}}_{\alpha'\nu\nu'\alpha} =\;& \big(\varepsilon^c_{\nu'} - \varepsilon^v_\nu - \varepsilon^c_{\alpha'} + \varepsilon^v_\alpha\big)C^{\mathrm{x}}_{\alpha'\nu\nu'\alpha}\\
&+ V_{\nu'\alpha\nu\alpha'}\big[\,(1-f^c_{\alpha'})(1-f^v_\nu)\,f^c_{\nu'}f^v_\alpha - f^c_{\alpha'}f^v_\nu\,(1-f^c_{\nu'})(1-f^v_\alpha)\,\big]\\
&+ \sum_{\beta\beta'}\Big\{(f^v_\nu - f^v_\alpha)\,V_{\beta\alpha\nu\beta'}\big(C^{\mathrm{x}}_{\alpha'\beta\nu'\beta'} + C^c_{\alpha'\beta\nu'\beta'}\big) + (f^c_{\alpha'} - f^c_{\nu'})\,V_{\nu'\beta\beta'\alpha'}\big(C^{\mathrm{x}}_{\beta\nu\beta'\alpha} + C^v_{\beta\nu\beta'\alpha}\big)\,\Big\}\\
&+ \sum_{\beta\beta'}\Big\{f^c_{\beta'}V_{\beta'\beta\beta'\alpha'}C^{\mathrm{x}}_{\beta\nu\nu'\alpha} + f^v_{\beta'}V_{\beta'\beta\beta'\nu'}C^{\mathrm{x}}_{\alpha'\beta\nu'\alpha} - f^c_\beta\,V_{\nu'\beta\beta'\beta}C^{\mathrm{x}}_{\alpha'\nu\beta'\alpha} - f^v_{\beta'}V_{\alpha\beta\beta'\beta}C^{\mathrm{x}}_{\alpha'\nu\nu'\beta'}\,\Big\}\\
&+ \sum_{\beta\beta'}(f^c_\beta + f^v_\beta)\big[V_{\beta'\beta\beta\alpha'}C^{\mathrm{x}}_{\beta'\nu\nu'\alpha} + V_{\beta'\beta\beta\nu}C^{\mathrm{x}}_{\alpha'\beta'\nu'\alpha} - V_{\nu'\beta\beta\beta'}C^{\mathrm{x}}_{\alpha'\nu\beta'\alpha} - V_{\alpha\beta\beta\beta'}C^{\mathrm{x}}_{\alpha'\nu\nu'\beta'}\big]\\
&+ \sum_{\beta\beta'}\Big\{(f^v_\alpha - f^c_{\alpha'})\,V_{\beta\alpha\beta'\alpha'}C^{\mathrm{x}}_{\beta\nu\nu'\beta'} - (f^v_\nu - f^c_{\nu'})\,V_{\nu'\beta\nu\beta'}C^{\mathrm{x}}_{\alpha'\beta\beta'\alpha} + (1 - f^v_\alpha - f^c_{\nu'})\,V_{\nu'\alpha\beta\beta'}C^{\mathrm{x}}_{\alpha'\nu\beta'\beta}\\
&\qquad + (f^c_{\alpha'} - 1 + f^v_\nu)\,V_{\beta\beta'\nu\alpha'}C^{\mathrm{x}}_{\beta\beta'\nu'\alpha} + (f^c_{\nu'} - f^c_{\alpha'})\,V_{\nu'\beta\alpha'\beta'}C^{\mathrm{x}}_{\beta\nu\beta'\alpha} + (f^v_\alpha - f^v_\nu)\,V_{\beta\alpha\beta'\nu}C^{\mathrm{x}}_{\alpha'\beta\nu'\beta'}\Big\}\\
&- i\sum_{\xi}\delta_{\alpha\alpha'}\delta_{\nu\nu'}\big[\,g^*_\xi(f^v_\alpha - f^c_\alpha)\langle b^\dagger_\xi v^\dagger_\nu c_\nu\rangle + g_\xi(f^v_\nu - f^c_\nu)\langle b_\xi c^\dagger_\alpha v_\alpha\rangle\,\big]\;.
\end{aligned}
\tag{2.25}
$$

Although the quantity of terms makes this equation look very complicated, an interpretation of the single contributions is possible. The first two lines of Eq. (2.25) correspond to a calculation of C^{x} in singlet approximation. A theory restricted to this level was used in Ref. [65, 72] for quantum wells and in Ref. [124] for QDs. Note that the singlet factorization of six-operator averages already goes beyond the Hartree--Fock approximation, which corresponds to the singlet factorization of four-operator averages. Nevertheless, it is not consistent in the sense that all occurring operator averages are treated on the same level.[5] In the Hartree-Fock approximation the correlations $C^{\mathrm{x},c,v}$ are neglected altogether. The terms in the third line can be shown to provide screening according to the Lindhard theory for the Coulomb potential in

---

[5] As the photon-assisted polarization is a doublet quantity, all averages must be evaluated up to the doublet-level for consistency.

Eq. (2.18). The next line contains exchange-like scattering terms, followed by one line of direct scattering terms, identified by the indices on the Coulomb matrix elements [10]. The terms in the fourth sum are Coulomb renormalizations due to scattering between all possible states. The last line finally contains the contribution due to the light-matter interaction Hamiltonian in Eq. (2.6).

An equation similar to (2.25) for the intraband correlations $C^c_{\alpha'\nu\nu'\alpha} = \delta\langle c^\dagger_{\alpha'} c^\dagger_\nu c_{\nu'} c_\alpha \rangle$ is obtained along the same lines. We restrict ourselves here to the equation of motion for the correlations of the conduction-band electrons. A similar equation can be given for the valence-band carrier correlations $C^v_{\alpha'\nu\nu'\alpha} = \delta\langle v^\dagger_{\alpha'} v^\dagger_\nu v_{\nu'} v_\alpha \rangle$ by exploiting the symmetry properties of the Hamiltonian (2.1).

$$
\begin{aligned}
i\hbar\frac{\mathrm{d}}{\mathrm{d}t}\, C^c_{\alpha'\nu\nu'\alpha} =\ & -\left(\varepsilon^c_{\alpha'} + \varepsilon^c_\nu - \varepsilon^c_{\nu'} - \varepsilon^c_\alpha\right) C^c_{\alpha'\nu\nu'\alpha} \\
& - \left(V^*_{\alpha'\nu\nu'\alpha} - V^*_{\alpha'\nu\alpha\nu'}\right)\left[(1-f^c_\nu)(1-f^c_{\alpha'})\,f^c_{\nu'}f^c_\alpha - f^c_\nu f^c_{\alpha'}\,(1-f^c_{\nu'})(1-f^c_\alpha)\right] \\
& + \sum_{\beta\beta'}\Big\{(f^c_{\nu'}-f^c_\nu)\,V_{\nu'b\ \beta'\nu}\,C^{c+\mathrm{x}}_{\alpha'b\ \alpha\beta'} - (f^c_{\alpha'}-f^c_\alpha)\,V_{\alpha b\ \beta'\alpha'}\,C^{c+\mathrm{x}}_{\nu b\ \nu'\beta'} \\
& \qquad - (f^c_{\nu'}-f^c_{\alpha'})\,V_{\nu'b\ \beta'\alpha'}\,C^{c+\mathrm{x}}_{\nu b\ \alpha\beta'} + (f^c_\nu - f^c_\alpha)\,V_{\alpha b\ \beta'\nu}\,C^{c+\mathrm{x}}_{\alpha'b\ \nu'\beta'}\Big\} \\
& + \sum_{\beta\beta'}\Big\{f^c_{\beta'}V_{\beta'b\ \beta'\alpha'}C^c_{b\ \nu\nu'\alpha} + f^c_{\beta'}V_{\beta'b\ \beta'\nu}C^c_{\alpha'b\ \nu'\alpha} - f^c_b\,V_{\nu'b\ \beta'b}\ C^c_{\alpha'\nu\beta'\alpha} - f^c_b\,V_{\alpha b\ \beta'b}\ C^c_{\alpha'\nu\nu'\beta'}\Big\} \\
& + \sum_{\beta\beta'}\Big\{(f^c_b + f^v_b)\,V_{\beta'b\ b\ \alpha'}C^c_{\beta'\nu\nu'\alpha} + (f^c_b + f^v_b)\,V_{\beta'b\ b\ \nu}C^c_{\alpha'\beta'\nu'\alpha} \\
& \qquad - (f^c_b + f^v_b)\,V_{\nu'b\ b\ \beta'}C^c_{\alpha'\nu\beta'\alpha} - (f^c_b + f^v_b)\,V_{\alpha b\ b\ \beta'}C^c_{\alpha'\nu\nu'\beta'}\Big\} \\
& + \sum_{\beta\beta'}\Big\{(1-f^c_\alpha-f^c_{\nu'})\,V_{\nu'\alpha\beta'b}\ C^c_{\alpha'\nu b\ \beta'} - (1-f^c_{\alpha'}-f^c_\nu)\,V_{b\ \beta'\nu\alpha'}C^c_{b\ \beta'\nu'\alpha} \\
& \qquad - (f^c_{\alpha'}-f^c_\alpha)\,V_{\alpha b\ \alpha'\beta'}C^c_{b\ \nu\nu'\beta'} - (f^c_{\nu'}-f^c_{\alpha'})\,V_{b\ \nu'\beta'\alpha'}C^c_{b\ \nu\beta'\alpha} \\
& \qquad - (f^c_{\nu'}-f^c_\nu)\,V_{b\ \nu'\beta'\nu}\,C^c_{\alpha'b\ \beta'\alpha} - (f^c_\nu - f^c_\alpha)\,V_{\alpha b\ \nu\beta'}C^c_{\alpha'b\ \nu'\beta'}\Big\}
\end{aligned}
\tag{2.26}
$$

Here we have used the abbreviation $C^{c+\mathrm{x}}_{\alpha'\nu\nu'\alpha} = C^c_{\alpha'\nu\nu'\alpha} + C^{\mathrm{x}}_{\alpha'\nu\nu'\alpha}$. The terms can be interpreted in analogy to Eq. (2.25). However, the contribution due to the light-matter interaction vanishes for C^c and C^v. Note that the remaining Coulomb correlations can only redistribute carriers without changing the total population $\sum_\nu f^{c,v}_\nu$. Therefore, the changes of the carrier densities in each band are determined only by the photon-assisted polarization. From combination of Eqs. (2.17) and (2.20), one readily obtains

$$
\frac{\mathrm{d}}{\mathrm{d}t}\left(\sum_\nu f^c_\nu + \sum_\xi \langle b^\dagger_\xi b_\xi \rangle\right) = 0 \ ,
\tag{2.27}
$$

which reveals that a decrease (increase) of population in the conduction band is balanced by the increase (decrease) of the total photon number.

In the equations of motion (2.25) and (2.26) for the carrier correlations no dephasing terms appear. In Eq. (2.18) for the photon-assisted polarization we have introduced a phenomenological dephasing in order to account for the effects of carrier-phonon interaction. Without dephasing, the correlations remain undamped. To account for the effect of phonon interaction in the correlations the obvious choice would be to add a constant dephasing term in analogy to Eq. (2.18). However, it turns out that a constant diagonal dephasing term leads to an unphysical heating of the system. This has also been observed by Hoyer et al. in Ref. [62]. The solution to this problem is to use a microscopic dephasing model. However, dephasing of carrier-carrier correlations is provided by triplet terms generated by the phonon-interaction Hamiltonian [62]. At this stage we restrict ourselves to the doublet level, and a small constant dephasing is used in Section 2.5 together with carrier scattering due to interaction with LO-phonons [128], treated in relaxation-time approximation, in order to demonstrate the effect of dephasing of correlations. The scattering redistributes carriers towards a steady-state distribution and manages to compensate the artificial heating caused by the constant dephasing term. Nevertheless, a microscopic treatment of the phonon interaction to obtain the correct dephasing terms is desirable and work in progress.

2.4. Stationary Photoluminescence Spectrum

Before we look at the dynamics of the photoluminescence, we show results for the stationary spectrum. The equations are solved in the time domain using a fourth order Runge-Kutta method. Some numerical details are found in Appendix E. Due to the free oscillating part in Eqs. (2.18) and (2.25) a constant femtosecond stepsize is required. The material parameters are those used in Ref. [10] for an InGaAs QD system. We consider a density of $1.5 \cdot 10^{10} \, \mathrm{cm}^{-2}$ QDs on the WL and a gap energy of $1.52 \, \mathrm{eV}$. We assume that the excitation involves only carriers with one spin polarization, e.g., due to excitation with circularly polarized light. The dynamics of the carrier generation and relaxation happen on much faster timescales ($\sim 10 \, \mathrm{ps}$) than the recombination ($\sim 1 \, \mathrm{ns}$), and we assume a quasi-equilibrium distribution of carriers with given carrier density and temperature as an initial state for our calculation. This treatment is supported by separate studies of relaxation processes due to Coulomb interaction and interaction with LO-phonons [17, 100, 127, 128].

Due to this assumption the initial values for the correlation functions C^{x}, C^{e}, and C^{v} remain open. In an unexcited system, all correlation functions are zero and build up

during the carrier generation process according to their equations of motion. Starting a calculation with quasi-equilibrium population and vanishing correlation functions can lead to an abrupt build-up of correlations, resulting in unphysical oscillations of the correlation matrix elements that carry over to the population dynamics. To avoid these unphysical results, we numerically determine the initial conditions for the correlation functions from their equations of motion. For this purpose, we perform a separate calculation, where the carrier populations are adiabatically ramped up to their equilibrium values $\tilde{f}_\nu^{e,h}$ according to

$$\frac{\mathrm{d}}{\mathrm{d}t} f_\nu^{e,h} = \frac{\tilde{f}_\nu^{e,h}}{2} \frac{\pi}{\tau} \sin\left(\frac{\pi}{\tau} t\right) \qquad \text{for } 0 < t < \frac{\tau}{2} \; . \tag{2.28}$$

The resulting steady-state solutions of the equations of motion for the correlation functions provide the starting point of the time evolution discussed in the following. This approach can be placed into a physical context by taking a closer look at carrier scattering due to LO-phonons. Microscopic calculations of carrier relaxation due to scattering with LO-phonons [17], although performed for a different material system, suggest a typical time of a few picoseconds until the incoherently excited population is transformed into a steady-state distribution. In Figure 2.4 we show the population build-up of electrons (top panel) and holes (bottom panel) in the p- and s-shells after pulsed excitation of the wetting layer states for a temperature of 10K. The bold lines are the result of a non-markovian quantum-kinetic calculation including polaronic and memory effects, performed by Jan Seebeck in our group. Efficient relaxation is observed despite the frequently used argument of a phonon bottleneck, for detail refer to [17, 128]. The steady-state results of the quantum kinetic calculation are well reproduced by choosing effective relaxation times τ, in this case 3.5 ps for electrons and 1.5 ps for holes. The results are shown in Figure 2.4. Based on this, we use Eq. (2.28) with comparable relaxation times.

We define the time-dependent luminescence spectrum according to [42, 70] and consider the high-frequency-resolution limit of a detector to obtain

$$I(\omega) = \frac{\mathrm{d}}{\mathrm{d}t} \sum_\xi \langle b_\xi^\dagger b_\xi \rangle \Big|_{|\mathbf{q}|=\frac{\omega}{c}} \; . \tag{2.29}$$

Here the mode label contains $\xi = \{\mathbf{q}, \mathbf{e}_\mathrm{p}\}$. Using Eq. (2.17) leads to

$$I(\omega) = \frac{2}{\hbar} \sum_\nu |\bar{g}_\xi|^2 \operatorname{Re} \widetilde{\langle b_\xi^\dagger v_\nu^\dagger c_\nu \rangle} \; , \tag{2.30}$$

where $\widetilde{\langle b_\xi^\dagger v_\nu^\dagger c_\nu \rangle} = \langle b_\xi^\dagger v_\nu^\dagger c_\nu \rangle / g_\xi$ has been introduced. By means of this redefinition, the resulting quantity $\widetilde{\langle b_\xi^\dagger v_\nu^\dagger c_\nu \rangle}$ can be shown to depend only on the photon energy
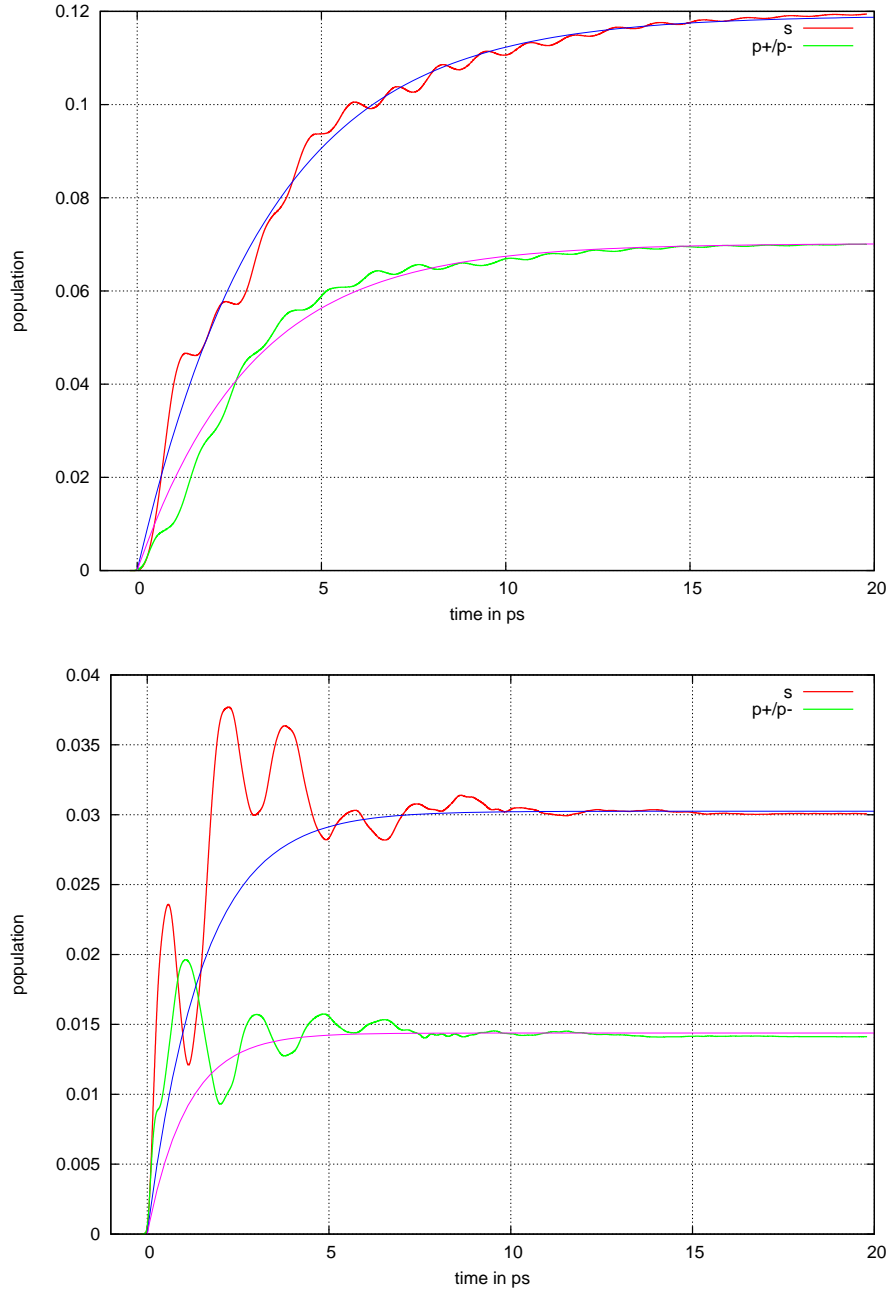
Figure 2.4.: Time evolution of the carrier population (top: electrons, bottom: holes) into a steady state after wetting-layer excitation at 10K. The oscillating lines represent the results of a non-markovian quantum-kinetic calculation, while the monotonic curves represent approximations based on the choice of an effective relaxation time of $\tau = 3.5$ (1.5) ps for electrons (holes).

$\hbar\omega = \hbar c q$ and neither on the direction nor on the polarization of the mode ξ. As a result the angular part and the polarization can be integrated out in Eq. (2.29), yielding the quantity $|\bar{g}_\xi|^2$ in Eq. (2.30) in a way similar to the Wigner-Weißkopf theory [92]. The total photon number is obtained from

$$I_{\text{tot}} = \int \mathrm{d}\omega \, I(\omega) \, . \tag{2.31}$$

The frequency-resolved photoluminescence (PL) spectrum after a time evolution of 50 ps is plotted in Figure 2.5 for two different temperatures of 200 K and 77 K. Scaled relative to the bandgap, the two peaks correspond to the s-shell resonance at about $-133\,\mathrm{meV}$ and the p-shell transition at about $-79\,\mathrm{meV}$. Both peaks are red shifted due to the Coulomb interaction from the non-interacting energies $\varepsilon_p^c + \varepsilon_p^v = -111\,\mathrm{meV}$ and $\varepsilon_s^c + \varepsilon_s^v = -55.5\,\mathrm{meV}$, respectively. Furthermore, the peak height is changed due to the Coulomb interaction.

To explain the origin of the peaks in the spectrum, we consider a simplified picture where Coulomb interaction and correlations (Hartree-Fock limit) are neglected. We can solve the equation of motion for $\langle b_\xi^\dagger v_\nu^\dagger c_\nu \rangle$ in the adiabatic regime to obtain

$$\frac{1}{g_\xi} \langle b_\xi^\dagger v_\nu^\dagger c_\nu \rangle = -i \, \frac{f_\nu^c (1 - f_\nu^v)}{\varepsilon_\nu^c - \varepsilon_\nu^v - \hbar\omega_\xi - i\Gamma} \, . \tag{2.32}$$

Inserting this in Eq. (2.29) yields two peaks, one at the free energy of the s-shell emission $\varepsilon_s^c - \varepsilon_s^v$, and one at the p-shell emission shown as dotted line in the left panel of Figure 2.5. The same arguments, but with less crude approximations, can be inferred from the Eliot-formula, which is frequently used in the discussion of PL [44, 70] and absorption spectra [58].

The results of the calculation on the doublet level are compared in the same figure to those obtained in the Hartree-Fock, or singlet approximation (dashed lines) for the source term of spontaneous emission. Remember that in the singlet factorization the correlations, which are doublet quantities, are neglected altogether. In the numerical evaluation we found the influence of the correlations C^c and C^v to be negligible in comparison to the electron-hole correlations C^x for the studied parameters. The PL at the s-shell is slightly reduced, while the p-shell PL becomes negative. Contrary to an absorption spectrum, where a negative peak corresponds to gain, this result is unphysical and an artifact of the Hartree-Fock approximation at low temperatures. It reflects a violation of the consistency required by the truncation scheme, indicating that for the calculation of a doublet-level quantity relevant processes must also be treated on the doublet level. In Chapter 3 this consistency requirement leads to the calculation of quadruplet level terms for the second-order photon correlation function,
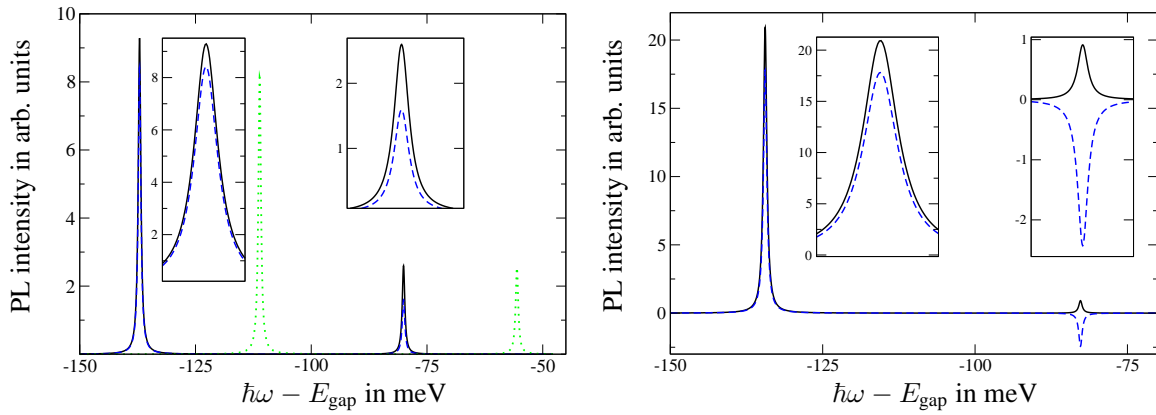
Figure 2.5.: Stationary PL spectra for $T = 200\,\mathrm{K}$ (left) and $T = 77\,\mathrm{K}$ (right). Initially the QD is populated on average with one electron and one hole. In both figures the solid line corresponds to the full calculation and the dashed line to the Hartree-Fock factorization. For comparison the dotted line shows a spectrum without Coulomb interaction. The insets show a magnification of the peaks.

which is determined by a quadruplet-level correlation function itself. In Ref. [65] the doublet correlations (2.22) were included, but factorized on the singlet level. As we have discussed, this corresponds to taking only the first two lines in Eq. (2.25) while neglecting the doublet contributions (due to the Coulomb- and the dipole Hamiltonian of the light-matter interaction). Although the PL signal is less prone to becoming negative, positivity is still not ensured. Only if the terms in the equations of motion for the correlations (2.22) are factorized on doublet level, do we find the spectrum to be positive for all temperatures. Positivity is also naturally ensured if a different approach based on Green's functions is chosen [65].

2.5. Time-Resolved Photoluminescence

In this section we study the influence of the correlations on the time-resolved PL and on the corresponding population dynamics. Before we discuss the numerical results obtained by the solution of the full set of equations derived in Section 2.3, it is instructive to analyze the source term in Eq. (2.18) in more detail to gain a deeper understanding of the decay behavior of photoluminescence in a semiconductor system.

2.5.1. Understanding the Role of Carrier Correlations in Quantum Dots

In the derivation of Eq. (2.18) the source term of spontaneous emission $g_\xi f_\nu^c (1 - f_\nu^v) + g_\xi \sum_\alpha C_{\alpha\nu\nu\alpha}^{\text{x}}$ originates from the operator average $\sum_\alpha g_\xi \langle c_\alpha^\dagger v_\alpha v_\nu^\dagger c_\nu \rangle$. An illuminating analysis is possible if one completely neglects the Coulomb interaction of carriers. Here, the source term of spontaneous emission with the four-operator expectation value (resulting from the carrier-photon interaction) can be evaluated in two limiting cases. The first is the Hartree-Fock approximation, where correlations among the carriers are neglected. The second corresponds to the one-electron two-level approximation, where one assumes that the relevant physics is determined by one confined shell for electrons and one for holes. The latter case is of particular interest, since atomic models are frequently used in the discussion of QDs.

Within the Hartree-Fock approximation, the source term of spontaneous emission is solely determined by the product $f_\nu^c (1 - f_\nu^v)$. In the absence of Coulomb interaction, one can formulate the stationary solution of Eq. (2.18) for the case of slowly varying populations to obtain

$$
\begin{aligned}
\frac{\mathrm{d}}{\mathrm{d}t} f_\nu^c &= -\frac{2}{\hbar} \operatorname{Re} \sum_\xi \frac{i \, |g_\xi|^2 \, f_\nu^c (1 - f_\nu^v)}{\varepsilon_\nu^c - \varepsilon_\nu^v - \hbar\omega_\xi - i\Gamma} \\
&= -\frac{f_\nu^c (1 - f_\nu^v)}{\tau_\nu^c} ,
\end{aligned}
\tag{2.33}
$$

where $1/\tau_\nu^c$ is the Wigner-Weißkopf rate of spontaneous emission for conduction-band carriers in the limit $\Gamma \to 0$ [92]. From this equation it is obvious that the decay of the population f_ν^c is non-exponential, unless f_ν^v is held constant by some mechanism, like background doping. Another way to think of it is that the decay rate becomes time dependent, if it is redefined as

$$
\frac{1}{\tilde{\tau}_\nu^c(t)} = \frac{1 - f_\nu^v(t)}{\tau_\nu^c} .
\tag{2.34}
$$

Furthermore, the rate of decay depends on the carrier density and is higher for smaller populations in the valence band. This behavior carries over to the PL according to Eq. (2.27). Due to the non-exponential PL decay a simple decay rate cannot be used to characterize the PL dynamics. This might appear surprising, because for a two-level atom an exponential decay behavior is known.

Let us consider the two-level approximation with a single carrier as the second limiting case. Carrier indices are dropped while they are not needed if the population dynamics is restricted to one confined electron and hole level. In the unexcited (excited) state for this two-level system the electron is in the valence- (conduction-) band state. For

the two spin polarizations, which are decoupled in the absence of Coulomb interaction, the independent processes then involve only the excitation of a single electron. This has a significant consequence for the evaluation of the source term of spontaneous emission. Within the two-level approximation, the successive application of more than one annihilation operator always yields zero, so that the source term $\langle c^\dagger v v^\dagger c \rangle$ reduces to f^c. Along the same lines discussed above, instead of Eq. (2.33) one obtains

$$\frac{\mathrm{d}}{\mathrm{d}t} f^c = -\frac{f^c}{\tau} \, , \tag{2.35}$$

which corresponds to the exponential decay behavior known from the two-level system. In this case, $1/\tau$ is the Wigner-Weißkopf rate for the considered two-level transition. From this analysis we deduce that the exponential decay within the two-level approximation is a manifestation of the fact that the excitation of a QD conduction-band carrier is rigidly linked to the absence of a QD valence-band carrier. In the electron-hole picture, this corresponds to fully a correlated electron-hole pair. On the operator level this is expressed as $c^\dagger v v^\dagger c = c^\dagger c$. In a semiconductor QD, however, several carriers are typically present and their correlations are subject to scattering and dephasing processes and must, therefore, explicitly be calculated.

2.5.2. Results for the Emission into Free Space

Now we turn to the numerical results of the SLE including Coulomb interaction. In Figure 2.6 we show the evolution of the time-resolved photoluminescence. Again, the initial carrier density is taken to be $1.5 \cdot 10^{10} \, \mathrm{cm}^{-2}$. For the solid line all correlations up to the doublet level have been included. The result of a calculation in the Hartree-Fock approximation, which we can now interpret to correspond to the situation of uncorrelated carriers, is shown as dashed line. In this case, the decay is clearly non-exponential, which is in accordance with Eq. (2.33). Keeping the discussion in the previous section in mind, it is obvious from the full calculation on doublet level that carriers are strongly correlated.

However, our approach so far does not account for any kind of dephasing of the correlations. This topic was already mentioned in Section 2.3, where phonon scattering was named as one physical mechanism providing such dephasing. Hoyer et al. have studied phonon scattering on a microscopic level for a quantum-well system. It is shown that dephasing of correlations is indeed provided, although this enters only via higher-order triplet terms [61, 62]. Extensions beyond the singlet-doublet factorization are not within the scope of this work. Nevertheless, we can account for the main features of scattering, which is dephasing of correlations and relaxation of the carrier
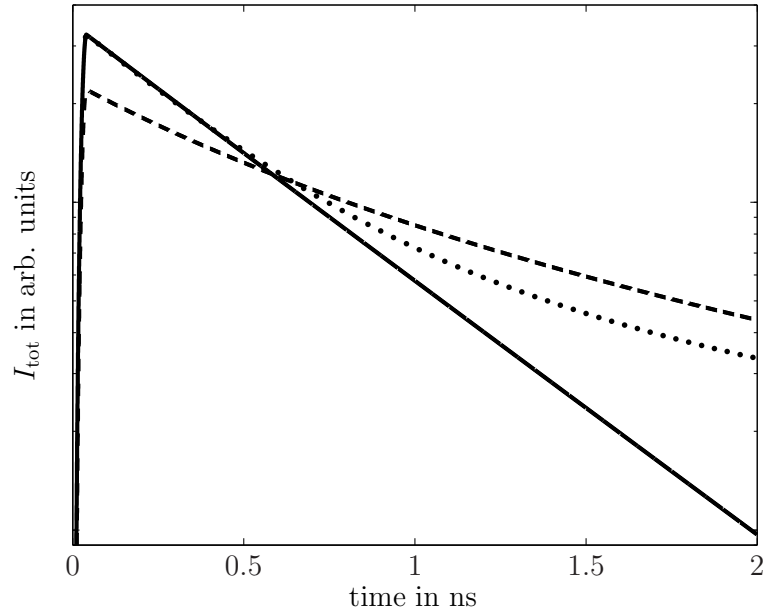
Figure 2.6.: Logarithmic plot of the time evolution of the quantum-dot photoluminescence. The dashed line corresponds to the calculation in singlet (Hartree-Fock) factorization and the solid line to the doublet level. For the dotted line the described phonon contributions were added to the doublet calculation and provide a damping mechanism for the correlations.

population towards a steady state, on a phenomenological level. A constant dephasing term $-i\gamma C^{\mathrm{x}}_{\alpha'\nu\nu'\alpha}$ is added on the right hand side of Eq. (2.25) and the scattering is treated within relaxation-time approximation by introducing

$$\frac{\mathrm{d}}{\mathrm{d}t} f^{c,v}_\nu \Big|_{\mathrm{relax}} = -\frac{f^{c,v}_\nu - F^{c,v}_\nu(T)}{\tau^{c,v}_{\mathrm{relax}}} \ , \tag{2.36}$$

in Eqs. (2.20) and (2.21), where we consider a Fermi-Dirac distribution $F^{c,v}_\nu(T)$ at the lattice temperature T, evaluated at every timestep for the corresponding carrier density.

Several recent experimental and theoretical investigations address the efficiency of carrier-phonon interaction in QDs. In the low-temperature and density regime, interaction of carriers with LA-phonons [78, 99, 145] provide the dominant dephasing mechanism, while at elevated temperatures the interaction of carriers with LO-phonons leads to very efficient dephasing [86]. The temperature dependence of the dephasing has been studied, e.g., in four-wave experiments [25, 26]. Even for the weakest dephasing values obtained there (few μeV at elevated temperatures), we find that the influence of carrier correlations on the PL decay is strongly reduced.

To demonstrate the effect of a very weak constant dephasing rate, $\gamma = 0.001\,\mathrm{meV}$ has been used according to Eq. (2.36) for the dotted line in Figure 2.6. The correlations

are drastically reduced so that a non-exponential signature of the decay is regained on longer timescales. Our numerical analysis shows that the results presented here are rather insensitive to the exact value of the relaxation time $\tau_{\text{relax}}^{c,v}$. For the discussed example, typical values of $\tau_{\text{relax}} = 1\,\text{ps}$ for electrons and holes are taken [17, 128]. Hoyer et al. have shown that a constant dephasing γ causes unphysical heating of the system. However, this effect is only weak for a small value for the dephasing and, additionally, the scattering term (2.36) counteracts the heating.

While for a consistent treatment of phonon scattering the inclusion of a microscopic description of the electron-phonon interaction is necessary, the important point is here that *any* kind of weak dephasing of the correlations will lead to deviations from an exponential decay.

2.6. Comparison with Experiments – Time-Resolved Photoluminescence of Doped and Undoped QDs

The development of the described theory was carried out side by side with experiments on both unstructured (no cavity) and structured (with cavity) QD samples performed in the group of Prof. Manfred Bayer in Dortmund [19, 124]. We present some of the results of this collaboration to provide direct experimental evidence for the discussed effects.

First we look at the emission of unstructured doped and undoped InGaAs QD samples. Experimental details of this work can be found in Ref. [19]. In the doped case the dopant density was chosen to be about equal to the dot density in each layer, so that an average occupation by a single electron or hole per dot can be expected.

The QD parameters are those used in the previous section, except for the QD density is taken to be $N = 10^{10}\,\text{cm}^{-2}$, the dipole moment is $16.8\,e\mathring{A}$ and the dephasing of the correlations is $0.05\,\text{meV}$. Even though the dephasing is weak it effectively destroys the correlations on a time scale of tens of picoseconds.

Figure 2.7 shows results for excitation into the p-shell. For the undoped situation we pump the system with equal electron and hole density $N_e = N_h = 0.35N$. In the n-doped case we assume on average one additional electron per QD, i.e. $N_e = N_h + N$ with again $N_h = 0.35N$. Apart from this difference in the initial conditions both curves are calculated with exactly the same parameters. Excellent agreement between theory and experiment can be observed. For the two different cases we see the following: In the situation of undoped QDs, we observe a non-exponential decay in
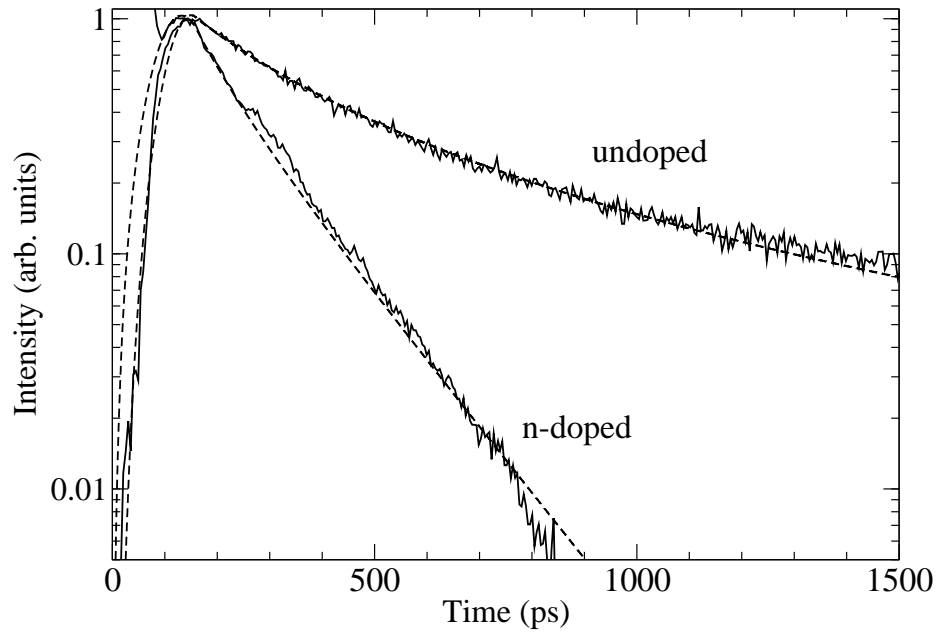
Figure 2.7.: Time-resolved PL for doped and undoped QDs excited into the p-shell. The calculation (dashed lines) agrees perfectly with the experimental data (solid lines).

agreement with our discussion of the emission of QDs into free space in Section 2.5. In contrast, the doped QDs show an exponential decay, which is faster by approximately a factor of two when compared to the undoped case.

To understand the origin of this different behavior, it is insightful to study the time evolution of the s-shell populations. These are depicted in Figure 2.8 for one spin subsystem. In the undoped case (top panel) the s-shell populations are zero at first. Due to the pump process and the subsequent carrier scattering, the population increases temporarily and then decays towards an empty system. In the n-doped case (lower panel) the electron occupation in the s-shell starts with the finite value of 0.5 (corresponding to an average of half an electron per spin direction) to account for the doping of one additional electron per QD. As can be seen, the temporal change of the electron population relative to the doping level remains small. According to Eq. (2.33), a constant electron population f_ν^e leads to an exponential decay of the hole population f_ν^h, and, hence, of the PL intensity.

These results clearly demonstrate the peculiarities of QD systems if thought of as 'artificial atoms' and underline the capability of our microscopic model to account for intrinsic semiconductor effects.
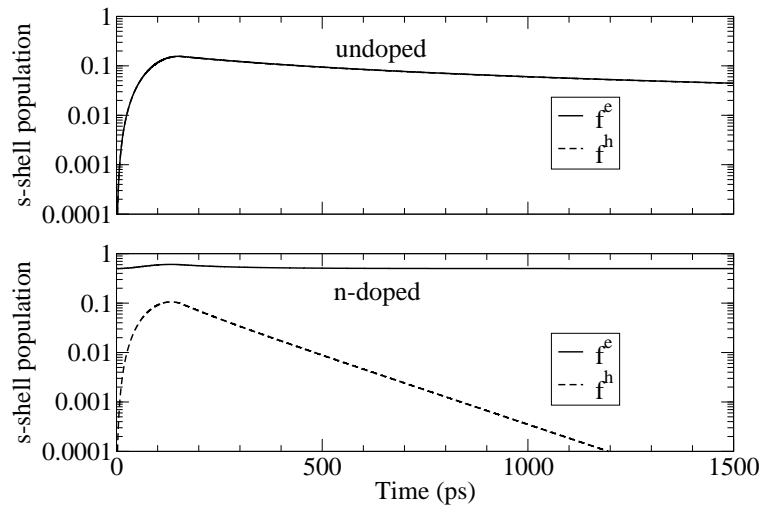
Figure 2.8.: Time evolution of electron and hole populations in the s-shell of undoped (top) and n-doped (bottom) QDs.

2.7. Time-Resolved Photoluminescence of QDs in Microresonators

In the remainder of this chapter we focus on QD-microcavity systems. The particular combination of QDs and microresonators offers a variety of new possibilities for device applications. Of particular interest is the design of efficient laser diodes with customized wavelength and emission properties. Additionally, QDs in microresonators are of considerable importance for fundamental studies and for quantum information research, e.g. as non-classical light sources.

So far, we have studied photoluminescence into free space, which we described by a continuum of plane wave modes. A non-exponential and excitation-density dependent decay was revealed to be a consequence of the semiconductor nature of QDs and a manifestation of missing correlations between electrons and holes. While we still expect these findings to hold in a cavity system, stimulated emission and absorption can have a strong effect on the decay of the PL. Cavity feedback is proportional to the number of photons in the cavity mode. State-of-the-art microcavities have very long lifetimes of hundreds of picoseconds, allowing for a large accumulation of photons in the long-lived modes even if the total spontaneous emission is small. An overview of various microcavity structures is given in the introduction and in Section 3.1. In the following we consider pillar microcavities with diameters of a few micrometers. A SEM (scanning electron microscopy) image of a typical structure in shown in Figure 2.9. Between two DBR (distributed Bragg reflector) mirrors, a layer of InGaAs QDs acting as the active medium is placed inside a GaAs λ-cavity. The confinement along the vertical direction is provided by alternating layers of high and low refractive index
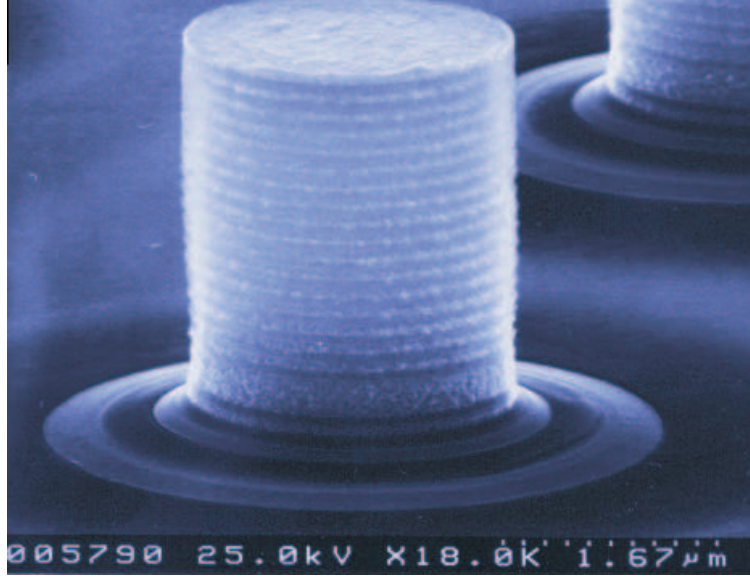
Figure 2.9.: SEM image of a pillar microresonator with InGaAs QDs of the type used in the experiments discussed in this section. The sample was grown in the group of A. Forchel, Universität Würzburg, picture taken from Ref. [14].

materials (AlAs/GaAs), each layer having a thickness of a quarter of the emission wavelength.

Placing an emitter into a microcavity can have numerous effects on its emission properties, first of all the enhancement and inhibition of the spontaneous emission rate, an effect being of great relevance in optoelectronics. The strength of the light-matter coupling can be tailored to a large degree by changing the geometry of the cavity and the position of the emitters relative to the maximum of the electromagnetic field inside the cavity, see also Figure 2.10. For a review we refer to Ref. [146] and the article by J.-M. Gérard in Ref. [93].

Depending on the strength of the light-matter coupling, two regimes are found, and both show characteristic effects whose experimental realizations have stirred excitement in the semiconductor community [50, 51, 55, 82, 106, 113, 157]. In an open cavity system several decay channels exist, like for example the emission into a continuum of leaky modes. If the decoherence introduced by the total losses happens on a slower timescale than the oscillation period, we speak of the *strong coupling regime*, where the system undergoes damped Rabi oscillations, revealing an exchange of energy between the emitter and the cavity mode. This behavior is similar to that of the ideal case of a closed cavity, where photons remain in the cavity mode until they get reabsorbed by the emitter. Due to the strong influence of the interaction, a level splitting occurs if the emitters get close to resonance with the cavity mode.

If the decoherence introduced by losses from the cavity mode is faster than the oscillation period, we speak of the *weak coupling regime*, where a monotonic relaxation of an excited emitter into the ground state takes place. This decay behavior is similar to the situation without cavity. However, the presence of the cavity alters the spontaneous emission rate in several ways: The photonic density of states, the amplitude of the electromagnetic field, and the angle between the field vector and the dipole of the radiating emitter are changed and finally determine the modified decay time τ of the emitter inside the cavity

$$\frac{\tau_0}{\tau} = F_P \frac{|\mathbf{E}(\mathbf{r})|^2}{|\mathbf{E}_{\mathrm{max}}|^2} \frac{\Delta\lambda_c^2}{4(\lambda_e - \lambda_c)^2 + \Delta\lambda_c^2} \cos^2\vartheta + \frac{\tau_0}{\tau_{\mathrm{leaky}}} \ . \tag{2.37}$$

This alteration of the spontaneous emission time is called the Purcell effect. Equation (2.37) is the result of an adapted calculation for atomic systems (J.-M. Gérard in Ref. [93]). Here τ_0 is the decay time in a spatially homogeneous, or unstructured medium. It is determined by the Wigner-Weißkopf rate of spontaneous emission [92]. The second term on the right hand side models the emission into leaky modes. The first term describes the QD emission at a wavelength λ_e into a cavity mode at wavelength λ_c. An emitter at location $\mathbf{r}$ is subject to the electric field $\mathbf{E}(\mathbf{r})$ whose amplitude varies between the maximum value $|\mathbf{E}_{max}|$ in a field antinode and zero for a node position. ϑ denotes the angle between the electric field vector and the dipole moment of the electronic transition. The Purcell factor F_P gives the enhancement or suppression of the emission decay rate in the resonator in comparison to that of the homogeneous medium,

$$F_P = \frac{3\lambda_e^3}{4\pi^2 n^3} \frac{d\,Q}{V}. \tag{2.38}$$

Here, Q is the quality factor of the resonator, V is the effective mode volume of the cavity with refractive index n, and d is the mode degeneracy. From Eq. (2.37) it can be seen that the Purcell effect is largest when the emitter is placed in the field maximum and the dipole orientation coincides with the electromagnetic field vector. While the dipole orientation is random in self-organized QDs, the cavity is typically designed to have as many emitters as possible in the field maximum. To give a better idea of how this is realized in the heterostructure design, the result of a mode calculation for a VCSEL- (vertical cavity surface emitting laser) structure is shown next to a typical SEM image of such a device in Figure 2.10. The field maximum coincides with the position of the spacer where the emitters are placed. The calculation is based on a Green's-function approach and was performed by Dr. Jan Wiersig, Universität Bremen.
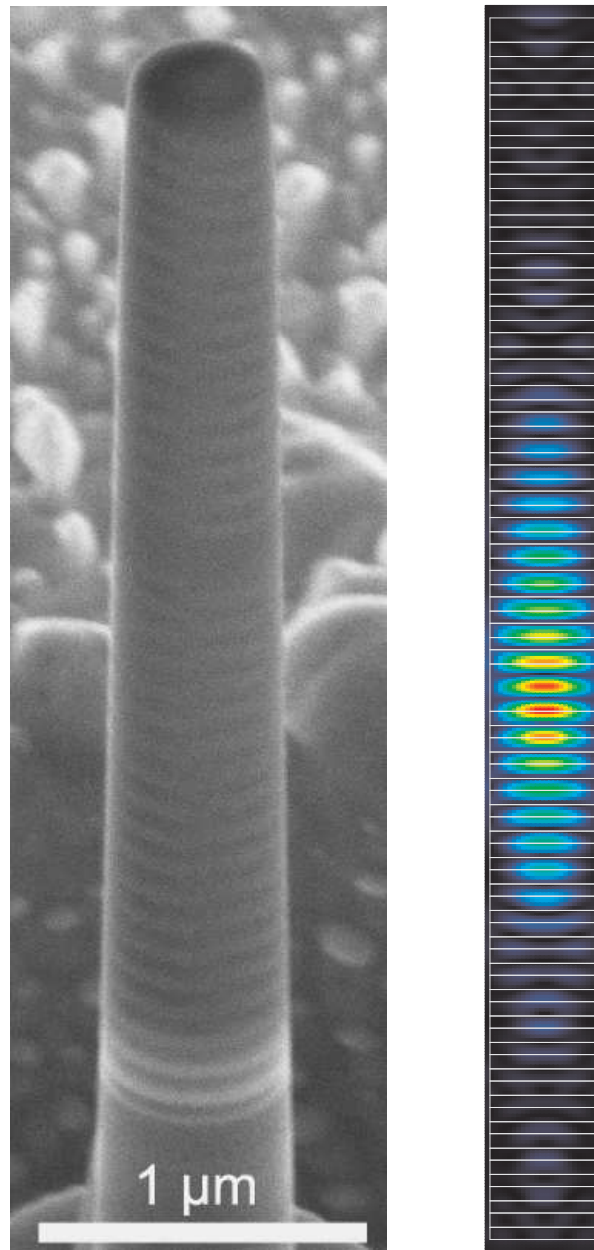
Figure 2.10.: Left: SEM image of a typical VCSEL structure with embedded II/VI QDs. The pillars have been processed by focussed ion beam lithography, the diameter is $0.5\,\mu$m. Courtesy of H. Lohmeyer, Univ. Bremen [84, 85]. Right: Strength of the electromagnetic field for the fundamental mode in a VCSEL-structure, courtesy of Dr. Jan Wiersig, Univ. Bremen. The position of the cavity coincides with the field maximum.

While the Purcell effect is of importance for the enhancement of spontaneous emission in microcavity laser devices and will be discussed in this context in the next chapter, we now focus on its visualization in time-resolved PL.

2.7.1. SLE for Open-Cavity Systems

In Section 2.3.1 we have derived the SLE for a system of QDs coupled to a continuum of photonic modes. With this we have modeled the emission into free space. Introducing a cavity has the consequence that photons emitted into a long-lived cavity mode remain in the vicinity of the QDs. This results in stimulated emission or absorption processes (cavity feedback) until the photons have left the cavity. In the derivation of the SLE these processes originate from the operator averages $\langle b^\dagger b c_\nu^\dagger c_\nu \rangle - \langle b^\dagger b v_\nu^\dagger v_\nu \rangle$. While we discuss the triplet-level correlations $\delta \langle b^\dagger b c_\nu^\dagger c_\nu \rangle$ and $\delta \langle b^\dagger b v_\nu^\dagger v_\nu \rangle$ in Section 3.2.2, the singlet-doublet factorization provides the cavity feedback term, which appears as the second term on the right hand side of the cavity-contribution to the photon-assisted polarization (2.18):

$$i\hbar \frac{\mathrm{d}}{\mathrm{d}t} \langle b_\xi^\dagger v_\nu^\dagger c_\nu \rangle \Big|_{\mathrm{cavity}} = -i\kappa_\xi \langle b_\xi^\dagger v_\nu^\dagger c_\nu \rangle - (1 - f_\nu^e - f_\nu^h) g_\xi \langle b_\xi^\dagger b_\xi \rangle \ . \qquad (2.39)$$

Depending on the sign of the population inversion in the bracket, this term provides stimulated emission (negative sign) or absorption (positive sign). Its particular form with $\langle b_\xi^\dagger b_\xi \rangle$ diagonal in the mode indices relies on the assumption of a discrete mode spectrum with well-separated peaks. In this case, coupling between different modes ξ cannot take place. A description of the system with a continuous mode spectrum with well-separated peaks can be shown to reproduce the results obtained without mode coupling if integrated quantities are considered. The cavity damping can be introduced via a complex frequency $\omega_\xi \to \omega_\xi - i\kappa_\xi/\hbar$. As a consequence, every time derivative of photon operators yields a damping term $\propto \kappa_\xi$, from which the first term in Eq. (2.39) arises. The dynamic equation for the photon number $\langle b_\xi^\dagger b_\xi \rangle$ is damped with a factor of $2\kappa_\xi$, which must be added to the time derivative on the left hand side of Eq. (2.17). With it the loss of photons from the cavity mode ξ after the lifetime τ_{cav}^ξ

$$\begin{aligned} \tau_{\mathrm{cav}}^\xi &= \frac{\hbar}{2\kappa_\xi} \\ &= \frac{Q_\xi}{\omega_\xi} \end{aligned} \qquad (2.40)$$

is introduced, where Q_ξ is the quality factor of the mode ξ.
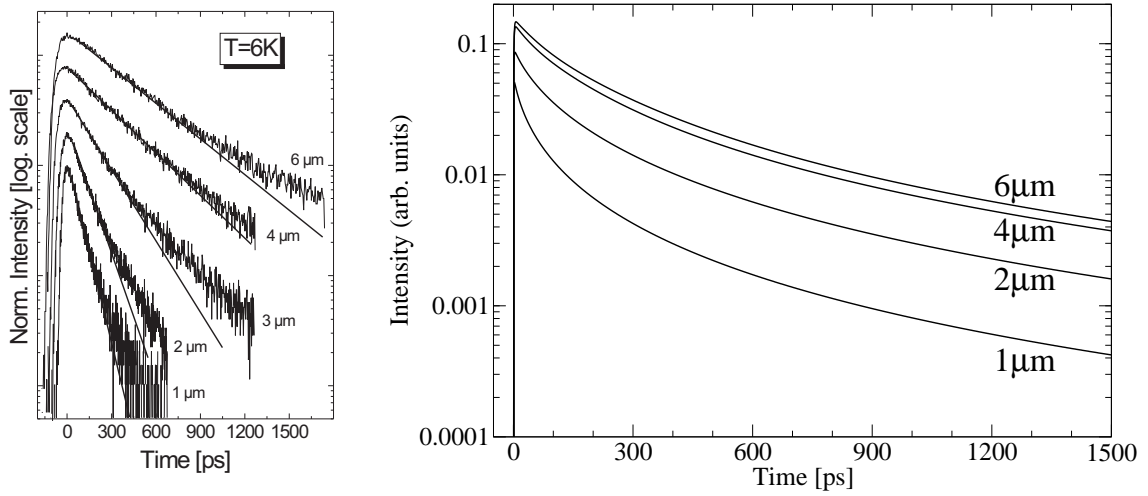
Figure 2.11.: Low excitation time-resolved PL emission for micropillars with different diameters. For clarity, the traces have been shifted vertically relative to each other. **Left: Experiment.** The excitation power density is 1.3 kW/cm². The decay times corresponding to the single exponential fits shown by the solid lines are: 400 ps (6μm), 315 ps (4μm), 200 ps (3μm), 110 ps (2μm), and 80 ps (1μm). **Right: Calculation.** Calculated photoluminescence of QDs in pillar microcavities with various diameters for an initial carrier density of $2 \cdot 10^9 \, \text{cm}^{-2}$.

2.7.2. Comparison with Experiments – Time-resolved PL of QDs in Microcavities

Figure 2.11 shows the decay of the time-resolved PL for detection at the energy of the respective fundamental optical mode of micropillars with different diameters, together with results from our microscopic theory for an ensemble of QDs. Experimental details are found in Ref. [124]. The intensity is plotted on a logarithmic scale. The excitation wavelength was set to 800 nm, corresponding to a creation of carriers in the GaAs barriers. This wavelength is also above the stop-band of the planar resonator. The low excitation power of 1.3 kW/cm² guarantees that the observed PL occurs in the spontaneous emission regime, where the Purcell effect is not masked by the cavity feedback.

The observed faster decay for decreasing pillar diameter is a consequence of the confinement-induced enhancement of the vacuum field amplitude that results in the Purcell effect. The reduction of the mode volume leads to an increase of the Purcell factor $F_P \propto Q/V$ according to Eq. (2.38), because for the discussed range of diameters the mode volume decreases faster than the Q-factors. For the decay of the signal over the first order of magnitude, the deviation from an exponential decay is rather weak. Straight lines indicating an exponential decay behavior have been added to
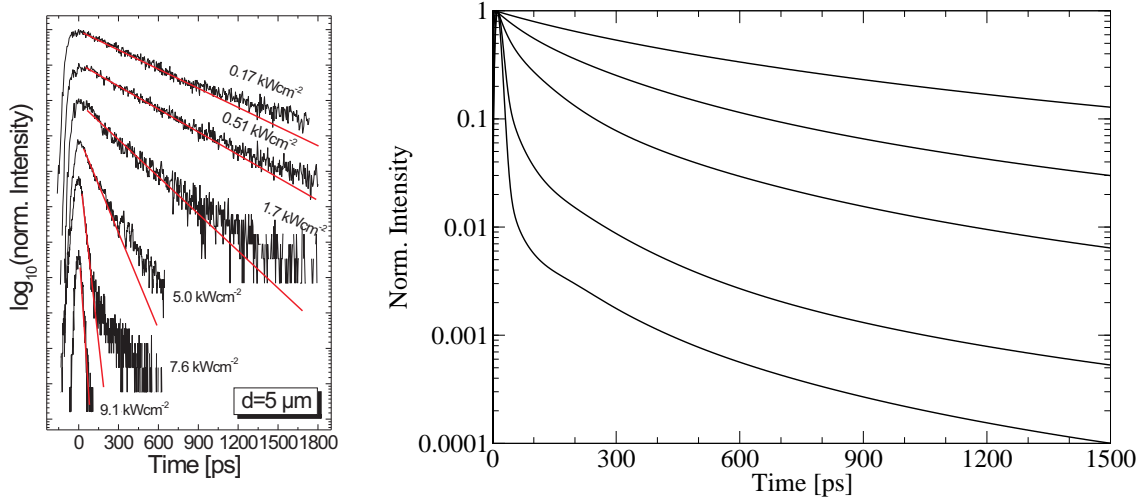
Figure 2.12.: PL decay of QDs in a $5\,\mu$m cavity at different excitation powers. **Left: Experiment.** The decay times corresponding to single exponential fits (shown by the solid lines) are: 550 ps (0.17 kW/cm^2), 475 ps (0.51 kW/cm^2), 265 ps (1.7 kW/cm^2), 120 ps (5.0 kW/cm^2), 30 ps (7.6 kW/cm^2), and 20 ps (9.1 kW/cm^2). $T = 6$ K. For clarity, the traces have been shifted vertically relative to each other. **Right: Calculation.** Calculated photoluminescence for an ensemble of QDs in a 6 μm diameter pillar microcavity with initial carrier densities from $1 \cdot 10^9$ cm^{-2} to $5 \cdot 10^9$ cm^{-2} in equidistant steps from top to bottom. For better comparison the results are normalized.

fit a T_1-time[6] to the initial decay. However, on a larger scale the decay data clearly reveals a non-exponential character.

The experimental results can be compared to our calculation in the right panel of Figure 2.11. With respect to the shape and the speed of the decay, we obtain good agreement with the measurements. The different heights of the curves can mainly be attributed to the fact that in larger pillars more carriers take part in the recombination dynamics. The differences between the measured and the calculated results close to $t = 0$, and in particular the slower rise of the PL signal observed in the experiment, can be attributed to the finite time resolution of the experimental setup, in addition to the fact that the optical carrier generation followed by relaxation processes was not modeled in our calculation.

To obtain more insight into the emission dynamics, a single micropillar was studied under varying excitation power. The left panel of Figure 2.12 shows the time-resolved

---

[6]Longitudinal relaxation time, here corresponding to the exponential decay of the population. The term originates from the phenomena of nuclear magnetic resonance (NMR). The T_2-time, on the other hand, describes the damping of a coherent polarization due to dephasing processes.

emission of a 5 μm pillar for different excitation powers, ranging from extremely low (measurement limit) to above the transition where stimulated emission sets in. This is visible in the extremely fast decay at the highest excitation power density. As the excitation power is decreased, the decay becomes slower and slower, but does not saturate. Even for the lowest excitation power, for which a time-resolved signal could be recorded, no saturated, power-independent decay is found. The same behavior in observed in our calculation (right panel): The rapidness of the decay strongly depends on the initial carrier density, which in the experiment is dependent on the strength of the optical pump pulse. In addition the non-exponential shape of the signal is clearly evident.

What we have observed in unstructured QD samples has been shown to persist in the presence of a cavity. These experiments are another example where QDs behave differently to what we expect from atomic systems. Again, no exponential decay is found, and the decay rate depends on the carrier density in the system, which we identified as an intrinsic semiconductor effect. This shows that it is not meaningful to introduce a decay time that depends only on the photonic density of states without including the influence of the carrier system. Moreover, it is an indication that also in other cases the description of QDs by means of atomic models may lead to false results.

2.8. Conclusion

In this chapter we have introduced a semiconductor theory for semiconductor quantum dots interacting with the quantized light field. The hierarchy problem inherent to the many-body problem has been addressed by means of the cluster expansion technique, which is used to characterize operator averages and to truncate the hierarchy.

In connection with the spectrum the influence of the Coulomb interaction and of carrier correlations was discussed. In particular we have learned how a violation of the consistency required by the cluster expansion method can lead to unphysical results.

By studying time-resolved emission without a resonator, we have shown that the decay behavior is strongly influenced by the presence or absence of excitonic correlations. We have discussed two limiting cases of i) uncorrelated carriers (Hartree-Fock approximation), leading to a non-exponential decay, and ii) fully correlated carriers (two-level approximation), resulting in an exponential decay. Our numerical results

reveal that correlations of the excited electrons and holes, treated on the singlet--doublet level, lead to an exponential decay of the photoluminescence, provided that dephasing of the correlations can be neglected, which is not the case in general. We have also demonstrated that a weak dephasing of the correlations leads to a clear departure from the exponential decay of the PL signal. This result provides an intrinsic explanation for experimental observations of non-exponential PL decays, in contrast to extrinsic effects like coupling to dark excitons or inhomogeneous broadening effects— effects often used to explain bi- or multi-exponential decays.

To underline our findings, we have summarized results of collaborations with the experimental group of Prof. Manfred Bayer, where measurements on samples with (micropillar) and without cavity were performed. The theory derived in this chapter clearly agrees very well with the experimental results, confirming both the non-exponentiality and the intensity dependence of the decay of the PL signal. Corresponding to the emission into free space, we have considered the case of n-doped QDs, which can formally be mapped to an atomic system of fully correlated carriers due to the abundance of holes. In agreement with our considerations of the limiting case of fully correlated carriers, we observe a fast exponential decay in these systems. Last but not least, we have studied the luminescence of QDs embedded in pillar microcavities, where the modified environment changes the emission behavior. While the observations of a non-exponential and excitation-intensity dependent decay remain unaltered in the presence of the cavity, we could observe a strong increase of the spontaneous decay rate with decreasing mode volume of the cavities in both experiment and theory, directly visualizing the Purcell-effect. In these experiments, the interplay of semiconductor effects, like the non-exponential decay, and cavity-quantum-electrodynamics, like the Purcell effect, is nicely demonstrated.

3. Laser Theory for Quantum Dots in Microcavities

In recent years, remarkable progress in semiconductor growth and processing techniques has enabled the fabrication of tailored optical microresonators [146]. Amongst the most popular ones are micropillars [105, 113], microdisks [94, 106], and, most recently, photonic crystals [9, 157]. The three-dimensional confinement of light in these structures leads to a discretization of the mode spectrum. The large mode separation due to the small resonator size enables single-mode lasing. Very small mode volumes in combination with a high-quality mode enhance the spontaneous emission (SE) rate into that mode, a phenomenon known as Purcell effect [110]. For device applications, less photons lost into non-lasing modes correspond to a higher efficiency, reflected in a SE coupling factor β close to unity. The SE coupling factor is defined as the ratio of SE into the laser mode divided by the SE into all available modes. With increasing β, the step-like 'threshold' in the output intensity of conventional $\beta \ll 1$ laser devices gradually disappears until the so-called 'thresholdless' laser is reached in the limit $\beta = 1$. This term is of great importance in the literature and the peculiarity of an apparently vanishing threshold has been widely discussed [31, 38, 41, 67, 108, 118]. Even if the input/output curve of a laser device reveals no indication of a threshold, the question of the coherence properties of the emitted light remains. Latest advances in the growth and design of semiconductor-QD microcavity lasers have now attained the regime of β-values close to unity experimentally [31, 104, 134, 138, 144]. For this reason, an understanding of the coherence properties of the emitted light and means to identify the threshold to coherent light emission is of great relevance for the design of microcavity laser devices.

From a device point of view, the gain material is equally important to the cavity design. QDs offer unique qualities as a gain material. Stronger insensibility to temperature variations and expected smaller linewidths are advantages over quantum wells, which are nowadays used as gain medium in many devices [4]. Most important, however, is the discrete density of states caused by the three-dimensional carrier confinement. Consequently, the spectral properties of QDs resemble the atomic case with transition energies that are determined by the choice of material and growth parameters. Thereby a tuning to the cavity resonances is possible.

In the literature, semiconductor-QD-based laser devices are almost without exception modeled by considering atomic two- or multi-level systems, resulting either in a set of rate equations [155, 156], or a master equation for the reduced density matrix [18, 98, 118, 148]. To describe the statistical properties of the emission from the microcavity in terms of the intensity correlation function, the latter approach has been used. Alternatively, for two-level systems the quantum regression theorem can be applied to obtain two-time operator averages from single-time ones [47, 73, 74, 92, 154]. All these quantum-optical models and the underlying approximations are well suited for atomic systems, but have to be reconsidered when applied to semiconductor systems. In QDs excitations can involve more than a single carrier. The resulting description of the interaction with the quantized light field is different when atomic systems with single-electron excitations and QDs with multiple excited carriers are compared, even though the elementary interaction processes remain the same. In addition to the modification of the light-matter interaction itself, it is also well-known from various semiconductor systems that the interaction among the excited carriers leads to effects that can modify or even dominate the emission properties and, hence, should be included in semiconductor models. Pauli-blocking of states, the Coulomb interaction of excited carriers [11, 149], their interaction with phonons, and a variety of resulting effects like energy renormalizations, contributions of new quasi-particles, or interaction-induced dephasing have been intensively studied also in QD systems. In atomic systems, interaction-induced effects are typically of minor importance and the single-particle excitations are subject to scattering and dephasing that is usually described via constant rates. Some of these effects were discussed in the previous chapter, among them the non-exponential decay of the luminescence with a carrier-density dependent decay rate, cf. Section 2.5. Also, unlike conventional four-level gas lasers, QD-based microcavity lasers usually do not operate at full inversion, resulting in considerable differences in the input/output curves. The same applies to the effects of Pauli blocking. Especially for excitation with short laser pulses, the output characteristics and the jump from below to above threshold becomes severely modified. If characteristic values, such as the β-factor, are derived from measured data, one must be aware of the differences between atomic and semiconductor laser models. Therefore, a semiconductor approach is highly desirable if QD-based laser devices are studied. A general semiconductor laser model based on a microscopic Hamiltonian has previously been used to study the influence of the carrier dynamics and many-body effects [32, 66], lasing without inversion [109], and noise spectra [142]. The effect of carrier scattering on relaxation oscillations has been studied by combining rate equations including a non-linear spontaneous emission term with a microscopic treatment of Coulomb interaction [88]. However, these approaches do not include correlations required to determine the photon second-order correlation function.

As is known from quantum optical and cavity-quantum-electrodynamical (CQED) approaches to the description of lasing in microresonators [118], an interpretation of the lasing onset and the nature of the emitted light more accurate than the input/output characteristics is given by a statistical analysis of the photon emission. The statistical properties of the light emission can be described in terms of the photon autocorrelation function at zero delay time

$$g^{(2)}(\tau = 0) = \frac{\langle n^2 \rangle - \langle n \rangle}{\langle n \rangle^2} \ , \tag{3.1}$$

where $n = b^\dagger b$ is the photon number operator for the laser mode. The development of a semiconductor laser theory and the calculation of $g^{(2)}(\tau = 0)$ for QD-based microcavity lasers is the topic of this chapter.

Based on the semiconductor luminescence equations introduced in the previous chapter, we now formulate a laser model to calculate both the light output and the photon autocorrelation function of microcavity lasers with QDs as the active material. This approach naturally includes the modified source term of spontaneous emission, Pauli-blocking, as well as many-body Coulomb effects. Most importantly, it possesses the capability to include the full spectrum of semiconductor effects in a consistent and straightforward way. Depending on which processes are deemed relevant in the considered regime, effects like inhomogeneous broadening or carrier scattering and dephasing due to interaction with phonons can be explicitly considered, either on a microscopic level or using appropriate approximations.

The laser model derived in this chapter can be stripped of all semiconductor effects to obtain the limiting case of atomic two-level systems with a single electron. Results obtained in this limit can directly be compared to results from quantum-optical models. In particular, the truncation scheme based on the cluster expansion method can be verified by comparing with master equation models that can be solved without the factorization of the electronic and photonic degrees of freedom. This is the topic of Chapter 5.

Also related to the description of lasing is the first-order coherence. Interference measurements can be used to obtain the coherence time of the emitted light. To numerically obtain the first-order coherence properties, an extension of our theory for the calculation of two-time operator averages is presented in Chapter 4.

This chapter is structured as follows. Preliminary to the derivation of the dynamic laser equations in Section 3.2, we give an introductory overview over microcavity laser systems and the classification of coherence properties. For the Hamiltonian, the equation-of-motion technique and the truncation and classification of operator
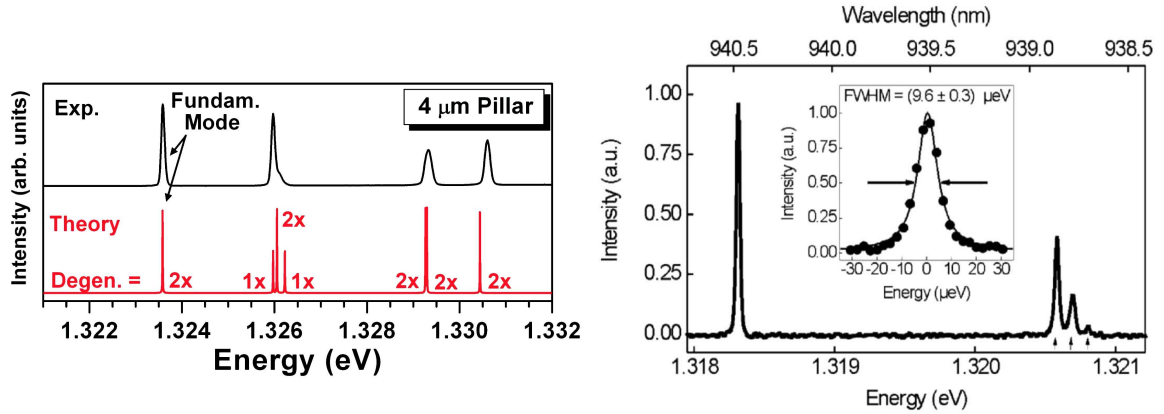
Figure 3.1.: For illustration purposes, we show the low-temperature PL spectra of two high-Q $4\,\mu$m micropillars, manufactured in the group of A. Forchel at the Universität Würzburg. The fundamental mode lies at the lowest energy, the Q-factor is determined by its width. **Left:** Measured spectrum above a calculation [144]. The Q-factor for the fundamental mode is $12\,300 \pm 500$, a typical value for microcavities currently used for laser devices. **Right:** Spectrum of a similar pillar of a newer generation from the same group [116]. Inset: high resolution spectrum showing the fundamental mode with a resolution limited linewidth of $9.6\,\mu$eV, corresponding to a ten-times larger Q-factor of $165\,000 \pm 8\,000$ compared to the pillar from the left panel.

averages by means of the cluster-expansion method, we refer to Sections 2.1–2.3. In Section 3.2.2 special emphasis is placed on the role of correlations beyond the doublet level that are required in order to calculate the second-order correlation function, for which analytical limits are discussed. Numerical results for both the input/output characteristics and the second-order coherence properties are presented in Section 3.3. A detailed comparison with experimental results of lasing in QD-micropillar structures is the topic of Section 3.4. Finally, the influence of pulsed and continuous wave excitation on the output characteristics in atomic and semiconductor lasers is studied in Section 3.5.

3.1. Preliminary Considerations about QD Microcavity Lasers

The laser equations that we now derive can be seen as an extension of the semiconductor luminescence equations (SLE) for microcavity systems, cf. Section 2.7.1. To accommodate the typical components of a laser model, several modifications and simplifications are introduced in the advance of the following section. To retain an overview, we introduce the considered system and describe the relevant physical processes that are accounted for in the laser model.

Coupled QD-cavity system.   When describing lasing from an ensemble of QDs in a microresonator, typically the resonator provides at least one (possibly degenerate) long-lived mode. In micropillars and photonic crystal cavities this is usually the so--called fundamental mode energetically lowest in the spectrum. In microdisks the long-lived modes are the higher-excited whispering gallery modes. The width of the resonance reflects the lifetime of the fundamental mode. In state-of-the-art semi-conductor microcavities, quality (Q-) factors (cf. Section 2.7) between 10^4–10^5 are achieved, resulting in very narrow linewidths $< 100\,\mu\text{eV}$ and long cavity lifetimes in the order of picoseconds. Too long cavity lifetimes, however, may reduce the output coupling required in a laser device beyond functionality. As an illustration, two typ-ical mode spectra of pillar microcavities are displayed in Figure 3.1. Cavities with Q-factors of the order of 10^4 (left panel) are typically used in the context of lasing. In the right panel the mode spectrum of a state-of-the-art micropillar with a Q-factor of the order of 10^5 is shown in comparison. Such cavities play a role for the generation of non-classical light, as well as quantum information technology, strong coupling and other fundamental studies.

When using QDs as the active material in microcavities, the coupling strength is determined by the spectral and spatial positions of the dots, cf. Eq. (2.8). The QDs off-resonance or only partly in resonance contribute less to the laser transition than those QDs, where the s-shell transition is resonant with the cavity mode and the placement coincides with the maximum of the electromagnetic field in the cavity [124]. The number of strongly coupling QDs can be estimated from the dot area density and the overlap of the cavity resonance with the inhomogeneously broadened ensemble of QDs. Each QD also possesses a natural linewidth that depends on many factors, like the temperature, the carrier density in the system, the material system and the depth of the confinement potential. However, with a typical value of $10\,\mu\text{eV}$ at $4\,\text{K}$ for the systems we consider in collaborations with experimentalists, this effect is much smaller than the inhomogeneous broadening (some meV). For micropillar cavities with diameters of a few microns, only a small number of tens of QDs can be considered to be in perfect resonance with the cavity mode.

Besides the laser mode other non-lasing modes exist. Due to the small size of the res-onator, the modes are well separated from each other so that the QD ensemble can be considered to couple mainly to one single mode. Still, a continuum of leaky modes pro-vides dissipation channels via spontaneous emission into these modes. These modes, as well as the more weakly-coupled cavity modes, provide the non-lasing modes. In our theoretical treatment, the dynamics of the non-lasing modes is eliminated adia-batically in order to introduce the β-factor that determines the fraction of the total

spontaneous emission (SE) directed into the laser mode:

$$\beta = \frac{\text{SE rate into laser mode}}{\text{total SE rate}} \ .$$

The effect of the non-lasing modes is that a fraction $1 - \beta$ of the total spontaneous emission is lost for the laser mode. In the regime where spontaneous emission dominates, i.e. below the laser threshold, the output-power is reduced by a factor of $1/\beta$, visible as a jump in the input/output curve. Note, however, that this is true only in atomic systems operating at full inversion, like conventional four-level gas lasers. For semiconductor lasers we find deviations from this well-established behavior. Above the intermediate threshold region, stimulated emission into the laser mode dominates, so that losses into non-lasing modes are irrelevant. As an illustration we refer the reader to Figure 5.2 on page 96 or to the literature [21, 118, 155], where input/output curves are displayed for an atomic system for various values of the β-factor.
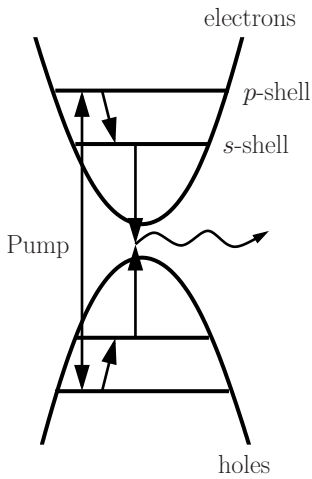
Figure 3.2.: QD laser model with carrier generation in the p-shells and the laser transition between the s-shells of electrons and holes.

So far we have considered intrinsic aspects of the coupled QD-cavity system. It remains to include a pump mechanism. Cavity losses were already discussed in Section 2.7.1, where they were introduced via a complex mode frequency. The pump process can be modeled in several ways. The most thorough treatment would include carrier generation in the barrier, the wetting layer, or in higher confined QD states by an optical pulse, followed by capture and relaxation processes described by the Coulomb and carrier-phonon interaction. It has been shown that both mechanisms lead to an efficient carrier scattering at low [127] and elevated temperatures [100, 128]. In such a consistent treatment, the scattering processes cause dephasing of polarizations and correlation functions at the same time. However, such an elaborate inclusion of the excitation and relaxation processes is beyond the scope of this work. Primarily we are interested in the development of a semiconductor laser model to learn about the influence of the semiconductor effects discussed in Chapter 2 and to study second-order coherence. Concentrating on these goals, we focus on the carrier dynamics in the QD s-shells that resonantly couple to the laser mode. Optical pumping in the p-shell is accounted for by a carrier generation rate and blocking factors. Relaxation into the s-shell is treated in a relaxation-time approximation. This simplified system is schematically shown in Figure 3.2.

Degrees of Second-Order Coherence. Following Glauber, the quantum states of light can be characterized in terms of photon correlation functions [54]. The coherence
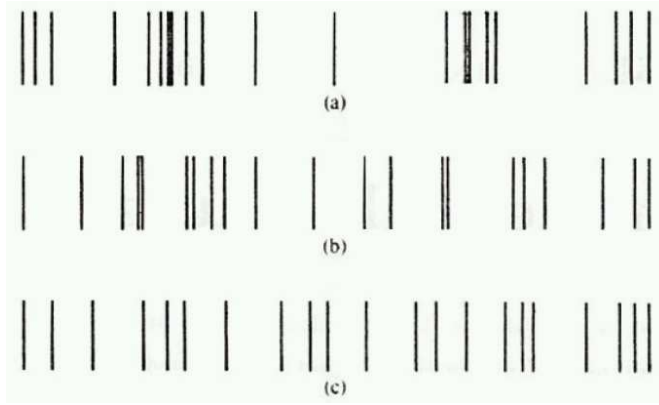
Figure 3.3.: Schematic description of thermal (a), coherent (b), and sub-poissonian (c) light emission. Each line represents a photon emission, the time progresses along the horizontal direction. The behavior of bunching (a) and antibunching (c) is reflected in a value of $g^{(2)}(0) = 2$ or 0, respectively. The trace of coherent light is $g^{(2)}(0) = 1$. The figure is taken from Ref. [87].

properties of the emitted light are reflected to a large degree in the photon statistics that is obtained from the second-order correlation function at zero-delay time $g^{(2)}(0)$. This function reflects the possibility of the correlated emission of two photons at the same time. As a visualization, one may consider three different cases of light emission from a thermal (a), a coherent (b), and a sub-Poissonian[1] (c) light source, depicted in Figure 3.3. In thermal light photons come in lumps so that there is an enhanced probability that two photons are emitted at the same time (bunching), reflected in a value of $g^{(2)}(0) = 2$. Antibunching is a characteristics of the single-photon emitter in (c), where a single emission is followed by a dark re-excitation time, so that two photons are never emitted simultaneously and $g^{(2)}(0) = 0$. In a laser (b), coherent light emission is statistically random, reflected in $g^{(2)}(0) = 1$.

The origin of the zero-delay $g^{(2)}(0)$ values of 2, 1 and 0 for thermal, coherent and sub-poissonian light can be understood by considering the respective states of the light field. For details we refer to Ref. [87]. From a theoretical point of view the description in the Fock basis is most convenient. For small photon numbers it is experimentally possible to prepare pure Fock or number states, which are the eigenstates of the number operator $\hat{n}$ as well as of the energy operator, i.e. for a number state $|n\rangle$

$$\hat{n}|n\rangle = b^{\dagger}b|n\rangle = n|n\rangle \ . \tag{3.2}$$

---

[1] In coherent light the photon number probability distribution is Poissonian, and the variance $(\Delta n)^2 = \langle n^2 \rangle + \langle n \rangle$ reduces to the mean photon number: $(\Delta n)^2 = \langle n \rangle$, and thus $\langle n^2 \rangle = 0$. Therefore, emitters with $\langle n^2 \rangle < 0$ ($\langle n^2 \rangle > 0$) are referred to as sub-Poissonian (super-Poissonian) light sources [87].

Thus, for arbitrary moments of the number operator one obtains

$$\langle \hat{n}^k \rangle = n^k \ . \tag{3.3}$$

From Eq. (3.1), which we reprint here for convenience,

$$g^{(2)}(\tau = 0) = \frac{\langle n^2 \rangle - \langle n \rangle}{\langle n \rangle^2}$$

it follows for the degree of second-order coherence

$$g^{(2)}(\tau = 0) = 1 - \frac{1}{n} \ , \tag{3.4}$$

which yields the signature $g^{(2)}(0) = 0$ of the single-photon emitter in the case $n = 1$. If the system can be described in terms of a mixture of coherent states all with the same absolute value, its probability distribution is Poissonian, i.e.

$$P_{\mathrm{coh}}(n) = \frac{\langle n \rangle^n}{n!} \, e^{-\langle n \rangle} \tag{3.5}$$

while, at the same time, the averages $\langle b \rangle = \langle b^\dagger \rangle = 0$ are preserved, cf. §11.8.6(d) in Ref. [89]. The factorial moments of a Poisson distribution are given by

$$\langle n(n-1) \ldots (n-k+1) \rangle = \langle n \rangle^k \ , \tag{3.6}$$

so that $g^{(2)}(0) = 1$ follows from Eq. (3.1). This result is even more easily obtained if one uses the property that coherent states are the eigenstates of the creation and annihilation operators. Rewriting Eq. (3.1) in terms of photon operators for photons in the laser mode

$$g^{(2)}(\tau = 0) = \frac{\langle b^\dagger b^\dagger b b \rangle}{\langle b^\dagger b \rangle^2} \ , \tag{3.7}$$

the application of the operators on a coherent state merely yield numbers and both the nominator and the denominator are equal. For the case of thermal light, the system cannot be expressed in terms of a pure state but is determined by a density matrix in the basis of the energy eigenstates, which are the Fock states. The probability distribution for the photon number is given by the Plank distribution

$$P_{\mathrm{th}}(n) = \frac{\langle n \rangle^n}{\left(1 + \langle n \rangle \right)^{n+1}} \tag{3.8}$$

with the factorial moments

$$\langle n(n-1) \ldots (n-k+1) \rangle = k! \langle n \rangle^k \ . \tag{3.9}$$

From Eqs. (3.1) and (3.9) follows the degree of second-order coherence $g^{(2)}(0) = 2$ for thermal light.

Calculation of Second-Order Coherence in the Semiconductor Formalism. In order to calculate the photon statistics numerically, the hierarchy of coupled equations must be extended to quadruplet-level photon correlations (the concept of correlation functions is described in Section 2.2). Expressing Eq. (3.7) according to Eq. (2.12d) in terms of correlation functions, $\delta\langle b^\dagger b^\dagger bb\rangle = \langle b^\dagger b^\dagger bb\rangle - 2\langle b^\dagger b\rangle^2$,[†] the autocorrelation function can be written in terms of the quadruplet correlation function $\delta\langle b^\dagger b^\dagger bb\rangle$:

$$g^{(2)}(\tau = 0) = 2 + \frac{\delta\langle b^\dagger b^\dagger bb\rangle}{\langle b^\dagger b\rangle^2} \ . \tag{3.10}$$

For consistency, in all equations of motion operator averages must be taken up to the four-particle level.

In the following we proceed with the derivation of the semiconductor laser equations. We do not consider the most general case, but restrict ourselves to the systems and goals discussed above. In doing so, a consistent framework is provided that can be adapted and extended if required, e.g., for the description of superradiance, normal mode coupling, or lasing at room temperature.

3.2. Dynamic Laser Equations

We use the Hamiltonian and the notation introduced in Section 2.1. Operator averages are obtained by means of the equation of motion technique described in Section 2.3. To underline the analogy to the semiconductor luminescence equations, we keep the equations in a general form. The specifications of the QD model described in the previous section are then included in a second step. Again we use the fact that polarization-like averages of the form $\langle v_\nu^\dagger c_\nu\rangle$ vanish due to the incoherent carrier generation, and so does the expectation value of the photon operators, $\langle b_\xi\rangle = 0$. For the dynamical evolution of the photon number $\langle b_\xi^\dagger b_\xi\rangle$ in the mode ξ and the carrier populations $f_\nu^e = \langle c_\nu^\dagger c_\nu\rangle$, $f_\nu^h = 1 - \langle v_\nu^\dagger v_\nu\rangle$, the contribution of the light matter interaction H_D in the Heisenberg equations of motion leads to

$$\left(\hbar\frac{\mathrm{d}}{\mathrm{d}t} + 2\kappa_\xi\right)\langle b_\xi^\dagger b_\xi\rangle = 2\,\mathrm{Re}\sum_{\nu'}|g_\xi|^2\,\langle b_\xi^\dagger v_{\nu'}^\dagger c_{\nu'}\rangle\ , \tag{3.11}$$

$$\hbar\frac{\mathrm{d}}{\mathrm{d}t}\,f_\nu^{e,h}\bigg|_\mathrm{opt} = -2\,\mathrm{Re}\sum_\xi|g_\xi|^2\,\langle b_\xi^\dagger v_\nu^\dagger c_\nu\rangle\ . \tag{3.12}$$

[†]The factor of two arises from the two realizations for this factorization. Since $\langle b\rangle = \langle b^\dagger\rangle = 0$ for a system without coherent excitation, cf. Section 2.3.1, only a factorization into doublets is possible.

Note that we have scaled $\langle b_\xi^\dagger v_\nu^\dagger c_\nu \rangle \rightarrow g_\xi \langle b_\xi^\dagger v_\nu^\dagger c_\nu \rangle$ with the light-matter coupling strength to have its modulus appear in the above equations.[2] In Eq. (3.11) we have introduced the loss rate $2\kappa_\xi/\hbar$. The mode index ξ labels cavity modes as well as leaky modes. For the laser mode, the loss rate is directly connected to the Q-factor of the laser mode ξ_l, $Q = \hbar\omega_{\xi_l}/2\kappa_{\xi_l}$. The dynamics of the photon number in a given mode is determined by the photon-assisted polarization $\langle b_\xi^\dagger v_\nu^\dagger c_\nu \rangle$ that describes the expectation value for a correlated event, where a photon in the mode ξ is created in connection with the transition of an electron from the conduction to the valence band. The sum over ν involves all possible interband transitions from various QDs, i.e., $\nu = \{\mu, \mathbf{R}\}$ with μ being the shell index and $\mathbf{R}$ the QD position. Similarly, the dynamics of the carrier population in Eq. (3.12) is governed by photon-assisted polarizations from all possible modes (both lasing and non-lasing modes).

The equation of motion for the photon-assisted polarization is derived in analogy to the previous chapter and now contains additional contributions beyond the doublet level:

$$
\left(\hbar\frac{\mathrm{d}}{\mathrm{d}t} + \kappa_\xi + \Gamma + i\left(\tilde{\varepsilon}_\nu^e + \tilde{\varepsilon}_\nu^h - \hbar\omega_\xi \right) \right) \langle b_\xi^\dagger v_\nu^\dagger c_\nu \rangle =
$$
$$
f_\nu^e f_\nu^h - \left(1 - f_\nu^e - f_\nu^h \right) \langle b_\xi^\dagger b_\xi \rangle
$$
$$
+ i\left(1 - f_\nu^e - f_\nu^h \right) \sum_\alpha V_{\nu\alpha\nu\alpha} \langle b_\xi^\dagger v_\alpha^\dagger c_\alpha \rangle + \sum_\alpha C_{\alpha\nu\nu\alpha}^{\mathrm{x}}
$$
$$
+ \delta\langle b_\xi^\dagger b_\xi c_\nu^\dagger c_\nu \rangle - \delta\langle b_\xi^\dagger b_\xi v_\nu^\dagger v_\nu \rangle \; . \quad (3.13)
$$

The evolution of $\langle b_\xi^\dagger v_\nu^\dagger c_\nu \rangle$ is determined by the detuning of the QD transitions from the optical modes. Hartree-Fock (singlet) contributions of the Coulomb interaction with the Coulomb matrix element $V_{\nu\alpha\nu\alpha}$ lead to the appearance of renormalized energies $\tilde{\varepsilon}_\nu^{e,h}$ and to the interband exchange contribution that couples the photon-assisted polarizations from different states α. The source term of spontaneous emission is described by an expectation value of four carrier operators $\langle c_\alpha^\dagger v_\alpha v_\nu^\dagger c_\nu \rangle$, see Section 2.5.1. For uncorrelated carriers, the Hartree-Fock factorization of this source term leads to $f_\nu^e f_\nu^h$, which appears as the first term on the right hand side of Eq. (3.13). Correlations remaining after the factorization are provided by the Coulomb and light-matter interaction and are included in $C_{\alpha'\nu\nu'\alpha}^{\mathrm{x}} = \delta\langle c_\alpha^\dagger v_\nu^\dagger c_{\nu'} v_\alpha \rangle$.

The stimulated emission/absorption term in the second line appears as the singlet--doublet factorization of the initial operator averages $\langle b_\xi^\dagger b_\xi c_\nu^\dagger c_\nu \rangle - \langle b_\xi^\dagger b_\xi v_\nu^\dagger v_\nu \rangle$. It is proportional to the photon number $\langle b_\xi^\dagger b_\xi \rangle$ in the mode ξ, thus providing feedback due

---

[2] The notation is to understood as follows: A new quantity $\widetilde{\langle b_\xi^\dagger v_\nu^\dagger c_\nu \rangle} = \langle b_\xi^\dagger v_\nu^\dagger c_\nu \rangle / g_\xi$ is used and the tilde is dropped in the following.

to the photon population in the cavity. The correlations left after the factorization are given by the last two terms in Eq. (3.13). These are triplet-level carrier-photon correlations that were omitted in the treatment on the doublet level in the previous chapter. Higher-order correlations beyond the doublet level are discussed in Section 3.2.2.

In Eq. (3.13) there are two terms acting as a dephasing: Photon dissipation κ_ξ and carrier-carrier and carrier-phonon interaction-induced dephasing. For the latter a microscopic evaluation of these effects has been used in [62] for the case of quantum wells. Here the dephasing is included via a phenomenological damping constant Γ in connection with transition amplitudes $\propto v_\nu^\dagger c_\nu$. For a discussion we refer to Sections 2.3.1 and 5.3.5.

3.2.1. Laser equations

Following the path outlined in Section 3.1 we now formulate the laser equations for a coupled QD-microcavity system. We consider QDs with two localized shells for electrons and holes. The dots are embedded in a microcavity that provides one (potentially degenerate) mode with a large Q-factor that is in resonance with the QD s-shell emission. Higher cavity modes are assumed to be energetically well separated from this mode, and a continuum of leaky modes and other cavity modes constitute the background of non-lasing modes.

In the following scheme, several assumptions are made, which are justified by corresponding experimental conditions. While they provide a convenient formulation of the theory, these assumptions are no principle limitations and can be circumvented at the cost of a more complicated analytical and numerical formulation.

   i. We assume that optical processes involving the laser mode (stimulated and spontaneous emission as well as photon reabsorption) are exclusively connected to the s-shell transition. In this case, higher shells and WL states contribute only to the carrier dynamics.

   ii. In accordance with i) we neclect correlations between p-shell carriers and photons in the laser mode mediated by the light-matter interaction. These correlations are off-resonant, but can nevertheless become significant in the case that only one QD emitter couples to a single cavity mode. In the case of few QDs in an ensemble, the associated processes are less influential. For a discussion we refer to Section 5.3.5.

iii. Ultrafast carrier-scattering processes in QDs have been predicted in recent studies of carrier-carrier [100] and carrier-phonon [127, 128] interaction. Based on this, we assume that the carrier system is close to equilibrium, so that scattering processes can be described in relaxation-time approximation [100]. We consider systems at about 4 K. At these low temperatures up-scattering into energetically higher levels is negligible.

iv. To include the simplest possible pump process, we consider carrier generation in the p-shell at a given rate P. This can be traced back either to resonant optical pumping in connection with rapid dephasing, or it can be used to model carrier injection into the delocalized WL or bulk states and fast successive carrier capture and relaxation processes towards the s-shell.

v. For the non-lasing modes, stimulated emission and reabsorption of photons can be neglected. This is well justified, as photons spontaneously emitted into non-lasing modes rapidly leave the cavity. Therefore, they can neither provide feedback, nor build up correlations with long-lived photons in the cavity mode. In case of strong dephasing (provided by efficient carrier scattering) it is possible to analytically solve the equation for the corresponding photon-assisted polarization and to introduce a rate of spontaneous emission into the non-lasing modes.

vi. It has been shown in Ref. [124] that the major emission into the selected high-Q cavity mode is due to those QDs on resonance, whereas slightly detuned dots hardly contribute. The calculations in [124] were performed to describe the photoluminescence of an ensemble of QDs in a microcavity. We found the decay of an inhomogeneously broadened QD ensemble to coincide with that of an ensemble of identical QDs in resonance, with the light-matter coupling strength being chosen as the maximum value in the inhomogeneously broadened QD ensemble. This is depicted in Figure 3.4. In our calculations, rather than using a calculated light-matter coupling strength, the radiative lifetime is obtained from experiments and directly enters our theory as a parameter. This way, the influence of the detuned QDs is already included, as the actual light-matter coupling strength is then set by the radiative lifetime. Therefore, we can consider to a good approximation only those emitters in resonance, rather than using an inhomogeneously broadened sample of QDs. For a system of identical dots on resonance with the laser mode, which we assume to be non-degenerate, the occurring energy differences with the laser mode ξ_l, $\tilde{\varepsilon}_s^e + \tilde{\varepsilon}_s^h - \hbar\omega_{\xi_l}$, drop out in the equations of motion. In other situations the effect of inhomogeneous broadening may have to be explicitly considered. This is also argued in Ref. [147] with respect to the theory presented in this Chapter. Their claim, however, is
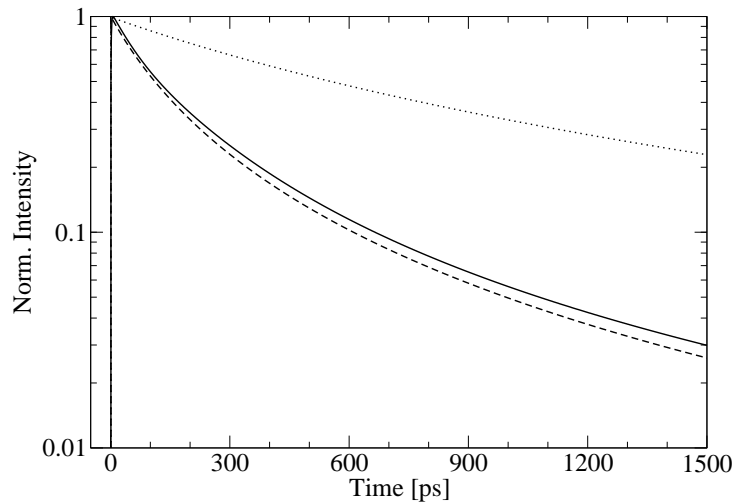
Figure 3.4.: Calculated photoluminescence of an ensemble of QDs with inhomogeneous broadening (solid line), for identical QDs with maximum coupling strength and on-resonance transitions (dashed line), and for identical QDs with averaged coupling strengths (dotted). The pillar diameter is $6\,\mu$m and the initial carrier density if $2 \times 10^9\,\mathrm{cm}^{-2}$. For details, see Ref. [124].

> based on merely two coupled QDs in the regime of strong coupling. We would
> like to emphasize that our argument applies to an ensemble of QDs in the weak
> coupling regime.

In the previous chapter we have derived the fundamental equations for the carrier and photon dynamics, which, on singlet-doublet level, are known as semiconductor luminescence equations. In order to describe a pumped laser system, we must incorporate carrier generation and the β-factor into the theory, as well as we must deal with the correlations appearing in Eq. (3.13). Note that the introduction of β is not strictly necessary, as the dynamics of the non-lasing modes can be explicitly calculated. However, a formulation of the theory in terms of β is convenient both for comparison with experiments and with other laser theories.

Regarding the treatment of many-body Coulomb effects, one can distinguish between two limiting cases. In the high-temperature regime, the WL states can accommodate a substantial carrier density that screens the Coulomb interaction between the QD carriers. At the same time, the Coulomb interaction between QD and WL carriers leads to a broadening and to energy shifts of the QD transitions. Calculations of QD gain spectra in this regime are presented in Ref. [86]. In the following we consider the low-temperature regime that was recently studied in several experiments [8, 124, 144], where the population of the WL states is expected to be marginal. The Hartree-like Coulomb effects between the QD carriers lead to intra- and interband interaction

effects and will be summarized in an effective transition energy and oscillator strength for the coupling to the laser mode.

In the laser regime, a substantial photon population in the long-lived cavity mode supports carrier-photon and photon-photon correlations. On the inclusion of these correlations in the laser equations we concentrate in this chapter. In principle also the explicit inclusion of carrier-carrier correlations (C^{x}) is desirable. However, for the calculations in this chapter, these are not included and left for further research. In the following we discuss to what extent we expect the effect due to carrier correlations to be small. Effects due to carrier correlations are most prominent when stimulated processes are small (well below the threshold), and negligible when stimulated emission dominates (above the threshold). This can be inferred from Eq. (3.13), where carrier correlations $C^{\mathrm{x}}_{\alpha\nu\nu\alpha}$ are directly connected to the Hartree-Fock source term of spontaneous emission $f^e_\nu f^h_\nu$, as both arise from the same initial operator average. In the same way the stimulated emission term $(1 - f^e_\nu - f^h_\nu) \langle b^\dagger_\xi b_\xi \rangle$ and the corresponding correlations $\delta\langle b^\dagger b c^\dagger_\nu c_\nu \rangle$ and $\delta\langle b^\dagger b v^\dagger_\nu v_\nu \rangle$ are connected by their common origin. For large photon numbers the stimulated emission terms can be expected to overpower the terms connected to the spontaneous emission. However, the photon number can only expected to be large well above the threshold. Far below the laser threshold the carrier correlations directly influence the radiative emission dynamics via Eqs. (2.18)–(2.21), as we have discussed in Section 2.5.1. Nevertheless, regarding the stationary photon number we expect significant modifications due to carrier correlations only in the regime where the spontaneous emission rate exceeds the cavity loss rate ("good cavity limit"). These considerations suggest that the influence of carrier correlations on the stationary properties, in particular on the input/output characteristics, is weak. On the other hand, if dynamical properties, like the switch-on behavior, are to be studied, these correlations should be included.

Under the discussed conditions we now derive the equations for the semiconductor laser model. The assumptions elaborated above and in the introductory part of this chapter are chosen to meet current experimental conditions under which microcavity lasing is achieved [7, 31, 114, 124, 138, 144]. In deviating situations, e.g. lasing at room temperature, appropriate modifications are required. It is the greatest strength of our microscopic model and the equation-of-motion technique that the accommodation of modifications is straightforward and follows a well-defined manner.

For the resonant s-shell/laser mode transition, the equation of motion (3.13) for the photon-assisted polarization takes the form

$$\left(\hbar\frac{\mathrm{d}}{\mathrm{d}t} + \kappa + \Gamma\right) \langle b^\dagger v^\dagger_s c_s \rangle = f^e_s f^h_s - (1 - f^e_s - f^h_s) \langle b^\dagger b \rangle + \delta\langle b^\dagger b c^\dagger_s c_s \rangle - \delta\langle b^\dagger b v^\dagger_s v_s \rangle \ , \ (3.14)$$

where, from now on, the index $\xi = \xi_l$ is omitted for the laser mode. In the equation of motion for the photon-assisted polarization of the non-lasing modes, the negligible photon population and the short lifetime of these modes allows for the omission of the feedback term and carrier-photon correlations,

$$\left(\hbar\frac{\mathrm{d}}{\mathrm{d}t} + \kappa_\xi + \Gamma + i\left(\tilde{\varepsilon}_s^e + \tilde{\varepsilon}_s^h - \hbar\omega_\xi\right)\right)\langle b_\xi^\dagger v_s^\dagger c_s\rangle\Big|_{\xi\neq\xi_l} = f_s^e f_s^h \; . \tag{3.15}$$

As a result, Eq. (3.15) can be solved in the adiabatic limit and the part $\xi \neq \xi_l$ of the sum in Eq. (3.12) can be evaluated, yielding a time constant τ_{nl} for the spontaneous emission into non-lasing modes according to the Weißkopf-Wigner theory [92],

$$\frac{2}{\hbar}\mathrm{Re}\sum_{\xi\neq\xi_l}\frac{|g_\xi|^2}{\kappa_\xi + \Gamma + i\left(\tilde{\varepsilon}_s^e + \tilde{\varepsilon}_s^h - \hbar\omega_\xi\right)} = \frac{1}{\tau_{\mathrm{nl}}} \; . \tag{3.16}$$

In a laser theory, one typically distinguishes between the rate of spontaneous emission into lasing and non-lasing modes, $1/\tau_l$ and $1/\tau_{\mathrm{nl}}$, respectively. Both rates add up to the total spontaneous emission rate $1/\tau_{\mathrm{sp}}$. It it convenient to introduce the spontaneous emission coupling factor β, which is given by

$$\beta = \frac{\frac{1}{\tau_l}}{\frac{1}{\tau_{\mathrm{sp}}}} = \frac{\frac{1}{\tau_l}}{\frac{1}{\tau_l} + \frac{1}{\tau_{\mathrm{nl}}}} \tag{3.17}$$

and to express the rate of spontaneous emission into non-lasing modes in terms of this β factor:

$$\frac{1}{\tau_{\mathrm{nl}}} = \frac{1-\beta}{\tau_{\mathrm{sp}}} \; . \tag{3.18}$$

For a further discussion of the time constants, see Appendix B.

With Eq. (3.12) one can now determine the population dynamics in the s-shell. For the spontaneous emission into non-lasing modes, the adiabatic solution of Eq. (3.15) is used according to Eqs. (3.16) and (3.18). Furthermore, we include a transition rate of carriers from the p- to the s-shell in an approximation where only downwards directed scattering is considered, $R_{p\rightarrow s}^{e,h} = (1 - f_s^{e,h}) f_p^{e,h}/\tau_{\mathrm{r}}^{e,h}$, and $g \equiv g_{\xi_l}$ to obtain

$$\frac{\mathrm{d}}{\mathrm{d}t} f_s^{e,h} = -\frac{2|g|^2}{\hbar}\mathrm{Re}\,\langle b^\dagger v_s^\dagger c_s\rangle - (1-\beta)\frac{f_s^e f_s^h}{\tau_{\mathrm{sp}}} + R_{p\rightarrow s}^{e,h} \; . \tag{3.19}$$

Here the first term describes the carrier dynamics due to the interaction with the laser mode, while the second term represents the loss of carriers due to recombination into non-lasing modes. The blocking factor $1 - f_s^{e,h}$ in $R_{p\rightarrow s}^{e,h}$ ensures that the populations cannot exceed unity.

The carrier dynamics for the p-shell can be written as

$$\frac{\mathrm{d}}{\mathrm{d}t} f_p^{e,h} = P\left(1 - f_p^e - f_p^h\right) - \frac{f_p^e f_p^h}{\tau_{\mathrm{sp}}^p} - R_{p\to s}^{e,h} , \qquad (3.20)$$

where a carrier generation rate P is included together with the Pauli-blocking factor $(1 - f_p^e - f_p^h)$. As the carrier generation takes place in the p-shell of each QD, P is to be understood as a "pump rate per emitter", in contrast to the pump rate $\tilde{P} = N_{\mathrm{emitter}}P$ typically appearing in atomic models, e.g. Eq. (5.2). The second term describes spontaneous recombination of p-shell carriers and the third contribution is the above-discussed carrier relaxation.

The scattering term $R_{p\to s}^{e,h}$ transfers carriers only from the p- to the s-shell but not vice versa. Thus, the relaxation rate is proportional to the population in the p-shell independently of temperature. As a result, the stationary values of the populations are not necessarily thermal and depend on the pump and scattering rates. Nevertheless, this is good approximation at low temperatures, where the p-shell deviates significantly from zero only if the s-shell is completely filled. In fact, we have performed calculations where carrier scattering between p- and s-shell was modeled by an evolution towards the equilibrium distribution analogous to Eq. (2.36) showing similar results at low and elevated temperatures. Note, however, that the carrier relaxation time in Eq. (2.36) differs qualitatively and quantitatively from the effective down-scattering time used in $R_{p\to s}^{e,h}$.

The resulting set of equations (3.19) and (3.20), together with (3.11) and (3.14) constitute the basic equations of the semiconductor laser model, describing the coupled dynamics for the photon number and the carrier population. It turns out that the inclusion of the carrier-photon correlations, which are given by the last two terms in Eq. (3.14), hardly modifies the results for the photon number. Neglecting the carrier-photon correlations in Eq. (3.14), the resulting set of equations corresponds to a truncation of the hierarchy on the doublet level. However, the inclusion of these correlations in Eq. (3.14) is of critical importance if $\langle b^\dagger v_s^\dagger c_s \rangle$ is used for the calculation of higher-order correlation functions, such as the photon autocorrelation function $g^{(2)}(0)$.

3.2.2. Extended Laser Equations and Photon Correlations

Now we turn to the extended set of laser equations including carrier-photon and photon-photon correlation functions. To access information about the coherence properties of the emitted light in order to characterize the threshold properties, we calculate

the second-order correlation function (3.10). The correlation function $\delta\langle b^\dagger b^\dagger bb\rangle$ appearing in this equation is a four-particle average, so that we must include all terms consistently up to the quadruplet level, cf. Section 3.1. Only photons from the laser mode are assumed to build up correlations. Therefore, in all correlation functions only photon operators for the laser mode are considered. As we consider only QDs in resonance with this mode, the free evolution energy terms $\tilde{\varepsilon}_s^e + \tilde{\varepsilon}_s^h - \hbar\omega$ drop out and are therefore not explicitly given in the following.

We calculate the second-order photon correlation function $g^{(2)}(0)$ from Eq. (3.10). The time evolution of the intensity correlation function $\delta\langle b^\dagger b^\dagger bb\rangle$ appearing in this equation is given by

$$\left(\hbar\frac{\mathrm{d}}{\mathrm{d}t} + 4\kappa\right)\delta\langle b^\dagger b^\dagger bb\rangle = 4\,|g|^2\,\mathrm{Re}\sum_{\nu'}\delta\langle b^\dagger b^\dagger b v_{\nu'}^\dagger c_{\nu'}\rangle\;, \tag{3.21}$$

where the sum involves all resonant laser transitions from various QDs. In this equation another quadruplet function enters, which represents a correlation between the photon-assisted polarization and the photon number. For the corresponding equation of motion we obtain

$$\begin{aligned}\left(\hbar\frac{\mathrm{d}}{\mathrm{d}t} + 3\kappa + \Gamma\right)\delta\langle b^\dagger b^\dagger b v_\nu^\dagger c_\nu\rangle = &-2\,|g|^2\,\langle b^\dagger v_\nu^\dagger c_\nu\rangle^2 - \left(1 - f_\nu^e - f_\nu^h\right)\delta\langle b^\dagger b^\dagger bb\rangle \\ &+ 2f_\nu^h \delta\langle b^\dagger b c_\nu^\dagger c_\nu\rangle - 2f_\nu^e \delta\langle b^\dagger b v_\nu^\dagger v_\nu\rangle \\ &- 2\delta\langle b^\dagger b c_{\nu'}^\dagger v_\nu^\dagger c_\nu v_{\nu'}\rangle + \delta\langle b^\dagger b^\dagger v_{\nu'}^\dagger v_\nu^\dagger c_\nu c_{\nu'}\rangle\;.\end{aligned} \tag{3.22}$$

Here, we have again scaled $\delta\langle b^\dagger b^\dagger b v_\nu^\dagger c_\nu\rangle \rightarrow g\,\delta\langle b^\dagger b^\dagger b v_\nu^\dagger c_\nu\rangle$ with the light-matter coupling g for the laser mode. The triplet carrier-photon, or population-photon correlations in the second line are the same as in Eq. (3.14), and their evolution is given by

$$\begin{aligned}\left(\hbar\frac{\mathrm{d}}{\mathrm{d}t} + 2\kappa\right)\delta\langle b^\dagger b c_\nu^\dagger c_\nu\rangle = -2\,|g|^2\,\mathrm{Re}\Big[&\delta\langle b^\dagger b^\dagger b v_\nu^\dagger c_\nu\rangle \\ &+ \sum_{\nu'}\delta\langle b^\dagger v_{\nu'}^\dagger c_\nu^\dagger c_{\nu'} c_\nu\rangle + \left(\langle b^\dagger b\rangle + f_\nu^e\right)\langle b^\dagger v_\nu^\dagger c_\nu\rangle\Big]\;,\end{aligned} \tag{3.23}$$

$$\begin{aligned}\left(\hbar\frac{\mathrm{d}}{\mathrm{d}t} + 2\kappa\right)\delta\langle b^\dagger b v_\nu^\dagger v_\nu\rangle = 2\,|g|^2\,\mathrm{Re}\Big[&\delta\langle b^\dagger b^\dagger b v_\nu^\dagger c_\nu\rangle \\ &- \sum_{\nu'}\delta\langle b c_{\nu'}^\dagger v_\nu^\dagger v_{\nu'} v_\nu\rangle + \left(\langle b^\dagger b\rangle + f_\nu^h\right)\langle b^\dagger v_\nu^\dagger c_\nu\rangle\Big]\;.\end{aligned} \tag{3.24}$$

The correlation functions in the sum, which have been scaled as $\delta\langle b^\dagger v_{\nu'}^\dagger c_\nu^\dagger c_{\nu'} c_\nu\rangle \to g\,\delta\langle b^\dagger v_{\nu'}^\dagger c_\nu^\dagger c_{\nu'} c_\nu\rangle$, $\delta\langle b c_{\nu'}^\dagger v_\nu^\dagger v_{\nu'} v_\nu\rangle \to g\,\delta\langle b c_{\nu'}^\dagger v_\nu^\dagger v_{\nu'} v_\nu\rangle$, obey equations of motion

$$\left(\hbar\frac{\mathrm{d}}{\mathrm{d}t}+\kappa+\Gamma\right)\delta\langle b c_{\nu'}^\dagger v_\nu^\dagger v_{\nu'} v_\nu\rangle = (1-\delta_{\nu\nu'})$$
$$\left[(1-f_{\nu'}^e-f_{\nu'}^h)\,\delta\langle b^\dagger b v_\nu^\dagger v_\nu\rangle - |g|^2\,\langle b^\dagger v_\nu^\dagger c_\nu\rangle^*\langle b^\dagger v_{\nu'}^\dagger c_{\nu'}\rangle^*\right]\,,\quad (3.25)$$

$$\left(\hbar\frac{\mathrm{d}}{\mathrm{d}t}+\kappa+\Gamma\right)\delta\langle b^\dagger v_{\nu'}^\dagger c_\nu^\dagger c_{\nu'} c_\nu\rangle = (1-\delta_{\nu\nu'})$$
$$\left[(1-f_{\nu'}^e-f_{\nu'}^h)\,\delta\langle b^\dagger b c_\nu^\dagger c_\nu\rangle + |g|^2\,\langle b^\dagger v_\nu^\dagger c_\nu\rangle\langle b^\dagger v_{\nu'}^\dagger c_{\nu'}\rangle\right]\,.\quad (3.26)$$

A closer look reveals that the correlation functions determined by Eqs. (3.25) and (3.26) only contribute if correlations between *different* QDs exist, i.e. superradiant coupling plays a role in the system. To see this, we refer to the dipole selection rules in cubic crystals, where optical transitions with a given circular light polarization are coupled to a particular electron spin and the corresponding hole total angular momentum. Specifically, the *s*-shell states for electrons are spin degenerate and the two spin states are coupled to different light polarizations. If we consider correlations between photons with the same circular polarization, we find they are linked to states for which only one electron or hole per *s*-shell and QD are available. In other words, annihilating two valence-band electrons in case of $\langle b c_{\nu'}^\dagger v_\nu^\dagger v_{\nu'} v_\nu\rangle$ and two conduction-band electrons in case of $\langle b^\dagger v_{\nu'}^\dagger c_\nu^\dagger c_{\nu'} c_\nu\rangle$ is only possible if these carriers belong to different QDs. Hence, for $\nu=\nu'$ these expectation values vanish altogether.[3] Thus, neither their factorization, nor the remaining correlation functions $\delta\langle b c_{\nu'}^\dagger v_\nu^\dagger v_{\nu'} v_\nu\rangle$ and $\delta\langle b^\dagger v_{\nu'}^\dagger c_\nu^\dagger c_{\nu'} c_\nu\rangle$ exist in the case $\nu=\nu'$. The remaining correlation functions referring to different QDs $\nu\neq\nu'$ are related to superradiant coupling. The same applies to the expectation value $\langle b^\dagger b^\dagger v_{\nu'}^\dagger v_\nu^\dagger c_\nu c_{\nu'}\rangle$, which also vanishes together with the corresponding correlation function for $\nu=\nu'$. Under the assumption that superradiance is weak in the system, the discussed correlation functions are neglected. If, however, the phenomenon of superradiant coupling itself is to be studied [22–24, 40, 103, 139, 140, 147, 148], the correlation functions must be included via their own equations of motion. Finally, the term $\delta\langle b^\dagger b c_{\nu'}^\dagger v_\nu^\dagger c_\nu v_{\nu'}\rangle$ in Eq. (3.22) is a variation of the carrier correlations $C_{\alpha'\nu\nu'\alpha}^{\mathrm{x}} = \delta\langle c_\alpha^\dagger v_\nu^\dagger c_{\nu'} v_\alpha\rangle$. For consistency reasons, this contribution is neglected in accordance with the omission of C^{x}.

Effects due to the Coulomb interaction of carriers can be included in the higher-order correlation functions along the same lines described in Chapter 2. Although we do

---

[3]In fact, this is the case already on the operator level, i.e., before taking the average.

not explicitly consider these terms in our calculation for the arguments given in Section 3.2.1, we would like to point out the analogy between the terms on the doublet and quadruplet levels. The contributions to Eq. (3.22) remaining on the quadruplet level are given by

$$
i\hbar\frac{\mathrm{d}}{\mathrm{d}t}\delta\langle b^\dagger b^\dagger b v_\nu^\dagger c_\nu\rangle\Big|_{\text{Coul}} = -2\sum_\alpha (1 - f_\nu^e - f_\nu^h)V_{\nu\alpha\nu\alpha}\delta\langle b^\dagger b^\dagger b v_\alpha^\dagger c_\alpha\rangle
$$
$$
- 2(f_\alpha^e + f_\alpha^h)V_{\nu\alpha\nu\alpha}\delta\langle b^\dagger b^\dagger b v_\nu^\dagger c_\nu\rangle \ . \quad (3.27)
$$

The result shows an analogous structure like the Hartree-Fock Coulomb terms for $\langle b^\dagger v_\nu^\dagger c_\nu\rangle$ in Eq. (3.13) and can be interpreted accordingly as a renormalization of the single-particle energies and as interband exchange interaction causing additional renormalizations of the transition energies as well as a redistribution of oscillator strength between different QD transitions. Coulomb interaction contributions to the correlations $\delta\langle b^\dagger b c_\nu^\dagger c_\nu\rangle$ and $\delta\langle b^\dagger b v_\nu^\dagger v_\nu\rangle$ are analogous to those contributing to the carrier dynamics of f_ν^e and f_ν^h discussed in detail in Section 2.3.

3.2.3. Analytical results for $\mathbf{g^{(2)}(0)}$

Before the numerical results of the semiconductor model are presented, it is instructive to study analytical solutions for $g^2(0)$ in the two limiting cases of strong and weak pumping. For this purpose we use the stationary limit of Eqs. (3.11), (3.14), and (3.21)–(3.24). Considering the resonant s-shell contributions from identical QDs, we replace $\sum_{\nu'}$ by the number of QDs N. Inserting in Eq. (3.11) the photon-assisted polarization from Eq. (3.14), ignoring spontaneous emission for the above-threshold solution, and expressing the higher-order correlations with the help of Eqs. (3.23) and (3.24), we obtain from (3.10) and (3.21)

$$
g^{(2)}(0) - 1 = -\frac{\kappa(\kappa + \Gamma)}{2\left|g\right|^2 \langle b^\dagger b\rangle}\left(1 + \frac{\left|g\right|^2 N}{\kappa(\kappa + \Gamma)}\big(1 - f_s^e - f_s^h\big)\right) \ . \quad (3.28)
$$

Above the threshold the photon number becomes large, so that the limit $\langle b^\dagger b\rangle/N \gg 1$ can be fulfilled. In this case the right hand side vanishes and we obtain $g^{(2)}(0) = 1$, i.e. well above threshold the light is coherent.

For the limiting case of weak pumping, we seek again the stationary solution of our coupled system of equations, now under the assumption that in Eq. (3.14) the stimulated emission term and the higher-order correlations $\delta\langle b^\dagger b c_\nu^\dagger c_\nu\rangle$, $\delta\langle b^\dagger b v_\nu^\dagger v_\nu\rangle$ can be neglected due to the lack of a photon population. A convenient way to solve for the intensity correlation function $\delta\langle b^\dagger b^\dagger b b\rangle$ is to insert Eq. (3.22) into (3.21). The

higher-order correlations in Eq. (3.22) are replaced by the static solution of Eqs. (3.23) and (3.24), while in the latter $\langle b^\dagger v_\nu^\dagger c_\nu \rangle$ is replaced by Eq. (3.11), and $\delta\langle b^\dagger b^\dagger b v_\nu^\dagger c_\nu \rangle$ is traced back to $\delta\langle b^\dagger b^\dagger bb \rangle$ with the stationary solution of Eq. (3.21). As explained above, we ignore the quadruplet correlations occurring in Eq. (3.22). Together with Eqs. (3.10) and (3.11) we finally obtain

$$
\left(\frac{\kappa(3\kappa + \Gamma)}{|g|^2 N} + (1 - f_s^e - f_s^h) \right) \left[g^{(2)}(0) - 2 \right] =
$$
$$
- \frac{2(f_s^e + f_s^h)}{N} \left[g^{(2)}(0) - 1 \right] - \frac{2\kappa(3\kappa + 2\Gamma)}{|g|^2 N^2} \; . \quad (3.29)
$$

To evaluate this formula further, we restrict ourselves to the case

$$
\frac{\kappa^2}{|g|^2 N} \gg 1 \; , \quad\quad\quad\quad\quad (3.30)
$$

or $2\kappa/\hbar \gg N/\tau_l$, i.e. the cavity loss rate is much larger than the total rate of spontaneous emission into the laser mode. This regime we refer to as "bad cavity limit" [118]. Typically, lasers operate in this regime (cavities with very large Q-factors and lifetimes longer than the spontaneous emission time are used in the context of strong coupling and quantum information). We obtain

$$
g^{(2)}(0) = 2 - \frac{2}{N} \; . \quad\quad\quad\quad\quad (3.31)
$$

This is an important result, because it provides the statistics of thermal light in the limit of many QDs, $g^{(2)}(0) = 2$, and in the opposite limit of a single QD it gives the statistics of a single-photon emitter, $g^{(2)}(0) = 0$.

3.3. Numerical Results

We now present numerical solutions of the extended semiconductor laser theory including carrier-photon correlations based on Eqs. (3.11), (3.14), (3.19), (3.20), and (3.21)–(3.24) using an adaptive time integration algorithm. For more details about the numerical methods we refer to Appendix E. We consider a typical parameter set: The number of emitters is $\tilde{N} = 20$. The number used in the calculations is increased with decreasing β in order to have the thresholds occur at the same pump rate, i.e. $N = \tilde{N}/\beta$. For the spontaneous emission time enhanced by the Purcell effect we use $\tau_{\mathrm{sp}} = 50\,\mathrm{ps}$, and the cavity damping is $\kappa = 20\,\mu\mathrm{eV}$. The corresponding cavity lifetime is about $17\,\mathrm{ps}$, yielding a Q-factor of roughly $30{,}000$. The effective relaxation times for electrons and holes are taken to be $\tau_{\mathrm{r}}^e = 1\,\mathrm{ps}$ and $\tau_{\mathrm{r}}^h = 500\,\mathrm{fs}$, respectively.

3.3.1. Stationary Properties

In Figure 3.5 the autocorrelation function $g^{(2)}(\tau = 0)$ is shown atop the input/output curve for various values of the spontaneous emission coupling β. There are several striking features:

i. The jump of the intensity curve from below to above threshold is no longer determined by $1/\beta$, like in Figs. 5.2 and 5.4 (cf. p.96 and p.101, respectively) and many examples found in the literature [21, 118, 155], which are obtained from a laser theory for two-level systems in which only a single excitation is possible and reabsorption is negligible. This is of particular importance since measurements of the input/output characteristics are often used to experimentally deduce the β-factor according to the predictions of the two-level models. If the atomic $1/\beta$-behavior would be used to extract the β-factors from the curves in Figure 3.5, one would obtain 0.017 instead of 0.1, 0.0017 instead of 0.01, and 0.00017 instead of 0.001.

ii. The usual laser threshold in conventional lasers with low spontaneous emission coupling ($\beta \sim 10^{-6}$) is very abrupt. We see that for larger β values ($\beta > 0.1$), the s-shaped jump in the input/output curve becomes smeared out, and also the drop of the autocorrelation becomes softer.

iii. For small β values, the intensity jump is accompanied by a decrease of the second-order correlation function from the value $g^{(2)}(0) = 2$ for thermal light to $g^{(2)}(0) = 1$ for coherent light (cf. Section 3.1). For higher spontaneous emission coupling β, $g^{(2)}(0)$ remains smaller than two below the threshold. Corresponding to the discussion above, this behavior can arise either in the bad cavity regime if the number of emitters is small (compare Eq. (3.31)), or if the loss rate from the cavity becomes smaller than the rate of spontaneous emission into the cavity. In the latter case, and this is the reason for the decrease of sub-threshold value of $g^{(2)}(0)$ in Figure 3.5, a substantial population of photons builds up in the cavity mainly due to spontaneous emission processes, and exhibits a deviation from the signature of incoherent thermal light.

iv. At high pump intensities saturation effects due to Pauli blocking become visible in the input/output curve, effectively limiting the maximum output that can be achieved. The strength of the Pauli blocking depends on the number of available states in the pump levels and the number of scattering channels to quickly redistribute carriers. When pumping into the barrier, where the number of available states is larger than in the localized states, saturation effects will
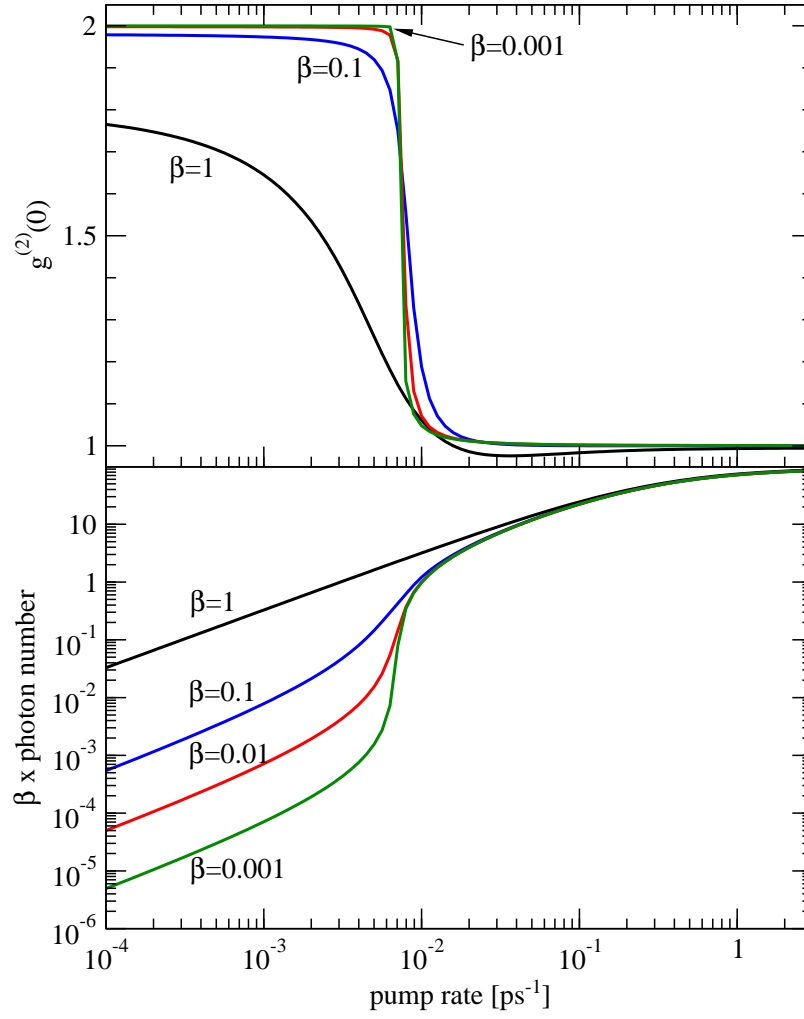
Figure 3.5.: Calculated output curve (lower panel) and autocorrelation function $g^{(2)}(\tau = 0)$ (upper panel) for $\beta =$1, 0.1, 0.01, and 0.001. The system is excited at a constant pump rate, corresponding to continuous wave excitation.
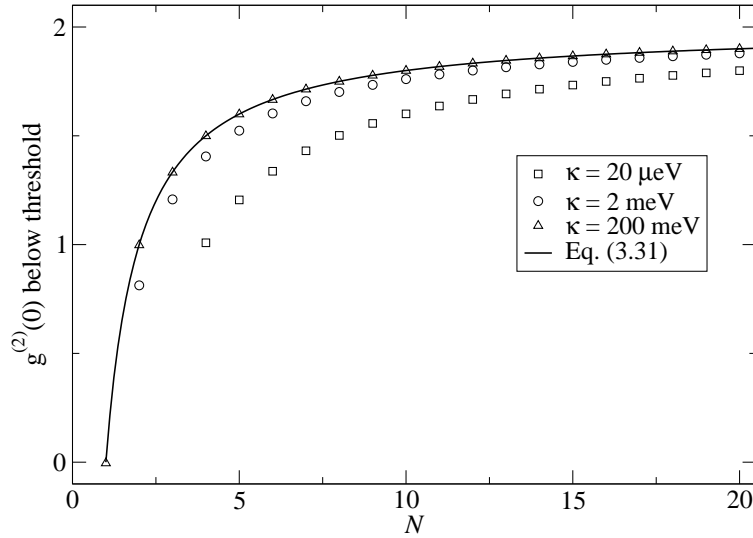
Figure 3.6.: Sub-threshold values of $g^{(2)}(0)$ for $\beta = 1$ obtained from the extended semiconductor laser model. The analytical approximation in the 'bad cavity' limit, Eq. (3.31), is compared to numerical results obtained with different values for the inverse cavity lifetime κ.

be less influential compared to the situation where higher localized states are pumped.

In Section 3.2.3 we have discussed the analytical solution of the semiconductor model for the autocorrelation function $g^{(2)}(0)$ below threshold in the 'bad cavity' limit $\kappa^2 \gg |g|^2 N$. In Figure 3.6 we show the sub-threshold value of the autocorrelation function versus the number of emitters N. The analytical solution Eq. (3.31) (solid line), which was derived for the limit of large κ, is compared to numerical solutions of the extended semiconductor laser model (open symbols) for $\beta = 1$ and various values of κ. All other parameters are the same as those used in Figure 3.5. If $\kappa = 200\,\mathrm{meV}$, the condition for the analytical solution is fulfilled and perfect agreement between analytical and numerical results is obtained. In this case, the thermal emission $g^{(2)}(0) = 2$ below the laser threshold is approached for a large number of emitters N. In the limit of one single QD, the antibunching signature $g^{(2)}(0) = 0$ is numerically recovered. On the other hand, in the theoretical limit of an infinitely good cavity $\kappa \to 0$, a constant value of $g^{(2)}(0) = 1$ is expected for atomic models [118]. The case of larger cavity lifetimes is displayed (circles and squares) and the trend of a decrease of the subthreshold value is observed. For the case of a small number of emitters in a very good cavity deviations from Eq. (3.31) are observed.

3.3.2. Switch-on Dynamics and Relaxation for Continuous-Wave Excitation

While for the input/output curves and the photon statistics only the stationary solution of the laser equations is of interest, from the time evolution insight on the population build-up due to pumping and scattering can be gained.

The switch-on dynamics of a laser system is depicted in Figure 3.7. The shown data is the time evolution that corresponds to pumping above threshold for the situation with (lower panel) and without (upper panel) carrier-photon correlations. The inset in the top panel magnifies the region where population is generated in the laser levels. In the initially empty system, the p-shell becomes populated due to pumping (dashed line). As soon as there is a population, relaxation redistributes carriers, resulting in an increase of the s-shell population (dotted line). Once there are carriers available in the s-shell, recombination due to spontaneous emission starts to take place, causing the photon population in the laser mode to build up (solid line). When stimulated emission starts to strongly depopulate the carrier system, which in turn reduces the optical gain, damped relaxation oscillations are observable. Finally, all quantities reach stationary values.

While in the top panel the influence of the higher order correlations (3.21)–(3.24) is omitted, corresponding to setting $\delta\langle b^\dagger b c_\nu^\dagger c_\nu\rangle$ and $\delta\langle b^\dagger b v_\nu^\dagger v_\nu\rangle$ equal to zero in Eq. (3.14), all correlations up to quadruplet level are included in the bottom panel. The stationary values become slightly modified compared to the top panel. The slight reduction of the photon population is marginal for the input/output curve that is typically displayed on a double-logarithmic scale. Also visible is an enhancement of oscillations, especially one additional oscillation period is introduced after about 75 ps before the actual relaxation oscillations take place. The unfamiliar manner of the oscillations is yet to be investigated.
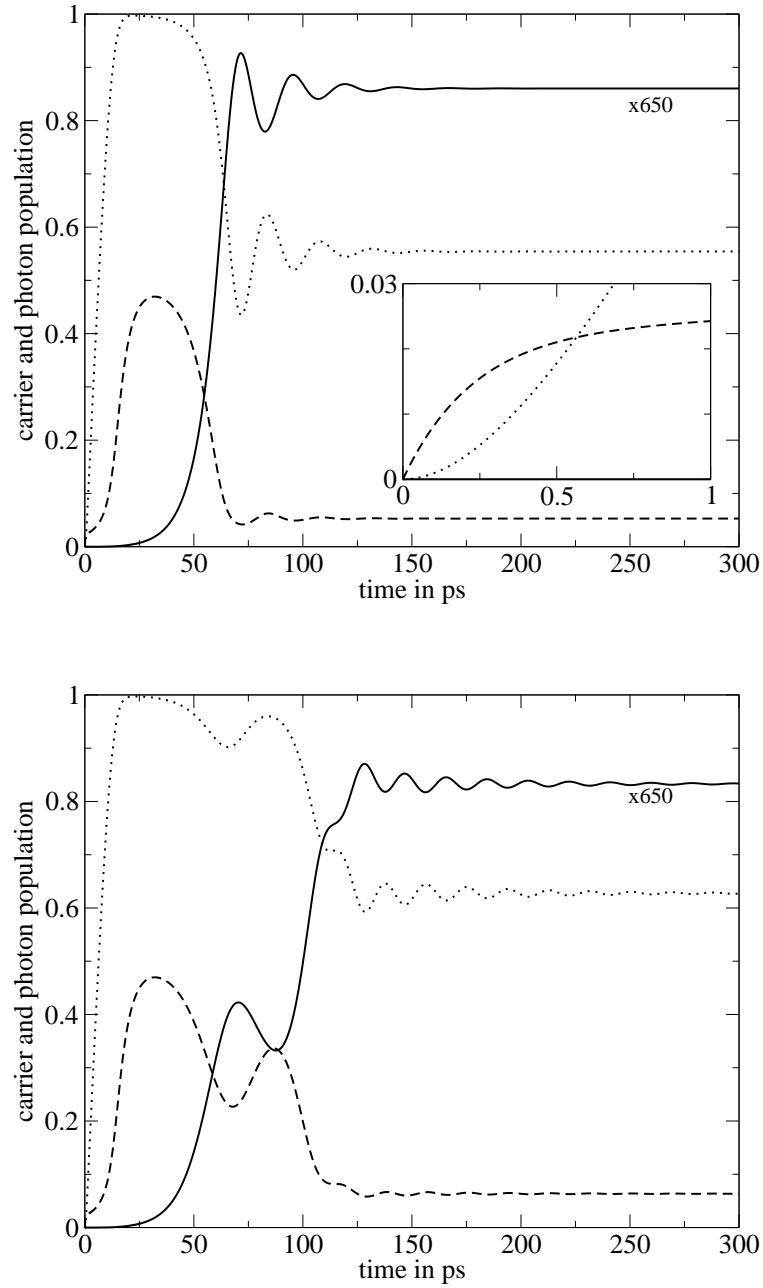
Figure 3.7.: Switch-on oscillations of the carrier (dotted line: *s*-shell, dashed line: *p*-shell) and photon population in the laser mode (solid line). The latter has been scaled down by a factor of 650. In the top panel correlations beyond doublet level have been suppressed, in the bottom panel they are included. The inset magnifies the region close to the origin.

3.4. Comparison with Experiments

A first direct application of our theory to micropillar QD lasing has been performed in close collaboration with the experimental group of Prof. Peter Michler in Stuttgart.
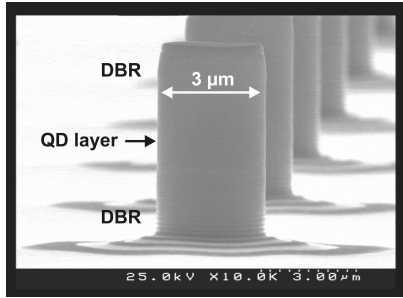
Figure 3.8.: $3\,\mu$m micropillar with InGaAs QDs as the active layer. From this type of structure the results presented in Figure 3.9 were obtained.

Measurements were performed on pillar microcavities with self-assembled InGaAs QDs as the gain medium. The pillar presented here has a diameter of $3\,\mu$m and is made out of 50 alternating layers of AlAs/GaAs, acting as distributed Bragg reflecting (DBR) mirrors due to the materials' different refractive indices [20, 144, 151]. The structuring was done by an etching technique [83], resulting in low roughness of the sidewall surfaces and an excellent quality of the samples. An scanning electron microscope (SEM) side view of one of the sample pillars is displayed in Figure 3.8; the cavity containing the QDs is indicated by the arrow in the middle of the resonator. The measurements of the autocorrelation function were done on a Hanbury-Brown and Twiss (HBT) setup [28], which is basically an interferometer for intensities. Located at the arms of the interferometer are two detectors that are coupled to a correlator. In dependence of the delay time τ between two events, the autocorrelation function can be extracted. Details are found in Refs. [143, 144].

The experimental results for the $3\,\mu$m and for another $4\,\mu$m pillar are summarized in Figure 3.9. The extracted photon autocorrelation function is shown (top panel) in relation to the corresponding input/output curve (bottom panel) for both pulsed and continuous wave (cw) excitation. Under varied optical excitation over four (cw: two) orders of magnitude, high output emission dynamics of up to 8 (cw: 5) decades are observed from each structure. In the pulsed series in panels (a) and (c) a characteristic s-shaped smooth intensity transition is apparent at intermediate excitation levels of $\sim 300\,\mu$W ($\sim 500\,\mu$W) for the $3\,\mu$m ($4\,\mu$m) pillar. The broadened transition region is a signature of a large spontaneous emission coupling, cf. Section 3.3.1, caused by the large Q-factor of the cavity and a short radiative lifetime enhanced by the Purcell effect. An equivalent trend is also found in the cw intensity traces in Figure 3.9 (b) and (d), where an observation of the smooth non-linear emission onset was experimentally limited to the lower branch. Pumping at higher powers would result in damaging the samples.

Looking at the top panels, we find that the autocorrelation function is peaked in the threshold region, rather than showing a monotonous transition from thermal
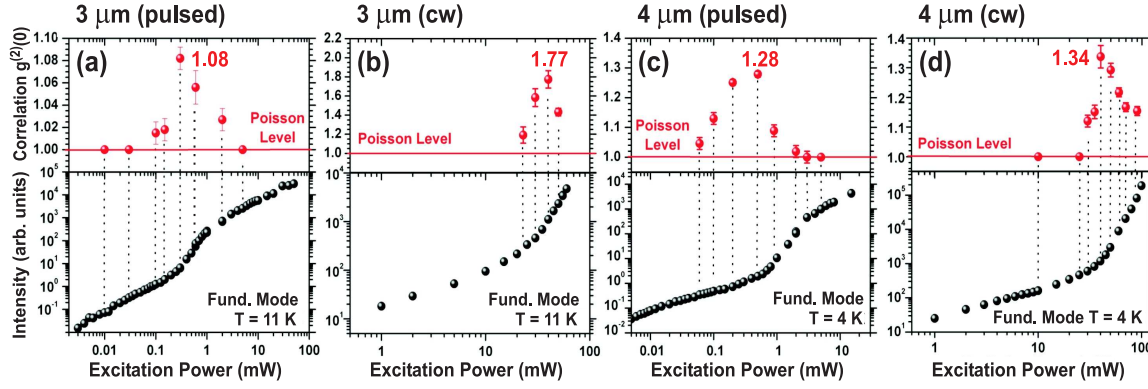
Figure 3.9.: (a) and (c) Integrated intensities (bottom) for the 3 and 4 μm pillars under non-resonant *pulsed* excitation. Strong photon bunching $g^{(2)}(0) > 1$ is found from corresponding correlation measurements (top) over a broadened regime around threshold. (b) and (d) Output intensity (bottom) and $g^{(2)}(\tau = 0)$ autocorrelation series on the 3 μm and 4 μm fundamental modes under *continuous wave* pumping, again revealing qualitatively strong field fluctuations around the threshold.

($g^{(2)}(0) = 2$) to coherent ($g^{(2)}(0) = 1$) emission. This is caused by the deficient temporal resolution of the setup. To distinguish between this insufficiently resolved experimental curve and the true autocorrelation function, we introduce the notation $\tilde{g}^{(2)}(0)$ for the experimental result. A quantitative analysis of this effect is given below.

The measured input/output curve (bottom) and intensity correlation function (top) for the 3 μm pillar is shown together with results obtained from our microscopic laser theory in Figure 3.10. The calculations are based on the parameters obtained for the measurements on the 3 μm pillar under pulsed excitation. With a cavity lifetime of $\tau_{\mathrm{cav}} = 13$ ps, a spontaneous emission time into the laser mode of $\tau_{\mathrm{lase}} = 250$ ps, and 42 resonant QDs, yielding $\beta = 0.12$, we obtain good agreement for the height and the shape of the output intensity jump (bottom panel). Saturation effects become visible in the high excitation regime, which occur due to Pauli blocking of the rapidly filled pump levels. To underline the importance of the saturation effects, the dotted line corresponding to a calculation where Pauli blocking is artificially switched off has been added to the figure.

As mentioned above, the measured autocorrelation function shows a peak around the threshold region. The reason for this lies in the limited time resolution of the HBT detector setup, for which avalanche photo diodes with a temporal resolution of approximately $\Delta t = 600$ ps are used. The autocorrelation function is a function of the delay time τ between two correlated events at the two detectors of the HBT setup. However, due to the limited time resolution the measurement is performed over a
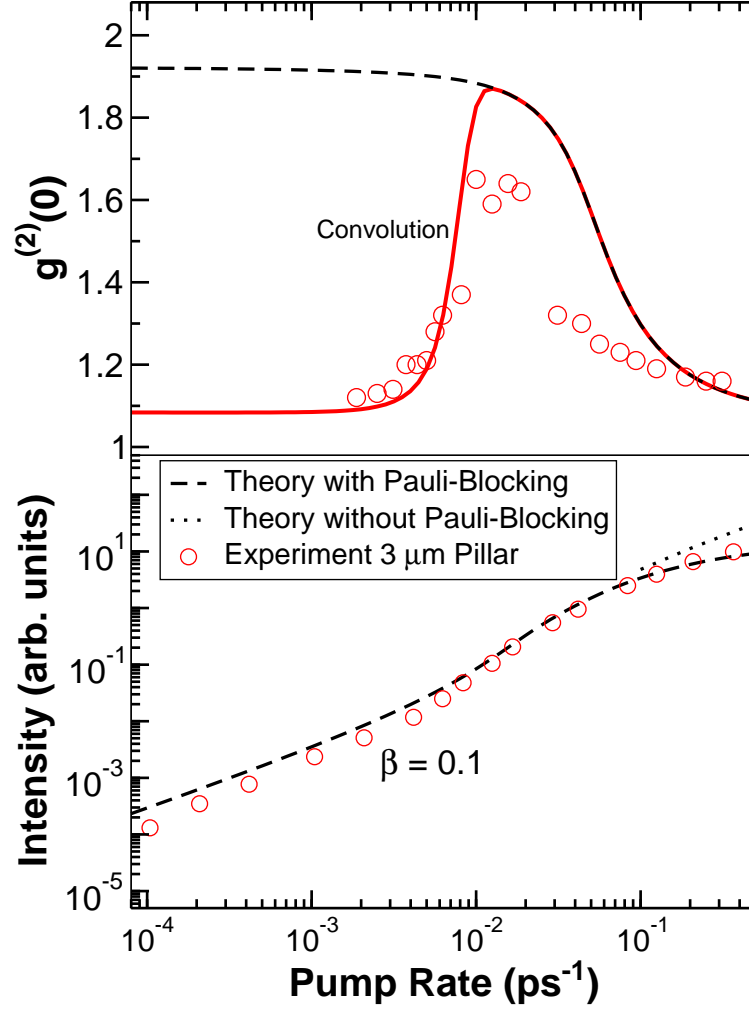
Figure 3.10.: Calculated results (dashed lines) and experimental data (circles): Input/output curves (bottom) together with the second-order coherence function (top). The experimental data is that of the $3\,\mu$m pillar from Figure 3.9(a). In the bottom panel a calculation with artificially suppressed Pauli blocking is shown as dotted line to underline the importance of saturation effects. In the top panel a convolution of the calculated second-order correlation function with an apparatus function reflecting the experimental temporal resolution τ_c is shown in accordance with Eq. (3.33) (red solid line), confirming that the peaked experimental result is caused by the limited time resolution of the detection setup.

much longer time window, during which the value of $g^{(2)}$ is averaged. If the coherence time of the output from the microcavity is much longer than the time resolution of the setup, this averaging effect is small. If the coherence time is much shorter though, the averaging will produce a result that is smaller than the true value at zero delay. To resolve this issue, the coherence time has been measured as a function of the excitation power. The results are displayed in Figure 3.11. Details about the coherence time and its connection to first order coherence are discussed in Chapter 4. While above the threshold the coherence time is larger ($> 700\,\mathrm{ps}$) than the time resolution, below threshold it is significantly smaller ($\approx 50\,\mathrm{ps}$).

To facilitate a direct comparison with the $\tilde{g}^{(2)}(0)$ measurements that are limited by the time resolution Δt, we use the following method. In a two-level system, the autocorrelation function as a function of the delay time decays to value of unity on the timescale of the coherence time τ_c. We determine $g^{(2)}(\tau)$ for each pump intensity from the calculated $g^{(2)}(0)$ by using

$$g^{(2)}(\tau) = 1 + \left(g^{(2)}(0) - 1\right) e^{-\frac{2|\tau|}{\tau_c}} , \qquad (3.32)$$

which holds exactly for thermal light. To evaluate this equation, the measured coherence times shown in Fig. 3.11 are adapted to our results in Figure 3.10. Then a convolution with an apparatus function describing the 'measurement profile' is performed. To a good approximation, this can be assumed to be a Gaussian with the width of the setup's time resolution $2\sigma = \Delta t$, i.e.

Figure 3.11.: Measured coherence times for the $3\,\mu\mathrm{m}$ pillar.

$$\tilde{g}^{(2)}(\tau) = \frac{1}{\sqrt{2\pi\sigma^2}} \int_{-\infty}^{\infty} d\tau' g^{(2)}(\tau - \tau') \exp\left(-\frac{\tau'^2}{2\sigma^2}\right) . \qquad (3.33)$$

The $\tau = 0$ value of this convolution is shown as a red line in the upper panel of Figure 3.10, reproducing the *measured* $\tilde{g}^{(2)}(0)$ correlation peak and its incomplete decay into full coherence. The theoretical result $g^{(2)}(0)$ is shown as a dashed line. The decrease in the autocorrelation function below the threshold is a result of the relatively high cavity quality (long cavity lifetime) in the samples, as discussed above. The fact that the correlation function does not reach a value of 1 even above the threshold shows that saturation effects in the pump levels prevent more carriers from being generated by harder pumping.

3.5. Pulsed and Continuous-Wave Excitation in Atomic and Semiconductor QD Lasers

For the characterization of quantum-dot-based microcavity lasers the evaluation of the input/output curves is the first step. In this section we concentrate on the information that can be obtained merely from the input/output curves of a laser device. In Section 3.3 it was described how the jump from below to above threshold does not scale with $1/\beta$ in QD microcavity lasers, as it is known from atomic systems. We have also discussed the influence of saturation effects on the upper branch of the input/output curve, i.e. at high excitation powers. While these discussions were based on stationary properties of a continuously excited system, we shall now study the modifications that occur if the system is excited by a pump pulse. In fact we will show how saturation effects can have a tremendous effect on the output characteristics and render a simple determination of the spontaneous emission coupling factor β completely impossible [52].

Before we turn to our semiconductor model, the basic features of pulsed excitation are discussed for atomic two-level systems that can be described by a rate equation model. The insight obtained from the atomic model facilitates a better understanding of the semiconductor case, where saturation additionally masks the basic effects of the pulsed laser dynamics and leads to a crossover behavior for different widths of the excitation pulse.

3.5.1. Pulsed Excitation in Atomic Systems without Saturation

For the case of an atomic four-level system with fast relaxation times the model can effectively be reduced to a two-level system where only the upper and lower laser level is considered. Then the system is described by two coupled equations (cf. Section 5.1), describing the dynamics of the photon number n

$$\dot{n} = -2\kappa n + \frac{\beta}{\tau_{\mathrm{sp}}}(1+n)N \qquad (3.34)$$

and the number of two-level systems N in an excited state

$$\dot{N} = -\frac{\beta}{\tau_{\mathrm{sp}}}nN - \frac{1}{\tau_{\mathrm{sp}}}N + P \ . \qquad (3.35)$$

Here, P is the pump rate, and $1/2\kappa$ and τ_{sp} are the cavity lifetime and the spontaneous emission time, respectively. The pump rate P is either a constant value in the case

of cw excitation, or a time-dependent pump pulse

$$P(t) = P_{\text{tot}} \frac{1}{\sqrt{2\pi\Delta t^2}} e^{\frac{-t^2}{2\Delta t^2}} \tag{3.36}$$

in case of pulsed excitation. The pulse area P_{tot} directly corresponds to the number of two-level systems excited by the pulse.

The rate of photons leaving the cavity is given by $2\kappa n$. For pulsed excitation the photon number changes dynamically, and the time integrated emission rate $\tilde{n}_{\text{pulsed}} = 2\kappa \int_{-\infty}^{\infty} dt\, n(t)$ yields the total number of emitted photons. The tilde denotes the measured photon number *outside* the cavity. In a cw measurement the situation is somewhat different. Two-level systems are excited at a constant rate, and after the switch-on dynamics the system finds into a stationary state where the rate of emitted photons per time is constant. The signal at the detector is nevertheless integrated over a time window T, so that the collected number of photons $\tilde{n}_{\text{cw}} = 2\kappa T n$ scales linearly with the integration time. Thus $\tilde{n}_{\text{pulsed}}$ and $\tilde{n}_{\text{cw}}$ can be compared only up to a scaling factor T. The same argument holds for the pump rate at which two-level systems are excited. While for pulsed excitation the total number of excited systems is given again by a time integral, in the cw case the excitation takes place at a constant rate and the total excitation scales again with the integration time T. For this reason, when comparing input/output traces of cw and pulsed excitation conditions on a logarithmic scale, the cw and pulsed curves can be shifted relative to each other along the diagonal.

We now turn to the input/output curves for the atomic system. In our example we consider a spontaneous emission time of $\tau_{\text{sp}} = 55\,\text{ps}$, a cavity lifetime $1/2\kappa$ of $19\,\text{ps}$ and $\beta = 0.027$. When discussing the semiconductor model in the following section, we use the same parameters. In the semiconductor case they are chosen to meet recent experiments [7]. The dashed line in Figure 3.12 corresponds to the case of cw excitation. Considering a pump pulse with $\Delta t \leq 10\,\text{ps}$, the input/output curves coincide with the cw result. The latter has been added to the figure with the pulsed results and corresponds to an integration time of $T \approx 150\,\text{ps}$, as is discussed above. The physical interpretation is that the number of excited two-level systems created by a sufficiently short pump pulse equals the number of excited two-level systems created by cw excitation with a carrier generation rate of $P = P_{\text{tot}}/T$. When the pulse is much shorter than the spontaneous emission time, the whole pump pulse is converted into excited two-level systems *before* the emission dynamics starts to take place. This can be inferred from Figure 3.13(a), where the time evolutions of the number of excited two-level systems N and of photons n are shown for a pulse length of 1 ps. For all curves in Figure 3.13 P_{tot} was chosen to correspond to the middle of the jump in the corresponding input/output curve, indicated by the circles in Figure 3.12.
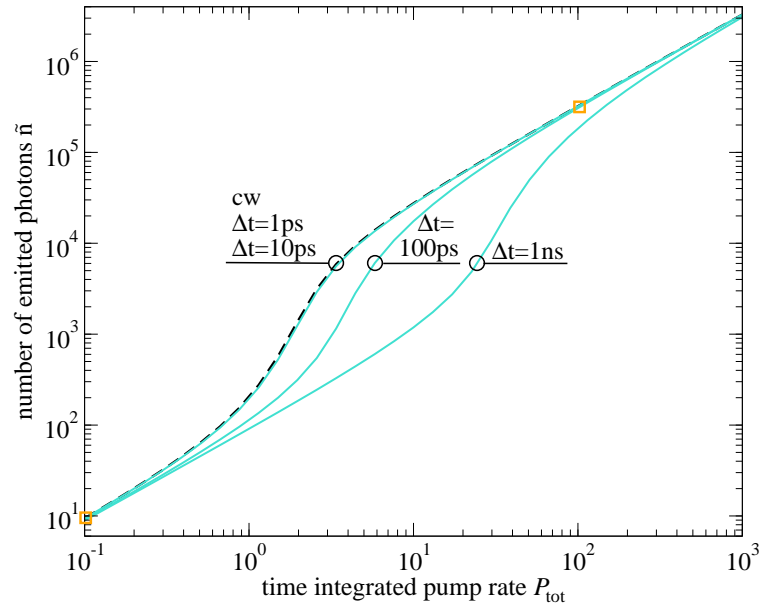
Figure 3.12.: Input/output curves for the atomic model for cw (dashed black line) and pulsed excitation with pulse widths $\Delta t =$ 1, 10, 100 and 1000 ps (solid blue curves). The curves for 1 and 10 ps pulse duration coincide with the cw result. The circles (orange squares) indicate the points on the input/output curves of which the time evolution is displayed in Fig 3.13 (3.14).
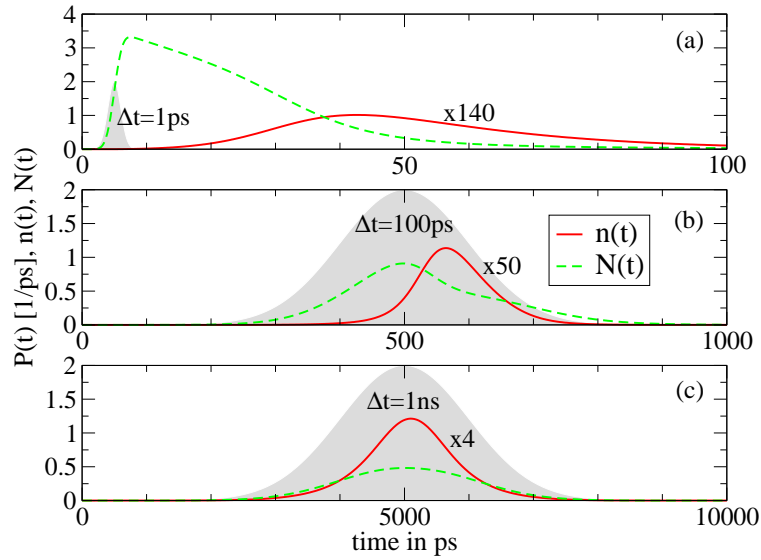
Figure 3.13.: Time evolution of the number of photons n (solid line, scaled up by the factors given in the figure) and excited two-level systems N (dashed line) after excitation with different pulse widths Δt (shaded area). Note the different timescales. In each panel P_{tot} corresponds to the marked points in Figure 3.12.
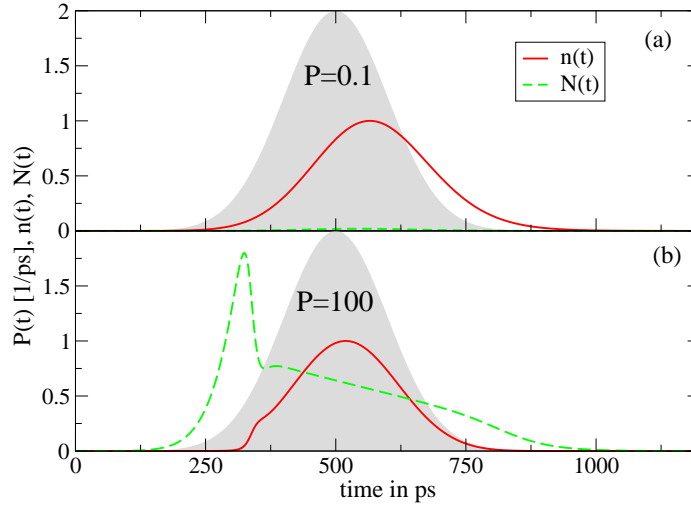
Figure 3.14.: For a pulse duration of $\Delta t = 100\,\mathrm{ps}$ the time evolution is shown in analogy to Figure 3.13. In panel (a) P_{tot} is chosen to be below the threshold, and in (b) above. The corresponding points on the input/output curve are indicated by the orange squares in Figure 3.12. The output intensity is normalized to unity.

For a longer pulse length of 100 ps a deviation from the cw result becomes apparent. Figure 3.13(b) reveals that now the pulse is broad enough for the emission dynamics to start already during the excitation. As two-level systems get excited, spontaneous emission already reduces their number before the stimulated emission starts to set in. Since only a fraction β of the spontaneous emission contributes to the emission into the laser mode, the part $(1-\beta)$ of excited two-level systems is lost for the emission into the laser mode, leading to a smaller number of photons in the input/output curve visible at equal pulse areas P_{tot}. The same holds for the 1 ns pulse, the time evolution of which is displayed in Figure 3.13(c).

Below the threshold only spontaneous emission takes place, so that the number of photons emitted into the laser mode is completely independent of the length of the pulse. This situation is depicted for an excitation length of 100 ps in Figure 3.14(a). Above the threshold the deviations visible in the threshold region for broad pulses disappear if the system is pumped hard enough. Then the system is driven faster into the regime of stimulated emission, as can be seen in panel (b) of the same figure.

To get a better understanding one may think of each point on the input/output curve corresponding to the time integral over the whole dynamics of the photon number n, as it is displayed exemplarily in Figs. 3.13 and 3.14. During the time evolution the system passes through different stages from spontaneous emission (when the system is mainly de-excited) to stimulated emission, and then back to mainly spontaneous

emission (after the stimulated processes have rapidly de-excited the system and only few excited two-level systems are left). The more pronounced the impact of spontaneous emission is, the greater the deviation from the cw result due to losses into leaky modes.

Above we have discussed the differences introduced into the system by pulsed excitation. It is important to note that the jump of the input/output curve from below to above threshold remains unaltered and displays the $1/\beta$ behavior known from cw-excited atomic laser models. We now turn to the semiconductor case.

3.5.2. Pulsed Excitation in Semiconductor Systems with Saturation

We describe the QD laser by the microscopic laser model that was introduced in Section 3.2 for N identical QDs with two energetically separated confined shells for electrons and holes. The transition from the lowest confined levels for electrons and holes is in resonance with the fundamental cavity mode, cf. Figure 3.2. The pulsed or cw excitation takes place in the p-shells of the QDs. Relaxation of carriers from the p- to the energetically lower s-shell is treated in relaxation time approximation. For the pump process and the relaxation, filling factors reflecting saturation due to Pauli blocking naturally ensure that the population is bound between zero and one.

We now present the results of the semiconductor model for the same material parameters that we have used in the atomic case. Additionally, relaxation times of 0.15 ps and 0.3 ps are used for holes and electrons, respectively, and the number of resonant QDs is $N = 170$. Note that these are realistic parameters for current micropillar laser devices [7]. In fact, the cw result displayed in Figure 3.15 corresponds to the calculation for the 2.6 μm pillar from Section 4.3. To avoid confusion, we anticipate that two different sets of input/output curves are shown in Figure 3.15: The solid lines represent the results of the semiconductor theory and are discussed with reference to the time evolution displayed in Figure 3.16, as was done before in the atomic case. The dashed lines display the same results without saturation effects. We first concentrate on the results including saturation effects. The input/output traces for pulsed excitation (thick lines) are shown in relation to the result for cw excitation (thin lines). Here, the time window assumed for the addition of the cw result to the figure is $T \approx 160$, cf. Section 3.5.1. Deviations between all five curves are striking, indicating a strong impact of the excitation pulse duration. While in the atomic case shorter pulses more closely resemble the cw results, here they show the strongest deviations due to strong saturation ($\Delta t = 1$ and 10 ps). This can be seen by looking at Figure 3.16 where the time evolution of the photon number and the electron
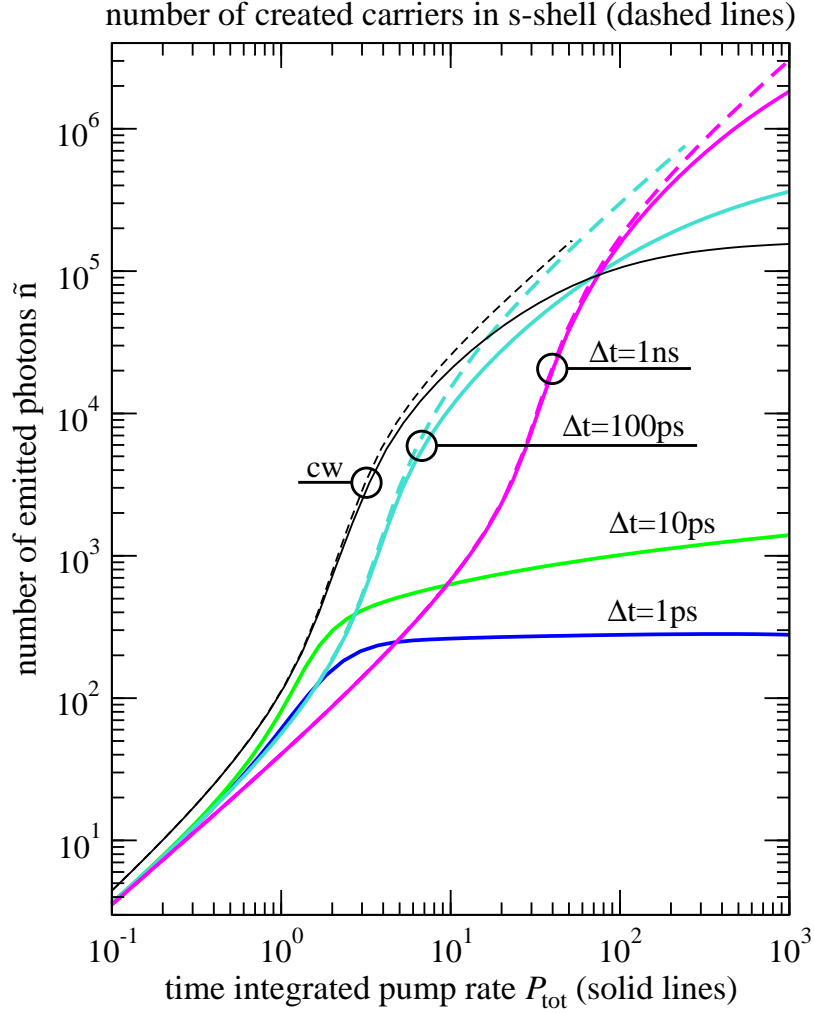
Figure 3.15.: Input/output curves for the semiconductor case for pulsed (thick lines) and cw excitation (thin lines). Shown are results for pulse widths of $\Delta t =$ 1, 10, 100 and 1000 ps. The solid lines correspond to the full semiconductor calculation, while the dashed lines indicate what the curves would look like without saturation effects. Note that the dashed lines resemble the situation depicted in Figure 3.12. Cw and pulsed results coincide for even lower pump powers ($P_{tot} < 10^{-2}$).
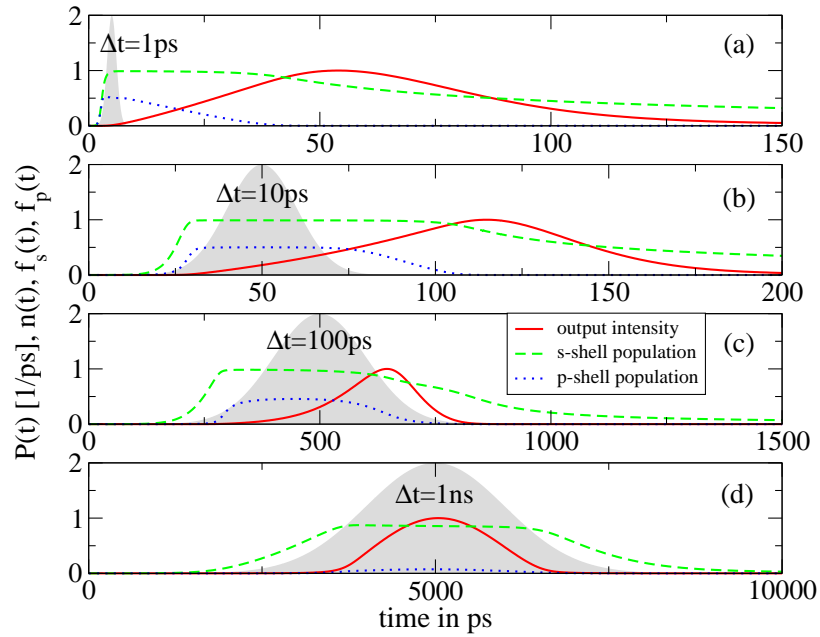
Figure 3.16.: Results of the semiconductor model. Time evolution for different pulse durations Δt and identical pulse areas of $P_{\text{tot}} = 100$. The plot is analogous to Figure 3.13, but in the semiconductor case the carrier population in the s- (green dashed line) and p-shell (blue dotted line) is shown.

population in the p- and s-shell is displayed for pump pulses, all with an area of $P_{\text{tot}} = 100$. The carriers created in the p-shell relax into the s-shell on a timescale of less than one ps. For pulse lengths much shorter than the spontaneous emission time (panels (a,b)) the population cannot be increased any further due to Pauli blocking, so that no more carriers are created by the pump pulse before the shells start to depopulate due to recombination processes. For $\Delta t = 1\,$ps this is not the case before the pulse is over, which explains the strong saturation of the input/output curve in Figure 3.15. Note that the considered optical pump process of the p-shell saturates for a carrier population $f_p^e + f_p^h = 1$, corresponding to transparency of the p-shell. In the $\Delta t = 10\,$ps case some emission can take place already during the excitation, so that in total more carriers can be created than in the previous case. As the pulse length becomes much longer than the spontaneous emission time, saturation effects become less important as the carrier generation is distributed over a longer time window with lower excitation. According to Figure 3.16(d) for $\Delta t = 1\,$ns the p-shell does not saturate at all.

The effect of Pauli blocking becomes even more distinct if the curves are shown without the effects of pump saturation. This can be demonstrated by replacing the area under the pump pulse P_{tot} on the x-axis by the rate of carriers truly created

in the QD *s*-shells. The corresponding curves have been added as dashed lines to Figure 3.15, to which the upper *x*-axis applies. Looking only at the dashed lines, the input/output curves in Figure 3.15 closely resemble the atomic case displayed in Figure 3.12. Referring to the discussion of the atomic case, emission after pump pulses much larger than the spontaneous emission time is subject to greater losses into non-lasing modes. The combination of the intensity reduction due to this effect for long pulses together with the saturation effects that are much more prominent for short pulses leads to the unfamiliar crossover behavior that is observed in Figure 3.15.

The presented results are of extreme relevance for current experiments where the input/output characteristics of semiconductor QD laser devices is used to determine the system parameters, especially the β-factor. Due to heating effects pulsed excitation is often preferred over cw excitation in experiments. Deviations in the height of the jump from below to above threshold have been observed for identical samples in the case of pulsed and cw excitation [144]. Typical experimental pulse durations are in the 1 ps range, resulting in a reduction of the jump as a caused by saturation effects, and thus misleads to estimate larger β-factors. Even in the case of cw excitation saturation can mask the upper branch of the input/output curve and lead to the prediction of wrong β-factors, which is clearly visible in Figure 3.15. It should be noted that the strength of the saturation effects depends on the number of available states where the excitation takes place. Here we consider carrier generation in the QD *p*-shells, leading to strong saturation. In case of WL excitation more carriers can be accommodated in the quasi-continuum states leading to weaker saturation effects at comparable pump intensities.

Even for a cw-excited QD laser showing no saturation at all the jump in the input/output curve is not given by $1/\beta$, as can be verified by looking at the blue line in Figure 3.15 where the deviation from this atomic result is approximately a factor of 2. This effect has been discussed before and is due to modifications to the source term of spontaneous emission, and the absence of complete inversion in the carrier system [53, 144].

3.6. Conclusion

In this chapter we have extended the semiconductor luminescence equations from Chapter 2 to a full semiconductor laser theory. Our model is applicable to any microcavity laser devices that use QDs as the active medium. Furthermore, by taking correlation functions up to the quadruplet level, we can calculate the photon second-order correlation function $g^{(2)}(0)$, which is crucial for the determination of the

threshold characteristics of semiconductor laser with high spontaneous emission coupling β.

We have presented representative results for current state-of-the-art QD lasers and found that the s-shaped intensity jump in the input/output curve becomes smooth for the large β-values that can be achieved with current microresonators. This broadened transition region is accompanied by a gradual change in the photon statistics from thermal to coherent emission. We have shown that a deviation from thermal emission is possible already below threshold in two cases: Either in microcavity lasers with few emitters, as we could show analytically, or in systems where the cavity lifetime exceeds the spontaneous emission time, resulting in an accumulation of photons in the cavity already in the spontaneous emission regime.

Finally, a theory-experiment collaboration was presented where our theory was used to characterize QD micropillar lasers. The broadened laser transition is observed also in the experiments. Above threshold saturation effects become visible, which are included in our semiconductor approach. The photon statistics of the emission has been measured on a Hanbury-Brown and Twiss setup. Explicitly considering the limited time resolution of the experimental setup, our calculations are in good agreement with the measurements.

With the intention to study to what extent information can be obtained merely from the input/output characteristics, we have investigated the influence of pulsed excitation in an atomic and a semiconductor-QD laser model. We have revealed a significant impact of the pulse duration on the input/output characteristics. It was shown that pulses shorter than the spontaneous emission time of the system coincide with the case of cw excitation if saturation is absent in the system (atomic case). Pauli-blocking of the carrier states (semiconductor case), on the other hand, results in the deviation from the cw result and in a reduction of the jump in the input/output curve especially for pulses shorter than the spontaneous emission time, but remaining visible even in the case of cw excitation. Ultimately, the implication is that, even though atomic laser models based on rate equations or a master equation approach provide convenient methods to fit the input/output characteristics of QD microcavity lasers, they are likely to miscalculate important parameters, like the β-factor.

Most importantly, our approach opens up the possibility to include the full spectrum of semiconductor effects in a consistent and well-defined manner. Besides a more complete inclusion of Coulomb correlations beyond the singlet level, relaxation and dephasing processes can also be treated on a microscopic level. Furthermore, interaction-induced correlations between different QDs, like superradiant coupling, can be studied. While these are future prospects, they outline the direction of future studies.

4. Calculation of Two-Time Operator Averages: First-Order Coherence in Quantum-Dot Microcavity Lasers

The coherence length of radiation is one of the most fundamental properties of a laser. Its knowledge is a crucial precondition for applications in interferometry and related areas. In recent years, intense research on the fabrication and physics of microcavity lasers has been performed due to their high potential for ultra-low threshold or even thresholdless lasers [8, 31, 38, 95, 102, 104, 114, 117, 138, 144]. Due to the lack of a clearly developed threshold in systems where the spontaneous emission coupling factor β approaches unity, the determination of the lasing onset becomes increasingly difficult. In Chapter 3 the second-order correlation function was used to identify the region of coherent emission in quantum-dot-based microcavity lasers. In this chapter, the coherence length of the emitted light will be investigated, which complements the studies of the autocorrelation function.

Although what follows can topically be understood as a part of the chapter "Laser Theory for Quantum Dots in Microcavities", it is devoted an own chapter. The calculation of two-time correlation functions is not a mere extension of the laser theory based on the semiconductor luminescence equations, but a new concept that can, in principle, be carried over to the calculation of other two-time quantities.

After a short introduction about first-order coherence, we demonstrate how correlation functions with two time arguments can be calculated and show theoretical results in Section 4.2. The theory has been developed in close collaboration with experimentalists. The achievements are presented in Section 4.3.

4.1. First Order Coherence

Coherence in usually associated with the occurrence of fringes in an interference experiment. In a Michelson interferometer, for example, a quasi-monochromatic beam is divided into two by a beam splitter. By means of a moving mirror, a time delay Δt is introduced to one of the beams before they are reunited. Only if this time delay

is shorter than the coherence time τ_{coh}, interference fringes can be observed between the two beams. The visibility of the interference fringes is directly described by the first-order correlation function, which we write in terms of photon operators for the laser mode

$$g^{(1)}(\tau) = \frac{\langle b^{\dagger}(t)b(t+\tau)\rangle}{\langle b^{\dagger}(t)b(t)\rangle} \ . \tag{4.1}$$

The loss of coherence carries over to the second-order correlation function $g^{(2)}(\tau)$. In Chapter 3 we were only concerned with its value at zero delay time. No matter if the light is thermal, coherent or exhibits an antibunching signature— the second-order correlation approaches a value of unity at long delay times. For thermal light this happens on the timescale of the coherence time [87]. The coherence time can be calculated from the first-order correlation function:

$$\tau_{\mathrm{c}} = \int_{-\infty}^{\infty} |g^{(1)}(\tau)|^2 d\tau \ . \tag{4.2}$$

4.2. Calculation of Two-Time Quantities

In quantum optics two-time operator averages can be conveniently accessed by invoking the quantum regression theorem [29, 154]. The quantum regression theorem, however, requires the equations of motion to be linear and, therefore, applies to two-level systems with single excitations. Due to the unavoidable factorization of the equations of motion in the semiconductor model, the initial linearity of the model is spoiled. With the source-term of spontaneous emission, our equations are nonlinear already on the singlet level so the quantum regression theorem in its usual form cannot be applied.

A straightforward approach lies in the equation-of-motion-technique itself with the time derivative now taken with respect to the delay time τ. In order to obtain the dynamics of a quantity $F(t, t+\tau)$ with respect to the time difference τ, in a first step the single-time problem is solved for $\tau = 0$. In a second step, the τ-evolution is evaluated according to its own equation of motion. The initial value is given by the $\tau = 0$ result obtained in the first step.

This method is now demonstrated in the calculation of the first order coherence function. We use the Hamiltonian and the methods introduced in the second chapter. In order to obtain non-rotating dynamical equations, we introduce

$$G(\tau) = e^{i\omega\tau}\langle b^{\dagger}(t)b(t+\tau)\rangle \ , \tag{4.3}$$

which obeys the following equation of motion

$$\left(\hbar\frac{\mathrm{d}}{\mathrm{d}\tau} + \kappa\right)G(\tau) = \sum_\nu g_\nu^* P_\nu(\tau) \;, \tag{4.4}$$

where have introduced the two-time photon-assisted polarization

$$P_\nu(\tau) = e^{i\omega\tau}\langle b^\dagger(t)v_\nu^\dagger(t+\tau)c_\nu(t+\tau)\rangle \;. \tag{4.5}$$

For the time evolution of the two-time photon-assisted polarization with respect to τ we find

$$\left(\hbar\frac{\mathrm{d}}{\mathrm{d}\tau} - i\left[\hbar\omega - (\tilde\varepsilon_\nu^e + \tilde\varepsilon_\nu^h)\right] + \Gamma\right)P_\nu(\tau)e^{-i\omega\tau} =$$
$$\sum_\xi g_\xi\,\langle b^\dagger(t)b_\xi(t+\tau)c_\nu^\dagger(t+\tau)c_\nu(t+\tau)\rangle$$
$$-\sum_\xi g_\xi\,\langle b^\dagger(t)b_\xi(t+\tau)v_\nu^\dagger(t+\tau)v_\nu(t+\tau)\rangle \;. \tag{4.6}$$

This equation can be simplified significantly if we endeavor the same assumptions that we have used in the definition of the laser system in Chapter 3, cf. Section 3.2.1. In the following we shall consider N identical quantum dots that are on resonance with the laser mode, so that the complex energy term in Eq. (4.6) vanishes and the state indices, now only referring to s-shell carriers, can be dropped. Furthermore, terms coupling different modes are neglected according to the discussion in Section 2.7.1. With $g^{(1)}(\tau)$ being a doublet quantity (two-particle average) in the cluster expansion scheme, we truncate the hierarchy consistently at the same level. For the averages in the last two lines of Eq. (4.6) this is similar to the semiclassical factorization, i.e. the factorization of the photonic and electronic degrees of freedom. With these approximations, we finally arrive at the closed set of equations

$$\left(\hbar\frac{\mathrm{d}}{\mathrm{d}\tau} + \kappa\right)G(\tau) = g^*P(\tau) \;, \tag{4.7}$$

$$\left(\hbar\frac{\mathrm{d}}{\mathrm{d}\tau} + \Gamma\right)P(\tau) = gN(f^c - f^v)G(\tau) \;, \tag{4.8}$$

where we have introduced $P(\tau) = \sum_\nu P_\nu(\tau)$. These two first-order differential equations can be cast into a single one of second order

$$\left(\hbar^2\frac{\mathrm{d}^2}{\mathrm{d}\tau^2} + \hbar(\kappa + \Gamma)\frac{\mathrm{d}}{\mathrm{d}\tau}\right)G(\tau) = \left(|g|^2\,N(f^c - f^v) - \kappa\Gamma\right)G(\tau) \;, \tag{4.9}$$

which can be solved to give for the normalized first-order correlation function

$$\left|g^{(1)}(\tau)\right| = \frac{-\gamma_-}{\gamma_+ - \gamma_-}e^{-\gamma_+|\tau|} + \frac{\gamma_+}{\gamma_+ - \gamma_-}e^{-\gamma_-|\tau|} \tag{4.10}$$
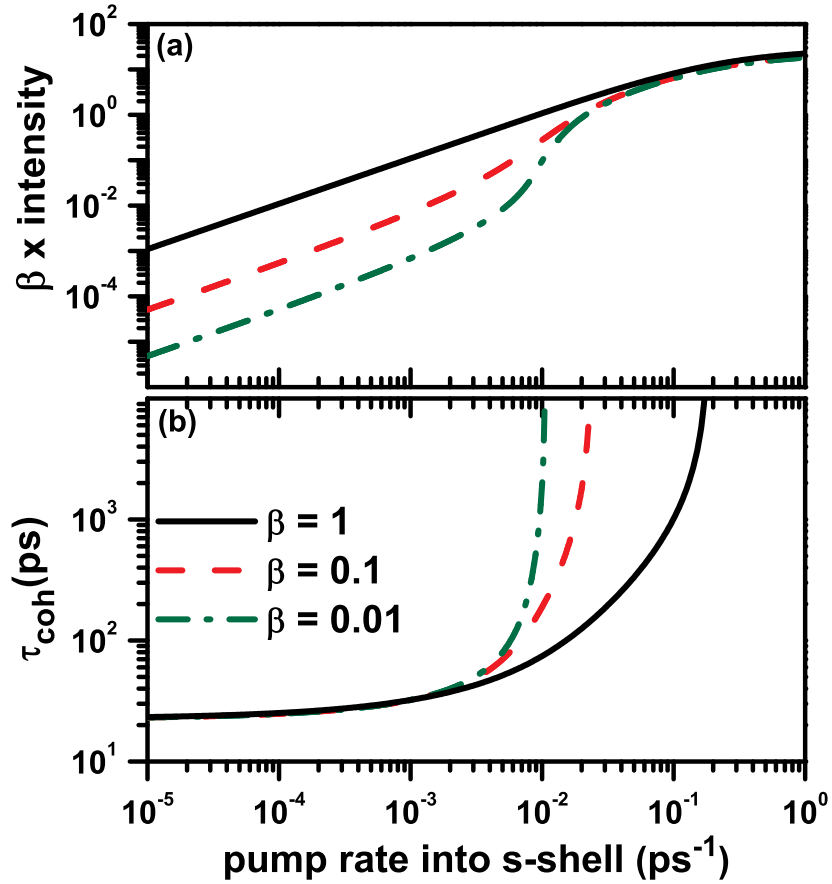
Figure 4.1.: Theoretical input/output curves (top) and coherence times (bottom) for various values of the β parameter. The curve for $\beta = 0.01$ equals that of the 6 μm pillar shown in Figure 4.2. For $\beta = 0.1$ and $\beta = 1$, 50 and 5 QDs have been used, respectively. All other parameters remain unaltered.

with

$$\hbar\gamma_{\pm} = \frac{\kappa + \Gamma}{2} \pm \sqrt{|g|^2 N(f^c - f^v) + \frac{(\kappa - \Gamma)^2}{4}} \ . \qquad (4.11)$$

The stationary populations of the lowest confined QD states f^c and f^v are obtained from the stationary solutions of the dynamic laser equations. From Eq. (4.2) and the equations above, we find for the coherence time

$$\tau_{\mathrm{c}} = \frac{1}{\gamma_+} + \frac{1}{\gamma_-} + \frac{\hbar}{\kappa + \Gamma} \ . \qquad (4.12)$$

In Figure 4.1 the coherence time obtained from Eqs. (4.11) and (4.12) is shown together with the input/output curves for three different values of the spontaneous emission coupling factor β. The parameters for the $\beta = 0.01$ curve are the following:

$N = 500$ QDs, total spontaneous emission time $\tau_{\text{sp}} = 80$ ps, homogeneous QD broadening $\Gamma \approx 200$ μeV, and cavity losses $2\kappa = 30\mu$eV. For the $\beta = 0.1$ ($\beta = 1$) curve, $N = 50$ (5) QDs was used. As the threshold region is approached, a strong increase in the coherence time is observed. While below threshold the value lies between 20 and 30 ps for all three curves, the coherence time is found to increase slower with increasing pump power in cavities with larger spontaneous emission coupling: At comparable points on the input/output curves, we find that devices with a larger β factor display shorter coherence times. An illustrative explanation is that fluctuations introduced by spontaneous emission processes decrease the coherence in the system, and at higher β values more spontaneous emission is coupled into the laser mode. At the same time, even in the 'thresholdless' case of $\beta = 1$, the slower, but nevertheless distinct rise in the coherence time indicates the beginning of the threshold region.

4.3. Comparison with Experiments

In collaboration with the group of Prof. Peter Michler in Stuttgart we have performed studies of first-order coherence in elliptical micropillar structures with InGaAs QDs as the active medium. Details about growth and experimental setup can be found in Refs. [7, 8]. The field-correlation measurements were performed on a Michelson interferometer consisting of a 50/50 non-polarizing beam splitter and two retro-reflectors orthogonal to each other, one of them movable. The interference pattern was recorded with an avalanche photo diode. As the mode spectrum is non-degenerate in elliptical pillars [8] [93, article by Gérard], the measurements were performed on the component with higher energy. A typical mode spectrum is shown in Figure 4.2(a), the fundamental mode (left peak) is well separated from the higher excited modes.

In the lower panel of Fig 4.2 the input/output curves are shown for the pillars with 6, 2.6 and 1.8 μm diameter. An s-shaped smooth transition from spontaneous to dominating stimulated emission is observed for all pillars, as it has been in many experiments with high-β lasers [114, 138, 144], cf. also Chapter 3. In analogy to Section 3.4 we calculate the input/output characteristics of the microcavity samples by using the extended laser equations derived in Section 3.2. With the following parameters we find a consistent overall description and an estimate of the structural parameters of the experiment. For the 6 μm pillar a number of 500 QDs (2.6 μm: 170, 1.8 μm: 80) is used, along with a total spontaneous time of 80 ps (2.6 μm: 55 ps, 1.8 μm: 45 ps) and a homogeneous QD broadening of $\Gamma \approx 200$ μeV. Furthermore, we consider the measured Q-factors of 44, 500 (6 μm), 38, 000 (2.6 μm) and 20, 000 (1.8 μm) that have been derived from coherence time measurements around the transparency point (where the system switches from absorption to gain) via Fourier transformation

[49]. The β-factor is used to fit the height of the jump in the input/output curves to the experiment. The results are shown as solid lines in Fig.4.2. For the 6 μm and 2.6 μm pillar we obtain β-values of 0.01 and 0.03, respectively. For the smallest pillar heating effects cause instabilities that limit the maximum excitation power. This becomes clearly visible above an excitation power of 3 mW. A β value of 0.05 has been estimated in this case by extrapolation.[1]

The coherence properties of the fundamental mode emission have been investigated by direct measurements of the first-order correlation function, which is possible by the analysis of the visibility $V(\tau)$ of interference fringes observed at the output port of the Michelson interferometer according to $V(\tau) = (I_{\max} - I_{\min})/(I_{\max} + I_{\min}) = \left|g^{(1)}(\tau)\right|$ [87]. Therefore, the coherence time of the fundamental mode at a certain power can be obtained from the evolution of the visibility with increasing delay times τ. An example of such highly resolved interference fringes is shown in the inset of Figure 4.3 with more than 95% visibility around zero delay. Visibility measurements were carried out at different pump powers covering the whole transition regime between spontaneous to dominating stimulated emission. Results from the fundamental mode emission of the 2.6 μm pillar are presented in Figure 4.3. A clear qualitative change of the visibilities from a Gaussian-like profile to a more exponential behavior can be observed within the transition regimes of all investigated micropillars. In addition to the experimental data, the first-order correlation function according to Eqs. (4.1) and (4.11) is shown as solid lines in the same figure. As can be seen, the theory predicts the coherence times and lineshapes of the visibilities very well.

The qualitative change of the lineshape can also be seen in the analytical solutions of the coherence function. Expanding Eq. (4.1) in a Taylor series reveals the Gaussian-like characteristic in the decay of $|g^{(1)}(\tau)|$, as the term linear in τ drops out. Considering the solutions $\gamma_\pm$ at transparency, $f^c - f^v = 0$, we get $\gamma_+ = \Gamma \gg \gamma_- = \kappa$, yielding a decay that is close to exponential $|g^{(1)}(\tau)| = e^{-\gamma_- \tau}$.

The decay of the first order coherence function gives direct access to the coherence time according to Eq. (4.2). The coherence times extracted from the measurements shown in Figure 4.3 and for two other pillars are shown in Figure 4.4. Interference measurements at low pump powers yield coherence times around 20–30 ps, corresponding to linewidths of 140–90 μeV. A nonlinear increase of τ_c is observed near and above the transition region. For the 6 μm pillar the coherence time increases from 30 ps to $\sim$ 990 ps. The solid lines represent the numerical results obtained from

---

[1]For all pillars the parameters were determined not only by matching the input/output characteristic, but also the decay of the first-order correlation function and the coherence time. Thus, even with uncertainties in the upper branch of the measured output intensity, we can reproduce the overall behavior with the chosen parameters.

Eqs. (4.11) and (4.12). They are in good agreement with the results derived from the measurements[2], although there is a tendency of a slight underestimation of the coherence time visible far below threshold.

At this point it is important to highlight that with the 6 μm pillar ($\beta = 0.01$), the longest achievable coherence length is $l_c = c\tau_c \approx 30$ cm, whereas significantly smaller values of $l_c \approx 7.5$ cm ($\beta_{2.6\mu m} = 0.03$) and ≈ 3 cm ($\beta_{1.8\mu m} = 0.05$) can be obtained from the smaller-sized structures. The value of τ_c at a given power level is strongly affected by the value of β, namely the residual contribution of spontaneous (incoherent) processes coupled into the emission channel. Our calculation for various β-values in the previous section highlights this feature as well, as can be seen in Figure 4.1.

4.4. Conclusion

In this chapter an extension of the laser model from Chapter 3 to two-time quantities has been discussed using the first-order coherence function $g^{(1)}(\tau)$ as an example. For the stationary limit of this particular case, and restricting ourselves to the doublet-level in the cluster expansion, an analytic solution could be obtained for the coherence time and the first-order coherence function itself.

A steep non-linear increase in the coherence time is observed around the laser transition. In particular, at comparable points on the input/output curve, lasers with larger β factors are found to exhibit a shorter coherence time. This is accompanied by a gradual change in the decay characteristics of $g^{(1)}(\tau)$ from Gaussian-like to exponential. These findings are very well explained by the analytical solution of the first-order coherence function.

In general, the described method can be used to calculate other two-time quantities. It must be realized, however, that the number of equations of motions required to be solved increases rapidly with increasing order, as commutation relations do not apply to operators with differing time arguments. For the second-order correlation function at finite delay times, a different approach based on a modified version of the quantum regression theorem has successfully been applied [150]. This topic, however, is not covered in this thesis.

---

[2]Depending on the shape of the measured visibility $V(\tau)$, a Gaussian or a Lorentzian fit function has been used to extract the coherence times.
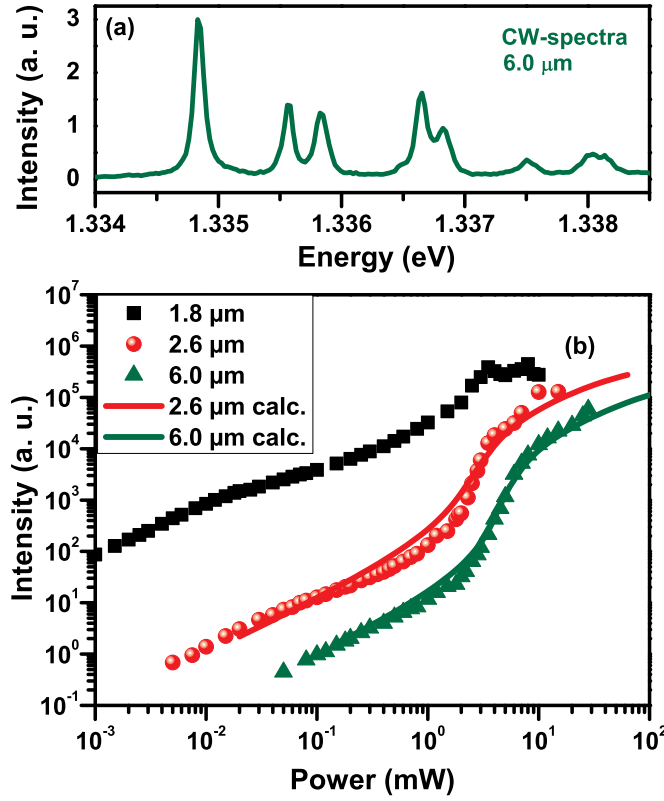
Figure 4.2.: (a) A typical high-resolution linearly polarized μ-PL spectrum taken at $P = 0.5$ mW from a 6 μm elliptical micropillar showing the fundamental and higher excited modes. (b) Excitation power-dependent output intensity of the fundamental mode emission from 1.8, 2.6, and 6 μm pillars in a log-log plot under non-resonant cw-excitation conditions. The curves are shifted for clarity. Due to heating effects at high excitation conditions, the upper branch of the 1.8 μm pillar is not fully covered. Solid lines represent the calculated curves from which β is determined. Theoretical results are shifted to match the mW scale of the experiment.
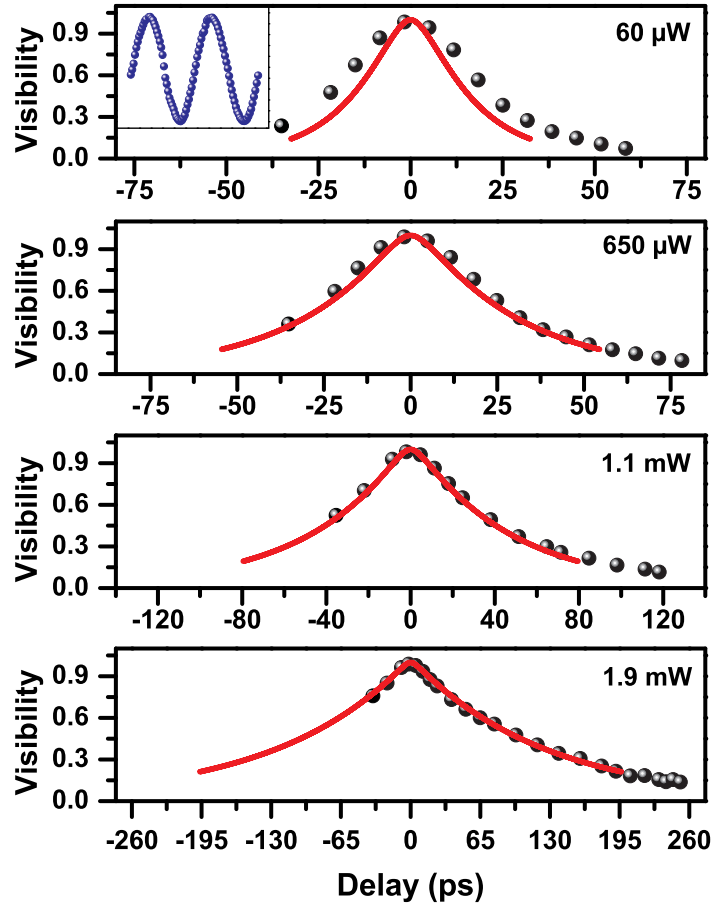
Figure 4.3.: Visibility curves of the fundamental mode emission from the 2.6 μm pillar at different excitation powers. A gradual change in the visibility profile from Gaussian-like to a more exponential behavior becomes evident with increasing excitation power. The calculation (solid lines) is in excellent agreement with the measured results (dots). Inset: a typical high resolution interference fringe from the fundamental mode at a certain delay time with $V(\tau)$ over 95%.
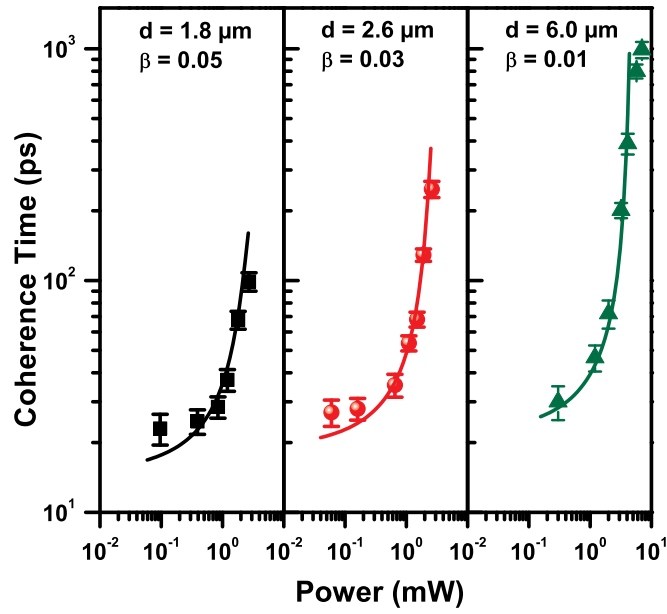
Figure 4.4.: Pump-power dependence of the coherence time τ_c of the fundamental mode emission for 1.8 (squares), 2.6 (spheres), and 6 μm (triangles) pillars in a log-log plot. A nonlinear increase in coherence time is observed for all pillars. As depicted in the figure, longer coherence times were observed for low-β pillars. An excellent agreement with the calculation (solid lines) is presented. Theoretical results are shifted to match the mW scale of the experiment.

5. Comparison with Atomic Models

Due to their discrete level structure, QDs are frequently referred to as 'artificial atoms'. To some extent the use of atomic models for the description of QDs is justified as long as many-body effects are negligible. In fact, without Coulomb interaction and under the assumption that QDs are true two-level systems, in which only a single excitation is possible, the semiconductor theory reduces to the atomic model, as we will show in this chapter.

In quantum optics, access to photon-intensity fluctuations can either be obtained by invoking the quantum regression theorem [92, 125, 154], or by using methods to calculate the diagonal density matrix for the coupled atom-photon system. Both methods are not directly applicable in semiconductors due to the presence of many-body effects, multiple excited carriers in a QD, and the modified source term of spontaneous emission. Nonlinearities are unavoidably introduced by the truncation of the theory. For the general case we have developed a comprehensive many-body treatment of the light-matter interaction in QD-based systems in the previous chapters. As it turns out, every equation-of-motion approach including either or both light-matter and Coulomb interaction inherits a hierarchy problem that must be truncated for calculations.

In this chapter we discuss three well-established quantum-optical models that are connected with each other and with the equation-of-motion approach that our semiconductor model is based on: The rate equations (Section 5.1) , the master equation (Section 5.2) and the Liouville/von-Neumann equation (Section 5.3). The rate equations are the most simple model to describe lasing. We show how they can be obtained from our semiconductor model in the 'atomic limit' mentioned above. The master equation yields the diagonal elements of the density matrix that describe probabilities. From the solution of the master equation the statistical properties of the emitted light can be calculated. Therefore, it is possible to compare both the input/output curve and the second-order correlation function obtained from the this density matrix approach and from the semiconductor model in the 'atomic limit'. Since no factorization of the correlations between the carrier and the photonic system is needed in the solution of the master equation, this comparison allows for a direct verification of the truncation of the infinite hierarchy of equations of motion by means of the cluster
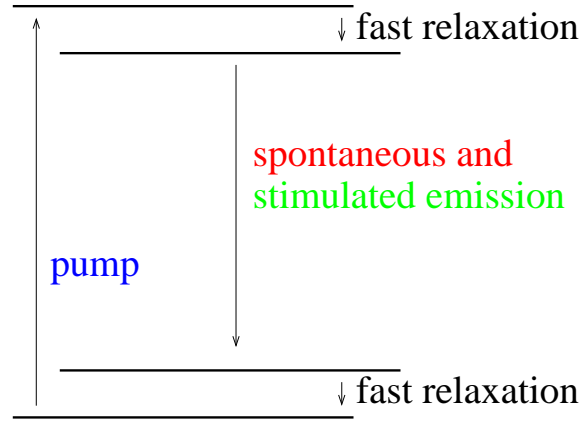
Figure 5.1.: The atomic rate equations describe the dynamics between the upper and lower laser levels. The dynamics of the upper and lower pump levels is adiabatically eliminated under the assumption of fast relaxation processes into and from the laser levels.

expansion technique. In the third part of this chapter, we present the most fundamental quantum-optical treatment of light-matter interaction, which is the solution of the Liouville/von-Neumann equation that yields the full density matrix. At the same time, it is possible to derive a hierarchy of equations of motion for operator averages from the Liouville/von-Neumann equation, which is demonstrated in Section 5.3.2. This hierarchy can be truncated by means of the cluster expansion method, so that an exact and a truncated version of the very same theory can numerically be compared. This offers the best possible verification of the truncation method that our semiconductor model is based on. Furthermore, it is possible to identify the derived equations of motion with those of the semiconductor laser model from Chapter 3 in the 'atomic limit', so that insight into the appearance of dephasing and scattering terms can be obtained (Section 5.3.5).

5.1. Rate Equation Limit of the SLE

In both atomic and semiconductor physics rate equations [21, 118, 156] are often used to describe lasing. Rate equations provide deterministic equations of motion for the population inversion and the light intensity. No further information about the properties of the light field can be obtained from this simple model, although two--time quantities can be derived from one-time quantities via the quantum regression theorem [92, 125, 154]. Access to the photon statistics can be obtained from more elaborate approaches, like the master equation that we discuss in the next section.

The frequently used rate equations can be derived in several ways, either phenomeno-

logically by introducing rates for the relevant processes indicated in Figure 5.1, or by tracing over the density matrix obtained from a master equation or the Liouville/von-Neumann equation (cf. Sections 5.2 and 5.3). In the latter case, correlations between atoms and photons are completely neglected, i.e., $\langle nN \rangle = \langle n \rangle \langle N \rangle$. Since these terms appear only in the contributions representing stimulated emission, the treatment of these processes then corresponds to a semi-classical picture. It is by no means necessary to truncate the equations of motion at the simplest possible level that leads to the rate equations. The truncation can be performed on a higher level in the hierarchy. For the additional terms separate equations of motion have to be formulated. This way, for example, it is possible to obtain insight into the statistical properties of the light field, represented by the photon-photon correlations $\langle n^2 \rangle$, via the equation-of-motion approach in an analogous fashion to the rate equations.

In the following we show how the atomic rate equation model can be obtained from the semiconductor theory developed in the previous chapter as a limiting case. In order to arrive at an atomic model, the semiconductor specific source term of spontaneous emission $f_\nu^e f_\nu^h$ in Eqs. (3.14), (3.19) and (3.20) is replaced by the electron population f_ν^e. This is because successive destruction of more than one carrier always yields zero in the case of a two-level system, where only one electron is present per independent emitter, in which case $c_\nu v_\nu = 0$. Then the source of spontaneous emission $\langle c_\alpha^\dagger v_\alpha v_\nu^\dagger c_\nu \rangle$ arising in Eq. (3.13) is found to reduce to $\langle c_\alpha^\dagger c_\nu \rangle \delta_{\alpha\nu} = f_\nu^e$. Furthermore, full inversion of the laser transition is assumed, $1 - f_s^h = \langle v_s^\dagger v_s \rangle = 0$, which is usually well justified for atomic four-level laser systems (but not for QDs). Finally we insert the adiabatic solution of Eq. (3.14) into Eq. (3.11). Introducing the number of excited emitters $\bar{N} = f_s^e N$, where N is the total number of emitters that arises from the sum over all states in Eq. (3.11), we find for the photon number $n = \langle b^\dagger b \rangle$ in the laser mode

$$\frac{\mathrm{d}}{\mathrm{d}t} n = -2\kappa n + \frac{\beta}{\tau_{\mathrm{sp}}} \left[1 + n \right] \bar{N} \ . \tag{5.1}$$

The photon population is determined by the interplay of the cavity loss rate 2κ and the photon generation due to spontaneous processes $\propto \bar{N}$ and stimulated processes $\propto n\bar{N}$. The rate of photons leaving the cavity is given by $2\kappa n$. For the number of excited emitters we obtain from Eq. (3.19)

$$\frac{\mathrm{d}}{\mathrm{d}t} \bar{N} = -\frac{\beta}{\tau_{\mathrm{sp}}} n\bar{N} - \frac{1}{\tau_{\mathrm{sp}}} \bar{N} + \tilde{P} \ , \tag{5.2}$$

where, for atomic laser systems quite common, a constant pump rate $\tilde{P}$ has been used to describe the carrier-generation in the laser-transition level. Note that, in contrast to the pump rate per emitter in Eq. (3.19), $\tilde{P}$ corresponds to the total pump rate, see Section 3.2.1. The carrier recombination is determined by the stimulated emission
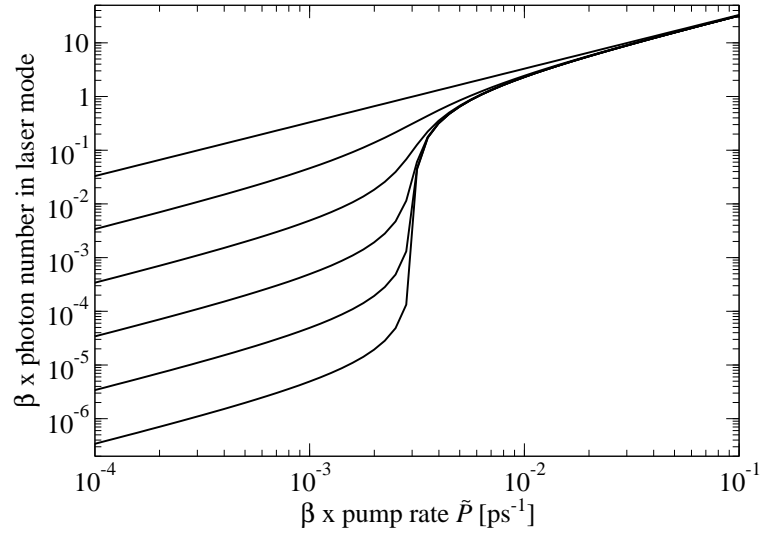
Figure 5.2.: Results from the atomic rate equations for $\beta = 1$ to 10^{-5} from top to bottom.

into the laser mode $\propto \beta/\tau_{\mathrm{sp}} = 1/\tau_l$, and by the spontaneous emission $\propto 1/\tau_{\mathrm{sp}}$ into all available modes.

With Eqs. (5.1) and (5.2) we have obtained the well-established rate equations. Results for the input/output curves for various values of the β-factor are shown in Figure 5.2. We choose the typical set of parameters that we also used in the previous chapter: $\tau_{\mathrm{sp}} = 50\,\mathrm{ps}$ and $\hbar\kappa = 20\,\mu\mathrm{eV}$. The corresponding cavity lifetime is about $17\,\mathrm{ps}$, yielding a Q-factor of roughly $30,000$. The curves show the typical intensity jump $\propto \beta^{-1}$ from below to above threshold. In the semiconductor case, where we have a nonlinear source term and incomplete population inversion, this is not the case. In the limit $\beta = 1$ the kink in the input/output curve disappears. The behavior of the jump is a commonly used criteria to estimate the β-factor from the measurements. For this reason it is important to note the differences between the results of this simple atomic rate equation model and the full semiconductor theory, cf. Figure 3.5. In semiconductor systems, even greater deviations from the $1/\beta$-height of the jump is to be expected for pulsed excitation due to saturation effects, see Section 3.5.

5.2. The Master Equation

In the previous section we have shown how the atomic rate equations are contained in the semiconductor laser equations derived in Section 3.2.1 as a limiting case. This is performed by replacing the QDs by two-level systems with only one possible excita-

tion. To arrive at the closed rate equations, terms up to the doublet level were kept, thus neglecting any carrier-photon and photon intensity correlations. Usually rate equations for the description of atomic [87, 118, 156] or semiconductor [21] systems are based on a phenomenological background. However, they can also be derived from density-matrix approaches, such as the master equation [118], by using certain approximations, like the factorization of the carrier and photonic degrees of freedom (semiclassical factorization), i.e. $\langle nN \rangle = \langle n \rangle \langle N \rangle$, where $\langle N \rangle$ is the number of excited atoms and $\langle n \rangle$ the photon number.

The solution of the master equation yields the diagonal elements of the density matrix without *any* truncation of correlations, and with it the possibility to obtain all relevant expectation values where all operators have equal time arguments. One important achievement of Chapter 3 is the calculation of the second-order photon correlation function $g^{(2)}(0)$, which relies on higher-order contributions in the cluster expansion. While photon correlations cannot be addressed in a rate equation model in the semiclassical limit (Section 5.1), they are contained in the master equation approach. To verify our approach in Chapter 3 to obtain the second-order correlation function from an equation-of-motion approach where correlations are taken up to the quadruplet level, we consider again the 'two-level' limit of the semiconductor model and compare the results for the input/output curve and for $g^{(2)}(0)$ with those obtained from the master equation model in the formulation of Rice and Carmichael [118].

5.2.1. The Master Equation

The master equation describes the evolution of the diagonal elements of the density matrix for the coupled atom-photon system. We introduce the notation

$$\rho_{n,N} = \langle n, N | \rho | n, N \rangle \tag{5.3}$$

for the matrix elements. As the diagonal matrix elements can be interpreted as the probabilities of states with N excited atoms and n photons in the cavity, often a simplified approach is taken to derive the time evolution. By considering all relevant processes that can act on a given state of the system, a birth/death model can be formulated where effective transition rates are introduced. This is illustrated in Figure 5.3. The figure is taken from Ref. [118], and in the notation of Rice and Carmichael λ is the cavity loss rate, P the pump rate and β is the spontaneous emission coupling factor. The arrows describe processes that can act on the state $\rho_{n,N}$, see the figure caption.
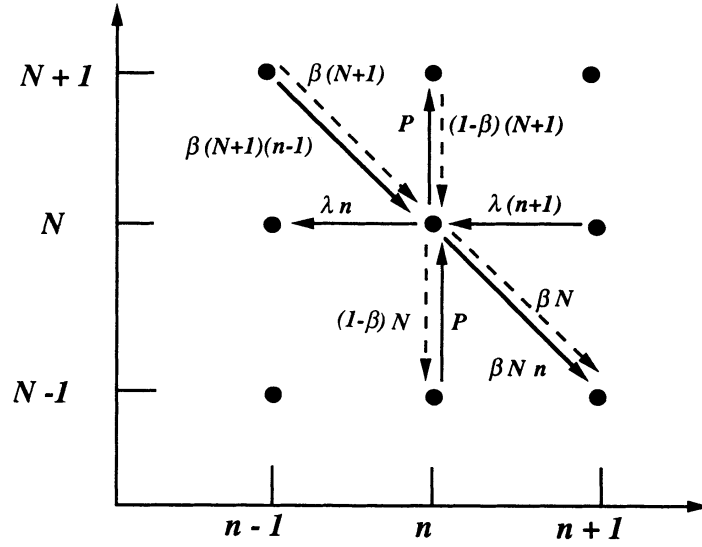
Figure 5.3.: Schematic representation of the relevant processes in the birth/death model. On the vertical axis the number of excited emitters N is shown, on the horizontal axis the number of photons n in the cavity mode. In the diagram, each dot stands for a matrix element of the diagonal density matrix $\rho_{n,N}$ and represents a state with the corresponding number of excited atoms and photons. Processes acting on a state with probability $\rho_{n,N}$ are: cavity losses, keeping the number of excited atoms unaltered and thus represented as horizontal line; pump process, keeping the number of photons unaltered and thus represented as vertical line; spontaneous and stimulated emission, where the number of excited emitters is reduced and the number of photons in increased, thus represented as diagonal lines. The figure is taken from Ref. [118].

As an example we consider the spontaneous emission into non-lasing modes, indicated as dashed lines in the vertical direction since the number of photons in the cavity remains unaltered by this process. The contribution to the equation of motion is read off the schematic as

$$\tau_{\text{sp}} \frac{\mathrm{d}}{\mathrm{d}t} \rho_{n,N}\Big|_{\text{nl}} = -(1 - \beta) \left[N\rho_{n,N} - (N + 1)\rho_{n,N+1} \right] . \tag{5.4}$$

The prefactor $(1 - \beta)/\tau_{\text{sp}}$ describes the rate of spontaneous emission into non-lasing modes, assuring that there is no emission at all into these modes in the case $\beta = 1$. There are two possibilities involving a state with N excited emitters, either a decay ('death') of the very same state (after emission a state with $N-1$ excited emitters is left), or its 'birth' by the decay of a state with $N+1$ excited emitters. The full master equation with all contributions displayed in Fig. 5.3 can be found in Ref. [118].

Being a phenomenological approach, it is not immediately clear that it is accurate.

It is justified by the fact that it reproduces the rate equations if quantum mechanical averages $\langle nN \rangle$ are factorized into photon and carrier number $\langle n \rangle \langle N \rangle$. With good intuition this also works the other way around: With some physical assumptions, the rate equations can be rewritten to yield the master equation, as is shown in Chapter 7 in Ref. [29]. Quantum optics, however, provides us with much more stringent methods for describing non-equilibrium open systems, like lasers. In the third section of this chapter we present a method for the calculation of the full density matrix $\langle n, j | \rho | n', j' \rangle$ by solving the Liouville/von-Neumann equation. The diagonal density matrix considered here can be recovered from that model by adiabatically eliminating the dynamics of the off-diagonal elements. In the adiabatic regime, the dephasing is sufficiently fast to dominate over the dynamics, so that the off-diagonal elements simply follow without delay their sources (incoherent regime). Furthermore, the contributions of the cavity losses to the dephasing of the off-diagonal density matrix elements need to be small [98].

5.2.2. Comparison with the Equation-of-Motion Approach

In order to facilitate a direct comparison between the input/output curve and the second-order correlation function obtained from the semiconductor approach in Chapter 3 and the master equation, we assume again a modified two-level version of the semiconductor model, in which only one excitation per emitter is possible. We have shown in Section 5.1 that the source term of spontaneous emission reduces to f_ν^e under this assumption. The fact that two carriers can never be successively annihilated, $c_\nu v_\nu = 0$ leads to a modification of the equation of motion (3.22) to

$$\left(\hbar \frac{\mathrm{d}}{\mathrm{d}t} + 3\kappa + \Gamma \right) \delta \langle b^\dagger b^\dagger b v_\nu^\dagger c_\nu \rangle =$$
$$-4 \left| g \right|^2 \langle b_\xi^\dagger v_\nu^\dagger c_\nu \rangle \, \mathrm{Re} \langle b_\xi^\dagger v_\nu^\dagger c_\nu \rangle - \left(1 - f_\nu^e - f_\nu^h \right) \delta \langle b^\dagger b^\dagger bb \rangle + 2\delta \langle b^\dagger b c_\nu^\dagger c_\nu \rangle \, , \quad (5.5)$$

again neglecting the quadruplet-level correlation functions appearing on the right hand side and scaling with the light-matter coupling strength.[1] All other equations of motion for the correlations remain unmodified under the two-level assumptions. In order to quantitatively compare to the master equation given in Ref. [118], we must once more assume a fully inverted system, which is done by setting $1 - f_\nu^h = 0$ in the two-level version of Eq. (3.14) and in Eq. (5.5). Due to the coupling to the correlation

---

[1] For the derivation of this equation note that $c_\nu v_\nu = 0$ already on the operator level, i.e. before taking the expectation value. In particular $\sum_{\nu'} b^\dagger b c_{\nu'}^\dagger v_\nu^\dagger v_{\nu'} c_\nu \equiv \sum_{\nu' \neq \nu} b^\dagger b c_{\nu'}^\dagger v_\nu^\dagger v_{\nu'} c_\nu$. As a consequence, the term $\nu = \nu'$ drops out *before* the expectation value is taken and the factorization is performed, regardless of the fact that the factorized expectation values $\langle b^\dagger v_\nu^\dagger c_\nu \rangle \langle b c_{\nu'}^\dagger v_{\nu'} \rangle$ are not zero.

functions in Eq. (3.14), an adiabatic solution in the spirit of the rate equations (5.1) and (5.2) is no longer possible. Nevertheless, the numerical steady-state solution can be directly compared to the results of the master equation approach. The master equation itself relies on the adiabatic elimination of the dynamics of the off-diagonal density-matrix elements, which has no influence on the steady-state results.

We solve Eqs. (3.11) and (3.13) together with Eqs. (3.19) and (3.20) for the population dynamics of the laser and pump level (with $f_\nu^e f_\nu^h$ replaced by f_ν^e for the spontaneous emission). This allows us to avoid the introduction of a number of excited two-level systems. For the direct comparison with the master equations, $R_{p \to s}^{e,h}$ is used as a measure for the carrier generation rate at the laser transition level.

Figure 5.4 shows numerical results from our truncated cluster expansion model applied to two-level systems, in comparison to results obtained from the master equation. The values for the parameters κ, $\tilde{N}$, and $\tau_{\rm sp}$ were taken from Section 5.1 and are the same as for Figure 5.2. Additionally relaxation rates entering $R_{p \to s}^{e,h}$ for both electrons and holes of 1 ps, and a dephasing $\Gamma = 1.36\,\mathrm{meV}$, corresponding to a dephasing time of approximately 500 fs, was used. The figure shows the second-order correlation function atop the input/output curve for various values of the β-factor. Looking at the input/output curves, we see that the equation-of-motion approach agrees convincingly well with the results from the master equation for all values of β. Regarding the autocorrelation function in the top panel, there is excellent agreement for small values of the β-factor. A deviation of roughly 5% becomes apparent as β is increased to unity, and the results are in good agreement regarding the onset and the end of the transition from thermal to coherent light emission.

As mentioned above, the x-axis in Figure 5.4 corresponds to the number of carriers that are truly generated at the laser transition, rather than the carrier generation rate in the pump levels. This means that pump saturation effects due to Pauli blocking, although included in the calculation, are not visible in the figure.

The deviation between lines and symbols in Figure 5.4 is a direct measure for the applicability of the theory with carrier-photon correlations truncated on the quadruplet level by means of the cluster expansion method. The agreement between the truncated (cluster expansion) and non-truncated (master equation) description of atomic two-level systems depends on parameters like the cavity lifetime and the spontaneous emission rate. For the above comparison, typical values of current microcavities have been used. Possible deviations between the two-level version of the cluster expansion model and the master equation must be considered alongside the modifications due to semiconductor effects, which can be significant. As long as the semiconductor theory is used for parameters where its two-level version is in agreement with the master
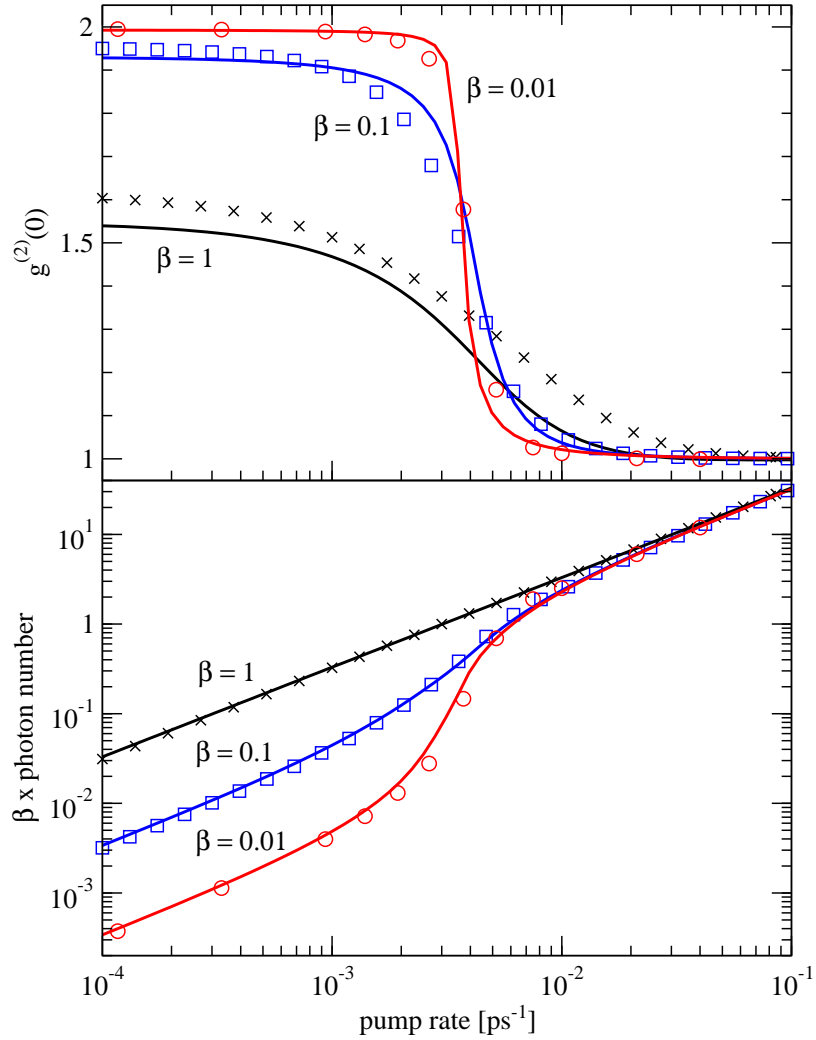
Figure 5.4.: Autocorrelation function (top) and input/output curve (bottom) for a fully inverted two-level system. Comparison between the master equation (symbols) and the two-level version of the semiconductor theory (solid lines) for $\beta = 1$, 0.1, and 0.01. On the x-axis the pump rate into the laser level is given. For the modified semiconductor theory, this corresponds to an effective carrier generation rate in the s-shell.

equation, we are reassured that the truncation can be applied with respect to the photonic correlations. The full semiconductor theory contains additional carrier-carrier correlations introduced by the Coulomb interaction. These are treated by means of the cluster expansion method in analogy to the correlations introduced by the light-matter interaction. In fact, the cluster expansion was developed to treat many-body effects of carriers [45], and successful applications include the photoluminescence of QDs [11, 44], and exciton formation in quantum wells [62].

5.3. Extended Jaynes-Cummings Model for a Single Electron System

So far we have studied two atomic laser models and their relation to the equation-of-motion approach our semiconductor theory is based on. The rate equations provide a deterministic description of the photon number, while the master equation for the diagonal elements of the density matrix gives access to the photon statistics. As we have discussed in the previous two sections, both models can be derived by a simple consideration of all relevant processes in the system, as is indicated in Figure 5.3. However, this constitutes more or less a phenomenological approach. Quantum optics provides us with much more stringent methods for describing non-equilibrium open systems, like lasers. We will now present an exact theory for the calculation of the full density matrix by solving the Liouville/von-Neumann equation.

To facilitate this paragraph, we consider in the following a single four-level system with one electron coupled to a single mode of an optical cavity. This system has been studied by Yi Mu and Craig Savage [98] in the context of the one-atom laser. The transfer of this concept to semiconductor systems is currently of great interest, as non-classical light sources are being realized with single-QDs [115]. The advantage of studying this particular system lies in the fact that it can be solved without any significant approximation. While in the birth/death model described in Section 5.2 only probabilities for the states of the system were considered, we can now obtain the dynamics of the full density matrix by solving the Liouville/von-Neumann equation numerically.

In a second step we will derive a hierarchy of equations of motion from the Liouville equation that we truncate in complete analogy to the semiconductor theory on the quadruplet level. In doing so we are once more able to test the truncation of equations of motion by means of the cluster expansion technique explained in Section 2.2. We show how the formalism can be translated to the semiconductor language with
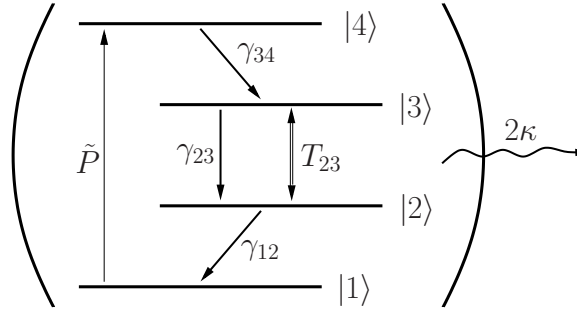
Figure 5.5.: Level diagram of the one-atom laser system. Electrons are excited at pump rate $\tilde{P}$ from the ground state $|1\rangle$ into the pump level $|4\rangle$. The rates γ_{34} and γ_{12} determine the scattering into and from the laser levels $|2\rangle$ and $|3\rangle$, which are coupled to the laser mode via the transition amplitude T_{23}. Emission into non-lasing modes is described by the rate γ_{23}. The cavity mode is coupled to a reservoir of radiative modes outside the cavity, giving the laser mode a finite lifetime $1/2\kappa$.

second-quantized carrier and photon operators. This enables us to draw conclusions about the structure of scattering and dephasing terms.

An extension of the Liouville/von-Neumann equation to N atoms is straightforward and provides a conclusive derivation of the master equation presented in the previous section. Furthermore, it includes coupling between different emitters due to the inclusion of the off-diagonal elements of the density matrix. A particular type of off-diagonal correlations between different atoms describe superradiant coupling, which is an interesting topic on its own.

The considered four-level system is depicted in Figure 5.5. The single electron, if in the ground state $|1\rangle$, can be excited into the pump level $|4\rangle$. Transition processes between the levels and the corresponding dephasing of the off-diagonal density matrix elements are introduced by coupling the atom to reservoirs. The interaction with these reservoirs is treated in the so-called Born-Markov approximation [29] and is contained in the resulting transition rates $\tilde{P}$ and γ_{ij} indicated in the level scheme. Of particular importance are fast transitions into the upper laser level $|3\rangle$ at the rate γ_{34} and rapid processes emptying the lower laser level $|2\rangle$ at the rate γ_{12}. For the transitions between the laser levels $|3\rangle$ and $|2\rangle$, the spontaneous emission into non-lasing modes, described by the rate γ_{23}, competes with the coupling to the laser mode via the transition amplitude T_{23}. By coupling also the laser mode to a reservoir as discussed above, cavity losses with a rate 2κ are introduced.

All these processes determine the time evolution of the density matrix of the coupled atom-cavity system. In the following the single contributions are discussed in detail.

5.3.1. Derivation of the Liouville/von-Neumann Equation for the Single Atom Laser

The time evolution of the full density matrix ρ can be obtained from its commutator with the Jaynes-Cummings Hamiltonian H_{JC} and the dissipative and pump processes are described by Lindblad terms $L\rho$ (that account for the above discussed coupling to the reservoirs [29]) according to

$$\frac{\mathrm{d}}{\mathrm{d}t}\rho = -\frac{i}{\hbar}[H_{\mathrm{JC}}, \rho] + L\rho \ . \tag{5.6}$$

The single contributions are discussed in the following.

Resonant optical transitions. We first consider the resonant coupling of the emitter to a single cavity mode, which corresponds to the famous and – in the absence of other processes – exactly solvable Jaynes-Cummings model. It is described by a Hamiltonian H_{JC} that contains contributions of the free atomic energies H^0, the free electromagnetic field H^0_{em}, and the Hamiltonian of the light-matter interaction H_{lm}. Spontaneous emission is a quantum-electrodynamical effect that enters the theory due to the quantization of the electromagnetic field. Damping terms will be added in a second step via external reservoirs for both the atomic and photonic systems, providing cavity losses and dephasing.

The basis of the atomic system is given by the energy eigenstates of the Hamiltonian

$$H^0 = \frac{1}{2}\hbar\omega_{23}\sigma_z \ , \tag{5.7}$$

which we denote as $|j\rangle$, $j = 2,3$, where $|2\rangle = \begin{pmatrix} 0 \\ 1 \end{pmatrix}$ and $|3\rangle = \begin{pmatrix} 1 \\ 0 \end{pmatrix}$. The atomic raising and lowering operators are given by a superposition of the Pauli spin matrices $\sigma_\pm = (\sigma_x \pm i\sigma_y)/2$, with

$$\sigma_x = \begin{pmatrix} 0 & 1 \\ 1 & 0 \end{pmatrix} \ , \qquad \sigma_y = \begin{pmatrix} 0 & -i \\ i & 0 \end{pmatrix} \ , \qquad \sigma_z = \begin{pmatrix} 1 & 0 \\ 0 & -1 \end{pmatrix} \ . \tag{5.8}$$

The raising and lowering operators can also be written as the outer products $\sigma_+ = |3\rangle\langle 2|$ and $\sigma_- = |2\rangle\langle 3|$, which is somewhat more intuitive. Their action on the basis states is naturally found to be

$$\begin{aligned} \sigma_+|2\rangle &= |3\rangle \ , & \sigma_+|3\rangle &= 0 \\ \sigma_-|2\rangle &= 0 \ , & \sigma_-|3\rangle &= |2\rangle \ . \end{aligned} \tag{5.9}$$

The free part of the electromagnetic field is given by the energy of all photons in the only available mode with frequency Ω

$$H_{em}^0 = \hbar\Omega b^\dagger b \ . \tag{5.10}$$

The eigenstates of the quantized electromagnetic mode are given by the number states $|n\rangle, \ n = 0, 1, 2, \dots$

The dipole interaction Hamiltonian is already known from Chapter 2. With the mode expansion of the electromagnetic field $\mathbf{E} = \left(\frac{\hbar\Omega}{2\epsilon_0 V}\right)^{1/2} \mathbf{U}(\mathbf{r})(b^\dagger + b)$ and the light matter coupling constant $g = -\mathbf{d}\left(\frac{\hbar\Omega}{2\epsilon_0 V}\right)^{1/2} \mathbf{U}(\mathbf{r})$, where $\mathbf{d}$, V and $\mathbf{U}(\mathbf{r})$ are the dipole moment, the volume and the function of the electromagnetic field mode, respectively, it takes the familiar form

$$H_{lm} = i\hbar g(b^\dagger \sigma_- - b\sigma_+) \ . \tag{5.11}$$

The basis states of the non-interacting atom-photon system we denote by $|n, j\rangle$,

$$|n, j\rangle = |n\rangle \otimes |j\rangle \ , \qquad n = 0, 1, 2, \dots \ , \tag{5.12}$$

where $n = 0, 1, 2, \dots$ is the photon number and $j = 1, 2, 3, 4$ is the level index. The Jaynes-Cummings Hamiltonian only acts on the laser transition between levels $|2\rangle$ and $|3\rangle$. We already include the pump level $|4\rangle$ and the ground state $|1\rangle$, as these states are subject to scattering, which we introduce further down. The photon operators have the well-known effect on the basis states

$$b^\dagger|n, j\rangle = \sqrt{n+1}|n+1, j\rangle \quad \text{and} \quad b|n, j\rangle = \sqrt{n}|n-1, j\rangle \ . \tag{5.13}$$

From this we infer that the light-matter interaction (5.11) couples only states with ± 1 in the photon number and level index, so that the Hilbert space of the many-body problem factorizes effectively into two-dimensional subspaces. Thus, when calculating the time evolution of the density matrix $\langle n, j|\rho|n', j'\rangle$ due to the interaction with the cavity mode, it suffices to consider the following three matrix elements[2]

$$\frac{\mathrm{d}}{\mathrm{d}t}\langle n, 2|\rho|n, 2\rangle\big|_{\mathrm{JC}} = g\sqrt{n}\left[\langle n-1, 3|\rho|n, 2\rangle + \langle n, 2|\rho|n-1, 3\rangle\right] \ , \tag{5.14a}$$

$$\frac{\mathrm{d}}{\mathrm{d}t}\langle n, 3|\rho|n, 3\rangle\big|_{\mathrm{JC}} = -g\sqrt{n+1}\left[\langle n+1, 2|\rho|n, 3\rangle + \langle n, 3|\rho|n+1, 2\rangle\right] \ , \tag{5.14b}$$

$$\frac{\mathrm{d}}{\mathrm{d}t}\langle n-1, 3|\rho|n, 2\rangle\big|_{\mathrm{JC}} = g\sqrt{n}\left[\langle n-1, 3|\rho|n-1, 3\rangle - \langle n, 2|\rho|n, 2\rangle\right] \ . \tag{5.14c}$$

The free parts H^0 and H_{em}^0 of the Hamiltonian contribute only a term in the equation of motion for the off-diagonal elements. This term vanishes under the assumption that the cavity mode is in resonance with the laser transition, i.e., $\omega_{23} = \Omega$.

---

[2]Note that $\langle n, 2|\rho|n-1, 3\rangle \equiv \langle n-1, 3|\rho|n, 2\rangle^*$, as can be seen from the corresponding equations of motion.

Cavity damping. Dissipation can be included in the density matrix formalism by coupling to a heat bath of harmonic oscillators. This model is commonly used in quantum optics to describe field damping, and here we consider the decay of the optical cavity mode via the coupling to a reservoir of radiative modes. The reservoir is treated in Born-Markov approximation and the degrees of freedom of the reservoir are traced out. In a descriptive picture, this constitutes an irreversible process and the source of dissipation. The result of this treatment are the damping terms in the Lindblad form [29, 81, 154]

$$L_{\text{cav}}\rho = \kappa(2b\rho b^\dagger - b^\dagger b\rho - \rho b^\dagger b) \tag{5.15}$$

that enter the Liouville equation (5.6). Note that here we have defined 2κ as the cavity loss rate with dimension $[1/s]$ in consistency with the scattering rates γ_{ij}. The Lindblad terms describe dissipation while ensuring that the trace of the density matrix is conserved. The resulting contributions to the Liouville equation are given by

$$\frac{\mathrm{d}}{\mathrm{d}t}\langle n,j|\rho|n,j\rangle\big|_{\text{cav}} = 2\kappa\big[(n+1)\langle n+1,j|\rho|n+1,j\rangle - n\langle n,j|\rho|n,j\rangle\big] , \tag{5.16a}$$

$$\frac{\mathrm{d}}{\mathrm{d}t}\langle n-1,3|\rho|n,2\rangle\big|_{\text{cav}} = 2\kappa\sqrt{n(n+1)}\langle n,3|\rho|n+1,2\rangle - \kappa(2n-1)\langle n-1,3|\rho|n,2\rangle . \tag{5.16b}$$

While the photon losses from the cavity described by the first equation correspond to those occurring in the master equation (indicated by the horizontal arrows in Figure 5.4), the second equation contains the effect of cavity damping on the laser transition. As the dynamics of the off-diagonal elements of the density matrix is eliminated in the master equation approach discussed in Section 5.2, these terms do not explicitly appear in the birth/death model (they are neglected under the assumption that the contributions of the cavity losses are small compared to the dephasing of the off-diagonal density matrix elements [98]).

Scattering and pumping. Carrier transitions other than those driven by the resonant transition amplitude T_{23} between the upper and lower laser level are described in terms of scattering rates. They are introduced in analogy to Eq. (5.15) as

$$L_{\text{scatt}}\rho = \sum_M \frac{\gamma_{ij}}{2}\big(2\sigma_{ij}^-\rho\sigma_{ij}^+ - \sigma_{ij}^+\sigma_{ij}^-\rho - \rho\sigma_{ij}^+\sigma_{ij}^-\big) , \tag{5.17}$$

where only the relevant scattering rates $M = \{\gamma_{12}, \gamma_{23}, \gamma_{34}\}$ are considered. As transitions are mediated via photons in the atomic model, the back-scattering processes, described by the rates $\gamma_{21}, \gamma_{32}, \gamma_{43}$, are highly unlikely at low temperatures and can

safely be neglected. Spontaneous emission into non-lasing modes is accounted for via γ_{23}.

The incoherent carrier pumping at rate $\tilde{P}$ from level $|1\rangle$ to $|4\rangle$ is modeled via

$$L_{\text{pump}}\rho = \frac{\tilde{P}}{2}\left(2\sigma_{14}^{+}\rho\sigma_{14}^{-} - \sigma_{14}^{-}\sigma_{14}^{+}\rho - \rho\sigma_{14}^{-}\sigma_{14}^{+}\right) . \tag{5.18}$$

Equations (5.15)–(5.18) and any form of damping in general is introduced the same way by coupling to a heat bath and integrating out the continuum of reservoir modes. For the cavity losses and carrier scattering, a physical interpretation is the coupling to the continuum modes of free space. For the pump process, however, such picture cannot be found. Note also that by modelling the incoherent pumping in a form analogous to the carrier scattering, the pump rate $\tilde{P}$ acts as a source of dephasing. Eq. (5.18) is one particular choice for the pumping between levels $|1\rangle$ and $|4\rangle$. Other choices are possible, so for example coherent pumping via an external field [98].

Considering all transitions indicated by the single-line arrows in Figure 5.5, the scattering contributions to the Liouville equation are the following:

$$\frac{\mathrm{d}}{\mathrm{d}t}\langle n,1|\rho|n,1\rangle\big|_{\text{sc}} = \quad -\tilde{P}\langle n,1|\rho|n,1\rangle + \gamma_{12}\langle n,2|\rho|n,2\rangle , \tag{5.19a}$$

$$\frac{\mathrm{d}}{\mathrm{d}t}\langle n,2|\rho|n,2\rangle\big|_{\text{sc}} = \quad \gamma_{23}\langle n,3|\rho|n,3\rangle - \gamma_{12}\langle n,2|\rho|n,2\rangle , \tag{5.19b}$$

$$\frac{\mathrm{d}}{\mathrm{d}t}\langle n,3|\rho|n,3\rangle\big|_{\text{sc}} = \quad -\gamma_{23}\langle n,3|\rho|n,3\rangle + \gamma_{34}\langle n,4|\rho|n,4\rangle , \tag{5.19c}$$

$$\frac{\mathrm{d}}{\mathrm{d}t}\langle n,4|\rho|n,4\rangle\big|_{\text{sc}} = \quad \tilde{P}\langle n,1|\rho|n,1\rangle - \gamma_{34}\langle n,4|\rho|n,4\rangle , \tag{5.19d}$$

$$\frac{\mathrm{d}}{\mathrm{d}t}\langle n-1,3|\rho|n,2\rangle\big|_{\text{sc}} = \quad -\frac{\gamma_{23}+\gamma_{12}}{2}\langle n-1,3|\rho|n,2\rangle . \tag{5.19e}$$

The subscript sc denotes all scattering processes including the pumping. Cavity losses were treated separately in Eqs. (5.16). In contrast to the off-diagonal element, the scattering contributions to the diagonal elements of the density matrix are trivial in the sense that they can be obtained from a phenomenological model, cf. Section 5.2. The consequences of the particular form of Eq. (5.19e) are discussed in Section 5.3.5. Equations (5.14), (5.16) and (5.19) determine the time evolution of the full density matrix. To this point the only approximation is the treatment of the cavity field damping and carrier scattering in Born-Markov approximation [154].

5.3.2. Equations of Motion for Operator Expectation Values

Having set up the Hamiltonian and the equations of motion for the matrix elements of the density matrix, the numerical solution of the Liouville equation is straightfor-

ward, though only feasible for small systems (few atoms). However, before we pursue this task, the connection to the equation-of-motion approach will be established. Instead of solving the full Liouville equation, we now derive a hierarchy of equations of motion for expectation values from the Liouville equation. Using the cluster expansion method to truncate this hierarchy, we will be able to compare the full to the truncated theory.

Operator averages are obtained from the density matrix by taking the trace over the atomic or photonic degrees of freedom

$$f_j = \sum_{n=0}^{\infty} \langle n, j | \rho | n, j \rangle \tag{5.20}$$

$$\langle n \rangle = \sum_{n=0}^{\infty} n \, \rho_n \tag{5.21}$$

$$\langle n^2 \rangle = \sum_{n=0}^{\infty} n^2 \rho_n \tag{5.22}$$

with the reduced density operator

$$\rho_n = \sum_{j=1}^{4} \langle n, j | \rho | n, j \rangle \ . \tag{5.23}$$

Having calculated the density matrix, operator averages and derived quantities, like the photon autocorrelation function

$$g^{(2)}(\tau = 0) = \frac{\langle n^2 \rangle - \langle n \rangle}{\langle n \rangle^2} \ , \tag{5.24}$$

follow directly.

Intending to reformulate the problem as a hierarchy of equations of motion, we now take the time derivative of the equations *for the operator averages* (5.20)–(5.22). As an example we consider the population in state $|3\rangle$. Adding all contributions to the Liouville equation from (5.14b), (5.16a) and (5.19c), we obtain

$$\begin{aligned}
\frac{\mathrm{d}}{\mathrm{d}t} \langle n, 3 | \rho | n, 3 \rangle = {}& 2\kappa \big[(n+1) \langle n+1, 3 | \rho | n+1, 3 \rangle - n \langle n, 3 | \rho | n, 3 \rangle \big] \\
& - \gamma_{23} \langle n, 3 | \rho | n, 3 \rangle + \gamma_{34} \langle n, 4 | \rho | n, 4 \rangle \\
& - g\sqrt{n+1} \big[\langle n+1, 2 | \rho | n, 3 \rangle + \langle n, 3 | \rho | n+1, 2 \rangle \big] \ .
\end{aligned} \tag{5.25}$$

According to Eq. (5.20) we write for the population f_3

$$
\begin{aligned}
\frac{\mathrm{d}}{\mathrm{d}t}f_3 = \frac{\mathrm{d}}{\mathrm{d}t}\sum_{n=0}^{\infty}\langle n,3|\rho|n,3\rangle = {} & 2\kappa\left[\sum_{n-1=0}^{\infty}n\langle n,3|\rho|n,3\rangle - \sum_{n=0}^{\infty}n\langle n,3|\rho|n,3\rangle\right] \\
& - \gamma_{23}\sum_{n=0}^{\infty}\langle n,3|\rho|n,3\rangle + \gamma_{34}\sum_{n=0}^{\infty}\langle n,4|\rho|n,4\rangle \\
& - g\sum_{n=0}^{\infty}\sqrt{n+1}\left[\langle n+1,2|\rho|n,3\rangle + \text{c.c.}\right] \\
= {} & -\gamma_{23}f_3 + \gamma_{34}f_4 - 2gT_{23} ,
\end{aligned}
\tag{5.26}
$$

where we have defined the transition amplitude of the laser resonance

$$
T_{23} = \sum_{n=1}^{\infty}\sqrt{n}\,\langle n-1,3|\rho|n,2\rangle
\tag{5.27}
$$

and used $T_{23} = T_{23}^*$, which can be verified by comparing the equations of motion for the matrix elements $\langle n-1,3|\rho|n,2\rangle$ and $\langle n,2|\rho|n-1,3\rangle$. According to Eq. (5.20), the second line of Eq. (5.26) becomes the sum of the populations. As the sums in the first line of Eq. (5.26) run over all possible photon numbers, the contributions of the cavity damping cancel. The time evolution of f_1, f_2 and f_4 is found along the same lines, so that we can summarize the population dynamics:

$$
\frac{\mathrm{d}}{\mathrm{d}t}f_1 = -\tilde{P}f_1 \;+ \gamma_{12}f_2 ,
\tag{5.28a}
$$

$$
\frac{\mathrm{d}}{\mathrm{d}t}f_2 = \qquad\quad -\gamma_{12}f_2 + \gamma_{23}f_3 + 2gT_{23} ,
\tag{5.28b}
$$

$$
\frac{\mathrm{d}}{\mathrm{d}t}f_3 = \qquad\quad +\gamma_{34}f_4 - \gamma_{23}f_3 - 2gT_{23} ,
\tag{5.28c}
$$

$$
\frac{\mathrm{d}}{\mathrm{d}t}f_4 = +\tilde{P}f_1 \;- \gamma_{34}f_4 .
\tag{5.28d}
$$

While the terms in the second column on the right hand side describe transitions due to carrier scattering, note that the physical meaning of the scattering rate γ_{23} in the third column is the spontaneous emission into non-lasing modes, i.e. the recombination between the laser levels $|2\rangle$ and $|3\rangle$ other than the resonant optical transition described by T_{23}. From the symmetry of Eqs. (5.28) it can be seen that the carrier number is conserved in the system. Note that the scattering depends only on the population of the out-scattering state. In a semiconductor, it would additionally depend on the non-population $1-f$ of the in-scattering state.

The time evolution of the transition amplitude T_{23} is derived in Appendix C and is given by

$$
\frac{\mathrm{d}}{\mathrm{d}t}T_{23} = -\left(\kappa + \frac{\gamma_{12}+\gamma_{23}}{2}\right)T_{23} + g\left[\langle n\rangle(f_3 - f_2) + f_3 + S_3 - S_2\right] .
\tag{5.29}
$$

This equation is of equivalent form as Eq. (2.18) for the photon-assisted polarization. Indeed we will proof this analogy in the following section. Looking at Eq. (5.29) it strikes that both the out-scattering and spontaneous emission into non-lasing modes are sources of dephasing for the transition amplitude. At the same time, the pump level $|4\rangle$ provides no dephasing to the laser transition amplitude, which contrasts the situation in a semiconductor system. The first and second term in the square bracket constitute stimulated and spontaneous emission contributions (see Appendix C). Furthermore, on the right hand side correlation functions appear that are defined as

$$S_1 = \sum_{n=1}^{\infty} n\langle n,1|\rho|n,1\rangle - \langle n\rangle f_1 \ , \tag{5.30a}$$

$$S_2 = \sum_{n=1}^{\infty} n\langle n,2|\rho|n,2\rangle - \langle n\rangle f_2 \ , \tag{5.30b}$$

$$S_3 = \sum_{n=1}^{\infty} n\langle n-1,3|\rho|n-1,3\rangle - \big[\langle n\rangle + 1\big]f_3 \ , \tag{5.30c}$$

$$S_4 = \sum_{n=1}^{\infty} n\langle n-1,4|\rho|n-1,4\rangle - \big[\langle n\rangle + 1\big]f_4 \ , \tag{5.30d}$$

and which are shown in Appendix C to obey the following equations of motion:

$$\frac{\mathrm{d}}{\mathrm{d}t}S_1 = -(2\kappa + \tilde{P})S_1 \ + \gamma_{12}S_2 - 2gT_{23}f_1 \ , \tag{5.31a}$$

$$\frac{\mathrm{d}}{\mathrm{d}t}S_2 = -(2\kappa + \gamma_{12})S_2 + \gamma_{23}S_3 - 2gT_{23}\big[\langle n\rangle + f_2\big] + 2g\Pi_{23} \ , \tag{5.31b}$$

$$\frac{\mathrm{d}}{\mathrm{d}t}S_3 = -(2\kappa + \gamma_{23})S_3 + \gamma_{34}S_4 + 2gT_{23}\big[\langle n\rangle + 1 - f_3\big] - 2g\Pi_{23} \ , \tag{5.31c}$$

$$\frac{\mathrm{d}}{\mathrm{d}t}S_4 = -(2\kappa + \gamma_{34})S_4 + \tilde{P}S_1 \ - 2gT_{23}f_4 \ . \tag{5.31d}$$

In this set of coupled equations we can identify contributions structurally similar to diagonal and off-diagonal dephasing of interband transitions in semiconductor systems, where the dephasing is connected to scattering processes. Diagonal dephasing is typically understood to correspond to a direct damping by the quantity itself, while off-diagonal dephasing is an additional contribution due to the coupling to all quantities of the same kind with different quantum numbers. Although Eqs. (5.31) do not describe interband transitions, the same structure is found.

The new correlation function is defined in analogy to Eq. (5.27) as

$$\Pi_{23} = \sum_{n=1}^{\infty} n\sqrt{n}\langle n-1,3|\rho|n,2\rangle \ , \tag{5.32}$$

only differing from T_{23} by a factor of n in the sum. Its equation of motion is given by

$$\frac{\mathrm{d}}{\mathrm{d}t}\Pi_{23} = -\left(3\kappa + \frac{\gamma_{12} + \gamma_{23}}{2}\right)\Pi_{23} + 2\kappa T_{23} + g\left[\langle n^2\rangle(f_3 - f_2) + (2\langle n\rangle + 1)f_3 + \tilde{S}_3 - \tilde{S}_2\right]$$

$$(5.33)$$

The quantities $\tilde{S}_i$ are defined like S_i in Eqs. (5.30) with an additional factor n in the sum. As will become clear a bit further down, they correspond to the quintuplet level in the cluster expansion and are factorized according to Eqs.(C.14) and (C.15), see Appendix C, so that we can rewrite Eq. (5.33) on the quadruplet level as

$$\begin{aligned}\frac{\mathrm{d}}{\mathrm{d}t}\Pi_{23} \approx &-\left(3\kappa + \frac{\gamma_{12} + \gamma_{23}}{2}\right)\Pi_{23} + 2\kappa T_{23} + g\big[\langle n^2\rangle(f_3 - f_2) + (2\langle n\rangle + 1)f_3 \\ &+ (2\langle b^\dagger b\rangle + 1)(S_3 - S_2) + 2S_3\big]\ .\end{aligned}$$

$$(5.34)$$

The approximation indicates that correlations on the quintuplet level are neglected after factorizing the correlations $\tilde{S}_2$ and $\tilde{S}_3$. With this the equations of motion close on the quadruplet level.

To complete the set of coupled equations we give the time evolution of the mean photon number

$$\frac{\mathrm{d}}{\mathrm{d}t}\langle n\rangle = -2\kappa\langle n\rangle + 2gT_{23}$$

$$(5.35)$$

and the mean square photon number

$$\frac{\mathrm{d}}{\mathrm{d}t}\langle n^2\rangle = -2\kappa\big[2\langle n^2\rangle - \langle n\rangle\big] + 4g\Pi_{23} - 2gT_{23}\ .$$

$$(5.36)$$

As an illustration we show in Appendix D how the rate equations can be obtained from the derived set of equations.

5.3.3. Correspondence to the Semiconductor Formalism

From the Liouville equation (5.14), (5.16) and (5.19) we have derived operator expectation values with their equations of motion (5.27)–(5.36) in the previous section. In the dynamical equations for the populations and the (squared) photon number new quantities T_{23}, Π_{23}, S_i and $\tilde{S}_i$ appear. We have anticipated that a factorization of the $\tilde{S}_i$ is consistent with a truncation on the quadruplet level, which we show in the following. To facilitate the comparison with the semiconductor laser model for Chapter 3, we denote the upper and lower laser levels with the carrier operators for the s-shells of the conduction band c_s, $c_s^\dagger$ and the valence band v_s, $v_s^\dagger$, respectively, and omit the state index for the s-shell in the following. The analogy is depicted in Figure 5.6.
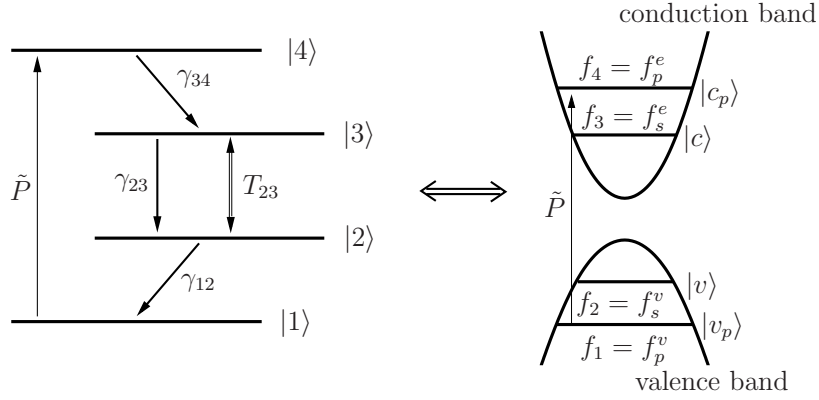
Figure 5.6.: 'Translation' between the atomic model introduced in Figure 5.5 and the semiconductor formalism, as explained in the text.

To establish a translation method between the operator method used in Sections 3.2.1 and 3.2.2 and the density matrix approach, we first consider the expectation value for the photon number $\langle b^\dagger b \rangle$ in the laser mode. It follows from taking the trace with the density matrix

$$
\begin{aligned}
\langle b^\dagger b \rangle &= \sum_{n,j} \langle n,j | \rho b^\dagger b | n,j \rangle \\
&= \sum_{n,j} \sqrt{n} \langle n,j | \rho b^\dagger | n-1,j \rangle = \sum_n n \sum_j \langle n,j | \rho | n,j \rangle \\
&= \sum_n n \rho_n = \langle n \rangle \ ,
\end{aligned}
\tag{5.37}
$$

where Eqs. (5.13) and (5.23) were used. It comes as no surprise that we obtain the identity $\langle b^\dagger b \rangle \equiv \langle n \rangle$, but it will help to understand the explicit form of T_{23} and Π_{23} in Eqs. (5.27) and (5.32). For the photon-assisted polarization we get

$$
\begin{aligned}
\langle b^\dagger v^\dagger c \rangle &= \sum_{n,j} \langle n,j | \rho b^\dagger v^\dagger c | n,j \rangle \\
&= \sum_n \sqrt{n} \sum_j \langle n-1,j | \rho v^\dagger c | n,j \rangle = \sum_n \sqrt{n} \sum_j \langle n-1,j | \rho \sigma_- | n,j \rangle \\
&= \sum_n \sqrt{n} \langle n-1,3 | \rho \sigma_- | n,3 \rangle \\
&= \sum_n \sqrt{n} \langle n-1,3 | \rho | n,2 \rangle = T_{23} \ .
\end{aligned}
\tag{5.38}
$$

In the second line we have identified the transition amplitude $v^\dagger c$ with the lowering operator for the laser transition defined in Eq. (5.9). For it there is only one possible transition causing the sum over the atomic states to drop out, revealing the identity between the photon-assisted polarization $\langle b^\dagger v^\dagger c \rangle$ and T_{23}.

From Eqs. (5.37) and (5.38) it can be concluded that two additional operators $b^\dagger b$ added to an arbitrary expectation value from the left merely yield an extra factor n under the sum while keeping the matrix elements unchanged, i.e.

$$
\begin{aligned}
\langle b^\dagger b b^\dagger v^\dagger c \rangle &= \sum_{n,j} \langle n,j | \rho b^\dagger b b^\dagger v^\dagger c | n,j \rangle \\
&= \sum_n n\sqrt{n} \langle n-1, 3 | \rho | n, 2 \rangle = \Pi_{23} \ .
\end{aligned}
\tag{5.39}
$$

The same holds for the mixed carrier-photon averages

$$
\langle b^\dagger b c^\dagger c \rangle = \sum_n n \langle n, 3 | \rho | n, 3 \rangle
\tag{5.40}
$$

$$
\langle b^\dagger b v^\dagger v \rangle = \sum_n n \langle n, 2 | \rho | n, 2 \rangle \ .
\tag{5.41}
$$

The cluster expansion method requires the use of true correlations rather than operator expectation values, as we have explained in Section 2.2. For Eq. (5.40), it is obtained according to $\delta \langle b^\dagger b c^\dagger c \rangle = \langle b^\dagger b c^\dagger c \rangle - \langle b^\dagger b \rangle \langle c^\dagger c \rangle$. Doing so we find that the S_i correspond to the population-photon correlation functions according to their definition in Eq. (5.30)[3]

$$
\delta \langle b^\dagger b c^\dagger c \rangle = \sum_{n=0}^\infty n \langle n, 3 | \rho | n, 3 \rangle - \langle n \rangle f_3 = S_3 \ ,
\tag{5.42a}
$$

$$
\delta \langle b^\dagger b v^\dagger v \rangle = \sum_{n=0}^\infty n \langle n, 2 | \rho | n, 2 \rangle - \langle n \rangle f_2 = S_2 \ .
\tag{5.42b}
$$

In order to rewrite Π_{23} as a correlation function we must restore normal ordering in Eq. (5.39) and factorize off the uncorrelated part:

$$
\begin{aligned}
\Pi_{23} = \langle b^\dagger b b^\dagger v^\dagger c \rangle &= \langle b^\dagger b^\dagger b v^\dagger c \rangle + \langle b^\dagger v^\dagger c \rangle \\
&= (2\langle b^\dagger b \rangle + 1)\langle b^\dagger v^\dagger c \rangle + \delta \langle b^\dagger b^\dagger b v^\dagger c \rangle \ .
\end{aligned}
\tag{5.43}
$$

If we now solve for the correlation function on the right hand side and take the time derivative, we obtain

$$
\begin{aligned}
\frac{\mathrm{d}}{\mathrm{d}t} \delta \langle b^\dagger b^\dagger b v^\dagger c \rangle &= \frac{\mathrm{d}}{\mathrm{d}t}\Big(\Pi_{23} - (2\langle b^\dagger b \rangle + 1)\langle b^\dagger v^\dagger c \rangle \Big) \\
&= -\left(3\kappa + \frac{\gamma_{12} + \gamma_{23}}{2} \right) \delta \langle b^\dagger b^\dagger b v^\dagger c \rangle - 4g\langle b^\dagger v^\dagger c \rangle^2 \\
&\quad + g(f_3 - f_2)\delta \langle b^\dagger b^\dagger b b \rangle + 2g\delta \langle b^\dagger b c^\dagger c \rangle \ ,
\end{aligned}
\tag{5.44}
$$

---

[3]Regarding S_3, relabeling n by $n-1$ under the sum yields the result in Eq.(5.30).

which we find to be equivalent to Eq. (5.5).[4] Here we have inserted the equations of motion (5.29), (5.34) and (5.35). Along the same lines we obtain the time evolution for $\delta\langle b^\dagger b^\dagger bb\rangle$:

$$
\begin{aligned}
\frac{\mathrm{d}}{\mathrm{d}t}\delta\langle b^\dagger b^\dagger bb\rangle &= \frac{\mathrm{d}}{\mathrm{d}t}\Big[\langle n^2\rangle - \langle n\rangle\big(2\langle n\rangle + 1\big)\Big] \\
&= -4\kappa\,\delta\langle b^\dagger b^\dagger bb\rangle + 4g\,\delta\langle b^\dagger b^\dagger bv^\dagger c\rangle \ .
\end{aligned}
\tag{5.45}
$$

Summary of the equations of motion for the one-atom laser system.   In the summary of equations we stick to the notation introduced in Section 5.3.2. Only for quantities rewritten in Section 5.3.3 to agree with the cluster expansion method, we use the notation already familiar from the semiconductor case.

The dynamics of the populations, the photon number and the transition amplitude are determined by Eqs. (5.28), (5.35) and (5.29), respectively. The carrier-photon correlations S_i evolve according to Eqs. (5.31), where we now replace Π_{23} in the equations for S_2 and S_3 by the true correlation function $\delta\langle b^\dagger b^\dagger bv^\dagger c\rangle$ according to Eq. (5.43), i.e.

$$
\frac{\mathrm{d}}{\mathrm{d}t}S_2 = -(2\kappa + \gamma_{12})S_2 + \gamma_{23}S_3 - 2gT_{23}\big[f_2 - \langle n\rangle - 1\big] + 2g\,\delta\langle b^\dagger b^\dagger bv^\dagger c\rangle \ ,
\tag{5.46}
$$

$$
\frac{\mathrm{d}}{\mathrm{d}t}S_3 = -(2\kappa + \gamma_{23})S_3 + \gamma_{34}S_4 - 2gT_{23}\big[f_3 + \langle n\rangle\big] - 2g\,\delta\langle b^\dagger b^\dagger bv^\dagger c\rangle \ .
\tag{5.47}
$$

The time-evolution of $\delta\langle b^\dagger b^\dagger bv^\dagger c\rangle$ is given in Eq. (5.44). This couples to the photon-intensity correlation $\delta\langle b^\dagger b^\dagger bb\rangle$, which evolves according to Eq. (5.45) and yields the second-order correlation function

$$
g^{(2)}(0) = 2 + \frac{\delta\langle b^\dagger b^\dagger bb\rangle}{\langle b^\dagger b\rangle^2} \ .
\tag{5.48}
$$

5.3.4. Numerical Results

What we have achieved in the previous sections are two approaches for solving the time evolution of an atomic one-electron system coupled to a single cavity mode: The full time evolution of the density matrix can be obtained from the numerical solution of the Liouville/von-Neumann equation. Alternatively, the truncated hierarchy of equations of motion for expectation values based on the cluster expansion technique can be solved.

---

[4]When comparing the equations of motion derived in this and the previous chapter, note that in Chapter 3 $\langle b^\dagger v^\dagger c\rangle$ and $\delta\langle b^\dagger b^\dagger bv^\dagger c\rangle$ are scaled with the light-matter coupling strength g, see for example Eqs. (3.11)–(3.13) and (5.5).

In the following, we distinguish between two different regimes: The situation where photons leave the cavity at a rate faster than the spontaneous emission into that mode is referred to as 'bad cavity limit'. On the other hand, the 'good cavity limit' describes the situation where photons can accumulate in a cavity mode with a lifetime longer than the spontaneous emission time already below threshold. For the latter case one intuitively expects a greater influence of photon correlations and, therefore, a greater deviation of the truncated theory from the full solution.
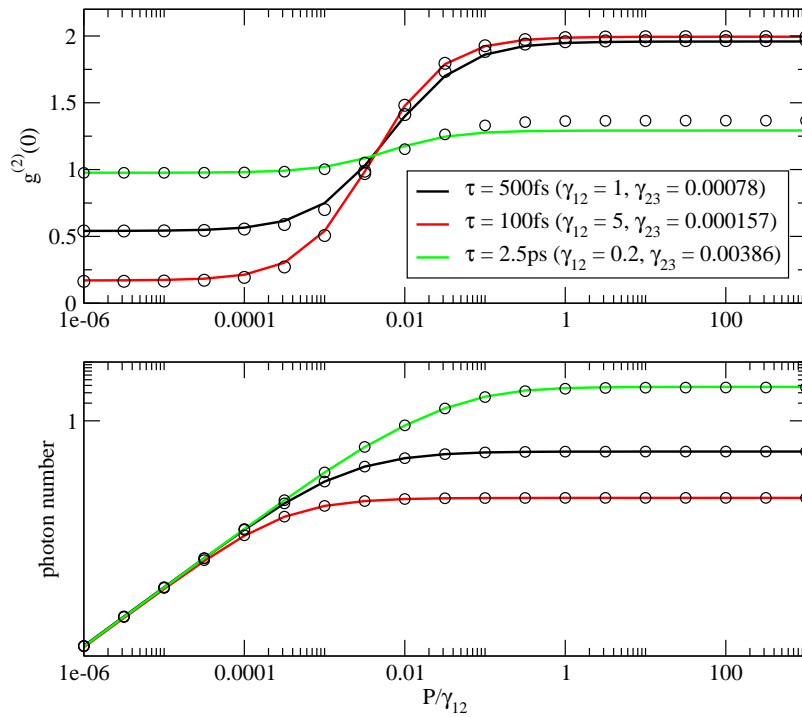
Figure 5.7.: Comparison of the exact Liouville/von-Neumann model (circles) with the truncated equation-of-motion approach on quadruplet level (solid lines). For all curves, $\beta = 0.5$, $\tau_{\mathrm{cav}} = 160\,\mathrm{ps}$, $g = 18\,\mu\mathrm{eV}$, and identical relaxation times $\tau_{12} = \tau_{34} = \tau$ are used.

In Figure 5.7 the circles are obtained by the solution of the Liouville equation (5.14)–(5.19) in a truncated Hilbert space, where it is ensured that the truncation does not have an influence on the numerical results by varying the size of the basis.[5] The solid lines correspond to the solution of the truncated hierarchy of equations of motion including terms up to the quadruplet level that is summarized on page 114. The cavity

---

[5]Note that the restriction to a set of relevant basis states is a technicality rather than an approximation to an otherwise exact theory. The implication of a 'truncation' should not be mixed up with the truncation of the hierarchy of equations of motion, which constitutes an approximation in the theory itself.

lifetime is chosen to be $\tau_{\text{cav}} \approx 160\,\text{ps}$, the spontaneous emission coupling $\beta = 0.5$ and the light-matter coupling $g = 18\,\mu\text{eV}$. The red and black curves correspond to calculations for the bad cavity limit with a spontaneous emission time $\tau_{23} = 4\,\text{ns}$ and $\tau_{23} = 850\,\text{ps}$, respectively. The green line corresponds to the good cavity limit with $\tau_{23} \approx \tau_{\text{cav}}$. As can be seen in the lower panel, the input/output curves show perfect agreement between the full and the truncated theory. In the upper panel the second-order correlation function $g^{(2)}(0)$ is shown. Here also perfect agreement is found, marginal deviations becoming visible only in the good cavity regime around and above the threshold region (green line).

The agreement revealed in Figure 5.7 is so far the most thorough proof of the validity of the cluster expansion truncation scheme. As the comparison is performed with a theory that is exact concerning factorization and truncation, it is truly a test of the factorization of the only occurring hierarchy, here introduced by the light-matter interaction, and is not obscured by other effects.

5.3.5. Dephasing Contributions and Analogy to the Semiconductor Formalism

Having shown that the cluster expansion method serves extremely well in the description of the coupled light-matter dynamics, we now turn back to the semiconductor formalism as it is introduced in Chapter 3. When comparing this model and the factorized form of the Liouville/von-Neumann equation in this paragraph, one must bear in mind that differences arise due to i) deviations between the considered systems (one electron system vs. QD system) and ii) different levels of approximations used in the derivation. Having identified the equations of motion for the atomic one-electron system in this section with the operator correlation functions that we know from the semiconductor approach, we can now compare the structure of the equations in detail. In particular, this will shine light on the appearance of dephasing terms.

In Eq. (5.42) we have identified the population-photon correlations $\delta\langle b^\dagger b c^\dagger c\rangle$ and $\delta\langle b^\dagger b v^\dagger v\rangle$. Taking a closer look at their equations of motion (5.31), it is obvious that the carrier scattering rates act as sources for what we have interpreted to be similar to diagonal and off-diagonal dephasing. Furthermore, via the off-diagonal dephasing, the dynamics of the carrier-photon correlations $\delta\langle b^\dagger b c^\dagger c\rangle$ and $\delta\langle b^\dagger b v^\dagger v\rangle$ for the laser transition are coupled to correlation functions of the same kind for the pump levels $S_1 = \delta\langle b^\dagger b v_p^\dagger v_p\rangle$ and $S_4 = \delta\langle b^\dagger b c_p^\dagger c_p\rangle$. In the dynamical equations (3.23) and (3.24) derived in Chapter 3 damping is provided only via the photonic system (expressed in terms of κ), and we have neglected carrier-photon correlations with the QD p-shell.

Differences are also found in the transition amplitude $T_{23} = \langle b^\dagger v^\dagger c\rangle$ for the laser resonance (5.38) and the correlation function $\delta\langle b^\dagger b^\dagger b v^\dagger c\rangle$. In the time evolution of

these quantities, given in Eqs. (5.29) and (5.44), respectively, dephasing enters via the rates γ_{12} and γ_{23}. Comparing the model from this section with the approach based on the semiconductor model, three points are of interest. In the single-atom model

i. dephasing is provided only due to scattering processes out of the laser transition. The scattering rate γ_{34} describing the transition into the upper laser level, however, does not provide dephasing. The reason for this lies in the one-electron approximation, where out-scattering is proportional only to the occupation of the level scattered from. In a semiconductor the occupation of both the in- and out-scattering states are relevant for scattering processes.

ii. the dephasing provided by γ_{23} is related to the spontaneous emission into non-lasing modes. In contrast to the other transition rates, this is mediated by coupling to the photonic system in both atomic and semiconductor systems. In the presented formulation of the semiconductor theory, dephasing due to radiative processes is understood to be contained in the dephasing constant Γ. Due to the long radiative lifetime of QDs, the induced dephasing time is extremely long [79] in comparison to the dephasing time introduced by ultrafast scattering processes. Thus, the contribution of the emission into non-lasing modes to the total dephasing of the transition amplitude and higher-order polarization-like correlations is expected to be small, i.e. $\gamma_{12} \gg \gamma_{23}$. This is true in general, but holds in particular for high-β lasers, where the contribution of non-lasing modes is suppressed by a factor of $1 - \beta$.

iii. the dephasing rates are in all cases related to the scattering rates. While this is also the case in a semiconductor system, the connection is somewhat more difficult. Carrier-phonon interaction causes a temperature and carrier-density dependent dephasing with diagonal and off-diagonal contributions. The dephasing as well as the in- and out-scattering terms are interconnected. In the derivation of the laser model this density-dependent scattering and dephasing is summarized as a constant dephasing Γ, e.g. in Eq. (3.13), and an effective scattering rate $R_{p \to s}^{e,h}$ is used in Eqs. (3.19) and (3.20) for the relaxation from the pump levels. In this approximate treatment of carrier scattering and dephasing, the inherent relation between both processes is lost if the values for Γ and the relaxation times are chosen independently, e.g. on the basis of experimental results.

The important point iii) addresses the approximate treatment of dephasing and scattering mechanisms that we have employed in the derivation of the laser model. An implementation of these processes on a microscopic level, e.g. via the interaction with

phonons, constitutes a considerable task worth an own dissertation's work. For the calculation of the photon second-order correlation function, contributions must be included up to quadruplet level in all of the appearing correlation functions. In Chapter 3 we have developed a theory aiming at the description of lasing and second-order coherence properties of an ensemble of QDs without having to deal with additional terms introduced by further interaction parts in the Hamiltonian. In fact, the results presented in Figure 5.4 demonstrate that our approach and the chosen approximations lead to consistent results already for small numbers of emitters. However, every approximation has its limits, which we find in the description of lasing from a *single* QD by means of the extended laser equations (cf. Section 3.2.2). In this case a treatment of carrier scattering and dephasing beyond the approximations used in Chapter 3 is required, as well as the inclusion of carrier-photon correlations with the p-shell carriers ($\delta\langle b^\dagger b v_p^\dagger v_p\rangle$ and $\delta\langle b^\dagger b c_p^\dagger c_p\rangle$). This can be concluded from studying the factorized version of the single-atom laser in this section, for which we have employed a trace-conserving treatment of scattering and dephasing via the much more easily implemented Lindblad terms.

5.4. Conclusion

What has been achieved with the work presented in this chapter is twofold: Firstly, we have examined the validity of the equation-of-motion approach and the cluster expansion truncation scheme in the developed laser theory. Equally important, we have established the connection to formalisms used in quantum optics for the description of atomic systems yielding significant insight into the structure and scope of application of our model.

Based on the reduction of the semiconductor laser model to a theory for atoms, we can compare the methods used in Chapter 3 to other atomic theories. In doing so, we have shown in the first section that the well-established atomic rate equations are recovered as a limiting case of our model. As the rate equations are insufficient for the description of photon correlations, we have invoked a master equation approach in Section 5.2. The obtained density matrix yields the probabilities for each state of the system, from which photon autocorrelation functions up to arbitrary order can be calculated without any truncation of correlations being involved. A comparison with the laser theory in the atomic limit for realistic parameters shows excellent agreement both for the input/output curve and the photon autocorrelation function, only with small deviations for lasers with extremely high spontaneous emission coupling.

In Section 5.3 the most rigorous approach is taken for the simplified model of a four-level atom with one electron, coupled to a single cavity mode. The light-matter

interaction in this system is governed by the Jaynes-Cummings Hamiltonian, while decoherence and damping follows a Markovian master equation. The dynamics of the system can be solved in two ways: Firstly, the Liouville/von-Neumann equation can be solved numerically, yielding an exact solution of the full density matrix of the system. Secondly, a hierarchy of equations of motion can be derived from the Liouville equation. By means of the cluster expansion method, we have truncated this hierarchy consistently on the quadruplet level. A comparison between both methods provides an ultimate test for the cluster expansion method and the sufficiency of a truncation on the quadruplet level if the photon second-order correlation function $g^{(2)}(0)$ is the aim of the calculation. The agreement revealed in this comparison even in the "good cavity regime" proves the sufficiency of the truncation on quadruplet level for the calculation of the photon statistics and the applicability of the cluster expansion method.

Furthermore, towards the description of the single-QD laser, the trace-conserving treatment of carrier scattering and dephasing in the single-atom model points out the significance of both diagonal and off-diagonal contributions to the dephasing. In a semiconductor theory these contributions enter e.g. via a microscopic treatment of the carrier-phonon or carrier-carrier interaction.

6. Conclusion

In the presented work we have developed and applied methods to describe the luminescence and laser emission from semiconductor quantum dots (QDs). From a microscopic Hamiltonian and Heisenberg's equations of motion the semiconductor luminescence equations were derived and used to study the photoluminescence dynamics. In both unstructured QD samples and QDs in microcavities we have identified the commonly observed non-exponential and carrier-density dependent decay of the luminescence as an intrinsic semiconductor property of QDs that reflects a lack of correlations between electrons and holes. We conclude that the description of the radiative decay using atomic models is not justified in the general case, as carrier correlations depend directly on many-body interaction processes and must therefore be explicitly calculated.

Based on the semiconductor luminescence equations, we have developed a laser theory for QDs in microresonators that allows for the calculation of coherence properties in terms of the second-order correlation function. As the equation-of-motion method does not require the equations to be linear, Coulomb correlations and other effects specifically important in semiconductor systems can be included in a straightforward way. In order to calculate the first-order coherence properties we have shown how the described model can be used to calculate two-time operator averages. With this and the second-order correlation function, we obtain a consistent overall picture of the laser transition in QD-based microcavity laser devices. At the large spontaneous emission coupling factors β that are currently obtained in state-of-the-art devices, the signature of the laser transition in the input/output characteristics is washed out and cannot be clearly identified anymore. At the same time, around the threshold region we observe a distinct rise in the coherence time by about two orders of magnitude, a change in the lineshape of the first-order correlation function from Gaussian-like to exponential, and a change in the second-order coherence properties from (close to) the signature of thermal ($g^{(2)}(0) = 2$) to that of coherent ($g^{(2)}(0) = 1$) light. These results distinctly characterize the threshold region even if a threshold is no longer directly visible in the intensity of the emitted light.

From atomic models it is expected that the output intensity shows a jump by a factor of $1/\beta$ at the threshold. For several reasons this does not apply to semiconductor

systems in general. The reabsorption present in the system modifies the height of the jump. The possibility to have more than single excitation in a QD modifies the spontaneous emission properties. Saturation effects of the pump levels, in combination with the small numbers of QDs typically present in microcavity lasers, can have a strong effect at higher excitation powers. The upper branch of the input/output curve can be masked to an extent where the threshold is not even fully developed. If in this case atomic models are used to extract parameters from measured data, the smaller jump in the input/output characteristics may be mistaken to be caused by a spontaneous emission coupling factor β larger than it truly is. We have shown that this effect is even more pronounced for pulsed excitation.

For a deeper understanding of the differences between QDs and atoms, and to verify our semiconductor approach, common methods in quantum optics for the computation of laser properties were reviewed and placed in relation to each other and to our semiconductor theory. As the most fundamental method we have discussed the Liouville/von-Neumann equation that yields the time-evolution of the full density matrix. This model can be reduced to a master equation that describes probabilities or to the well-known rate equations. Two points are important to notice: Firstly, in both approaches where the density matrix elements are calculated, information about the statistical properties of the light are preserved, whereas in the rate equation formulation this information is lost. And secondly, we have discussed that the rate equations are the most simple possible factorization in a reformulation of the first two approaches in a hierarchy of coupled equations of motion. In this context we place our semiconductor laser theory, which is based on an equation-of-motion approach. While rate equations typically describe the carrier system in terms of the expectation value of the number of excited two-level systems, the semiconductor approach is formulated in terms of population expectation values and transition amplitudes in a semiconductor basis. Also the hierarchy of equations is not truncated on the semiclassical level, but higher-order correlation functions are kept in a consistent manner. This enables us to calculate the coherence properties of the emitted light in terms of the second-order correlation function.

The close relation to the discussed atomic models allows for a direct comparison and a verification of the truncation scheme if the semiconductor model is considered in the limit of a single possible excitation. We have performed such tests and find that the truncation of the hierarchy, introduced by the light-matter interaction, on the quadruplet level delivers an accurate description of the laser properties including the second-order correlation function for realistic parameters.

Finally, we would like to point out that the presented work has been mutually inspired by the close and fruitful collaboration with experimental groups in Dortmund and

Stuttgart. Therefore, most of our results are shown side-by-side with results from recent experiments.

Future Directions

From here the work can be continued in several directions. While we have treated some aspects of our theory thoroughly and in great detail, in other parts we have used approximations that allowed us to obtain results on a simplified level. We have pointed out the limitations of those approximations and the circumstances under which a refinement is required.

We have shown that the influence of carrier correlations on the spontaneous emission properties can be drastic. The build-up and dephasing of correlations is of particular interest if the emission from semiconductor QDs into free space, or the emission from QD-based LEDs or weakly excited laser diodes is to be studied. To account for dephasing of correlations, an inclusion of carrier-phonon interaction on a microscopic level is desirable. An extension of the theory presented in Chapter 2 to the coherent regime would allow to study the build-up of carrier correlations and exciton formation, as well as the emission behavior under resonant excitation.

The laser theory in its particular form has been developed to describe current experiments, where single-mode lasing is achieved with an ensemble of QDs in a microresonator at low temperatures. In different situations, modifications are required, such as, for example, the explicit inclusion of the interaction with the wetting layer for lasing at room temperature. Furthermore, a more detailed treatment of Coulomb effects is desirable especially in the regime where spontaneous emission is the dominant emission mechanism. These are refinements of the theory in its present form and the expected corrections are small.

Of greatest interest are different effects which are currently being discussed in the literature. Superfluorescence and superradiant coupling in QD-based systems has been experimentally investigated and described by means of atomic models. Nevertheless, a treatment where the semiconductor nature of QDs is accounted for would be worthwhile. Finally, recent experiments point towards the direction of single-QD lasing. In contrast to the emission from an ensemble of emitters, for single-QD lasing the cavity lifetime must exceed the spontaneous emission time. In this regime correlations are strongly developed and dephasing terms are of enhanced importance. For a proper description in this regime, some assumptions that are valid for lasing from an ensemble of QDs must be revisited. Our investigations of the single atom laser in Chapter 5 have already indicated the direction for further research.

Appendices

A. Application of the Cluster-Expansion Method

In Section 2.2 the cluster-expansion method is introduced to consistently truncate the infinite hierarchy of equations of motion. Often questions arise in the direct application of the factorization scheme. The following examples aim at clarifying these issues.

Most conveniently, normal order is established before operator averages are factorized. However, it is not necessary as long as the order of operators is not altered in the factorized parts, i.e.

$$\langle b^\dagger b c c^\dagger \rangle = \delta\langle b^\dagger b\rangle\langle cc^\dagger\rangle + \delta\langle b^\dagger bcc^\dagger\rangle \;, \tag{A.1}$$

$$\langle b^\dagger b c^\dagger c \rangle = \delta\langle b^\dagger b\rangle\langle c^\dagger c\rangle + \delta\langle b^\dagger bc^\dagger c\rangle \;. \tag{A.2}$$

Both factorizations are correct, but note that different quantities appear on the right and left hand side of these equations.

Normal ordering can be performed before or after the factorization, which may become clear by looking at the following example. Direct factorization of the operator average $\langle b^\dagger bb^\dagger v^\dagger c\rangle$ into two doublets (denoted as $\delta\langle 2\rangle\delta\langle 2\rangle$) yields

$$
\begin{aligned}
\langle b^\dagger bb^\dagger v^\dagger c\rangle\Big|_{\delta\langle 2\rangle\delta\langle 2\rangle} &= \delta\langle b^\dagger b\rangle\delta\langle b^\dagger v^\dagger c\rangle + \delta\langle bb^\dagger\rangle\delta\langle b^\dagger v^\dagger c\rangle \\
&= \delta\langle b^\dagger v^\dagger c\rangle\big[1 + 2\delta\langle b^\dagger b\rangle\big] \;,
\end{aligned}
\tag{A.3}
$$

where the extra term in the last line results from the commutator for $[b, b^\dagger]_- = 1$. On the other hand, normal order can be established before the factorization, i.e.

$$
\begin{aligned}
\langle b^\dagger bb^\dagger v^\dagger c\rangle\Big|_{\delta\langle 2\rangle\delta\langle 2\rangle} &= \Big\{\langle b^\dagger v^\dagger c\rangle + \langle b^\dagger b^\dagger bv^\dagger c\rangle\Big\}_{\delta\langle 2\rangle\delta\langle 2\rangle} \\
&= \delta\langle b^\dagger v^\dagger c\rangle\big[1 + 2\delta\langle b^\dagger b\rangle\big] \;.
\end{aligned}
\tag{A.4}
$$

As the same commutation relation is used as in Eq. (A.3), one obtains the same result.

When starting from normal-ordered averages, the resulting factorizations are always normal-ordered as well. For each possible factorization, the operators are rearranged

such that the factorization can be performed as a splitting of the operator average into smaller operator averages, see the example below. This rearranging is performed for each possible factorization and always from the same initial expectation value. Commutators *only* yield a change in the sign for fermions, but never extra terms. The reason for this is that always the same operator average is factorized. If the operator average was brought into the desired order using proper commutation relations yielding additional terms, and if these terms were kept, *different initial* operator averages would actually be used in different factorizations.

As an example we consider the factorization of the quadruplet quantity $\langle b^\dagger b^\dagger v_{\nu'}^\dagger v_\nu^\dagger c_{\nu'} c_\nu \rangle$ into two doublets $\delta\langle 2 \rangle \delta\langle 2 \rangle$. One possibility is obtained from

$$\langle b^\dagger v_{\nu'}^\dagger c_{\nu'} \ b^\dagger v_\nu^\dagger c_\nu \rangle \ , \tag{A.5}$$

where the commutation of the underlined terms yields a minus sign. Bose operators, however, can be moved without changes of sign. The other possible factorization[1] requires commutation in two steps:

$$\langle b^\dagger b^\dagger v_{\nu'}^\dagger v_\nu^\dagger c_{\nu'} c_\nu \rangle \rightarrow -\langle b^\dagger b^\dagger v_\nu^\dagger v_{\nu'}^\dagger c_{\nu'} c_\nu \rangle \rightarrow +\langle b^\dagger v_\nu^\dagger c_{\nu'} \ b^\dagger v_{\nu'}^\dagger c_\nu \rangle \ . \tag{A.6}$$

Performing the truncations indicated by the gaps in Eqs. (A.5) and (A.6) yields

$$\langle b^\dagger b^\dagger v_{\nu'}^\dagger v_\nu^\dagger c_{\nu'} c_\nu \rangle \bigg|_{\delta\langle 2 \rangle \delta\langle 2 \rangle} = -\delta\langle b^\dagger v_{\nu'}^\dagger c_{\nu'} \rangle \delta\langle b^\dagger v_\nu^\dagger c_\nu \rangle + \delta\langle b^\dagger v_\nu^\dagger c_{\nu'} \rangle \delta\langle b^\dagger v_{\nu'}^\dagger c_\nu \rangle \ . \tag{A.7}$$

---

[1] Other factorizations are technically possible, but yield non-resonant terms.

B. Interplay of Time Constants

For the evaluation of our theory, we treat the rate of spontaneous emission into the non-lasing modes $1/\tau_{\mathrm{nl}}$ as an extrinsic parameter, which is determined by the properties of the laser resonator. Depending on the particular cavity design, other high-Q resonator modes as well as a quasi-continuum of low-Q leaky modes can contribute. The spontaneous emission into the laser mode can be calculated from the light-matter coupling strength $|g|^2 = |g_{\xi_l}|^2$ for this mode, the cavity lifetime $\hbar/2\kappa$, and the homogeneous dephasing Γ. Restricting the adiabatic solution of Eq. (3.14) to the spontaneous emission into the laser mode and using Eq. (3.12) to define the corresponding rate $1/\tau_l$ according to

$$\left. \frac{\mathrm{d}}{\mathrm{d}t} f_s^{e,h} \right|_{l,\mathrm{spont}} = -\frac{f_s^e f_s^h}{\tau_l} \ , \tag{B.1}$$

we find

$$\frac{1}{\tau_l} = \frac{2}{\hbar} \frac{|g|^2}{\kappa + \Gamma} \ . \tag{B.2}$$

With τ_l and τ_{nl} the β-factor follows from Eq. (3.17). In this thesis we present the figures in the common style where the β-factor is varied, as it is the most important parameter characterizing the cavity efficiency, while the total rate of spontaneous emission

$$\frac{1}{\tau_{\mathrm{sp}}} = \frac{1}{\tau_l} + \frac{1}{\tau_{\mathrm{nl}}} \tag{B.3}$$

is held constant. To achieve such a situation, for various β-values both τ_{nl} and τ_l need to be changed. Note that the latter requires a change of the light-matter coupling strength according to Eq. (B.2), which is possible for a given dipole coupling by a modification of the mode functions (cf. Eq. (2.7)), and/or by a change of the lifetime of the cavity mode. In Section 3.4 the presented theory is applied to pillar microcavities with various resonator diameters. In such a situation, the spontaneous emission into non-lasing modes is practically constant due to the unchanging contributions of leaky modes, while the spontaneous emission into the laser mode is modified by the Purcell

effect, see Section 2.7. The Purcell factor F_P is defined as the ratio of the rate of spontaneous emission into the cavity mode, $1/\tau_l$, to the rate of spontaneous emission into free space, $1/\tau_{\text{free}}$. We can express the β-factor in terms of F_P as

$$\beta = \frac{F_P}{dF_P + \frac{\tau_{\text{free}}}{\tau_{\text{nl}}}} = \frac{\frac{1}{\tau_l}}{\frac{d}{\tau_l} + \frac{1}{\tau_{\text{nl}}}} \ , \tag{B.4}$$

where additionally a possible degeneracy d of the fundamental mode has been included, see the article by J.-M. Gérard in Ref. [93].

C. Operator Equations of Motion in the Density Matrix Formalism

In the third section of Chapter 5 a density matrix formulation of the coupled atom--cavity system is used to derive a hierarchy of dynamic equations analogous to the laser equations obtained from the cluster expansion method under the assumption of two-level emitters. In the following we give the derivations of the occurring equations that were omitted in Chapter 5 for the sake of clarity.

Resonant transition amplitude. In Section 5.3.2 the equation of motion for the resonant transition amplitude T_{23} is given. By collecting the contributions from the Liouville equation (5.14c), (5.16b) and (5.19e), it follows from

$$
\begin{aligned}
\frac{\mathrm{d}}{\mathrm{d}t}T_{23} &= \frac{\mathrm{d}}{\mathrm{d}t}\sum_{n=1}^{\infty}\sqrt{n}\langle n-1,3|\rho|n,2\rangle \\
&= \kappa\sum_{n=1}^{\infty}\left[2n\sqrt{n+1}\langle n,3|\rho|n+1,2\rangle - (2n-1)\sqrt{n}\langle n-1,3|\rho|n,2\rangle\right] \\
&\quad - \frac{\gamma_{12}+\gamma_{23}}{2}\sum_{n=1}^{\infty}\sqrt{n}\langle n-1,3|\rho|n,2\rangle \\
&\quad + g\sum_{n=1}^{\infty}n\Big[\langle n-1,3|\rho|n-1,3\rangle - \langle n,2|\rho|n,2\rangle\Big] .
\end{aligned}
\tag{C.1}
$$

The cavity damping term can be rewritten by relabeling the indices

$$
\sum_{n=1}^{\infty}\left[2n\sqrt{n+1}\langle n,3|\rho|n+1,2\rangle - (2n-1)\sqrt{n}\langle n-1,3|\rho|n,2\rangle\right]
$$
$$
= \sum_{n=1}^{\infty}-\sqrt{n}\langle n-1,3|\rho|n,2\rangle , \quad \text{(C.2)}
$$

which yields

$$
\frac{\mathrm{d}}{\mathrm{d}t}T_{23} = -\left(\kappa + \frac{\gamma_{12}+\gamma_{23}}{2}\right)T_{23} + g\sum_{n=1}^{\infty}n\Big[\langle n-1,3|\rho|n-1,3\rangle - \langle n,2|\rho|n,2\rangle\Big] . \quad \text{(C.3)}
$$

C. Operator Equations of Motion in the Density Matrix Formalism

To further evaluate the two terms introduced by the light-matter interaction, we first consider their factorization. In the fashion of the cluster expansion method we will then define a correlation function by subtracting the factorization from the full expectation value.

The semiclassical factorization of the atomic and photonic degrees of freedom is expressed by the factorization of the density matrix

$$\rho = \rho_{\text{phot}} \cdot \rho_{\text{atom}} \ . \tag{C.4}$$

Then the extended basis states (5.12) factorize. Accordingly, for the matrix elements we get

$$\langle n, j | \rho | n', j' \rangle = \langle n | \rho_{\text{phot}} | n' \rangle \cdot \langle j | \rho_{\text{atom}} | j' \rangle \ . \tag{C.5}$$

Tracing out either the photonic or the electronic states yields the population functions f_j or the photon number probability p_n, respectively:

$$f_j = \sum_n \langle n, j | \rho | n, j \rangle = \langle j | \rho_{\text{atom}} | j \rangle \underbrace{\sum_n \langle n | \rho_{\text{phot}} | n \rangle}_{=1} \ , \tag{C.6}$$

$$p_n = \sum_j \langle n, j | \rho | n, j \rangle = \langle n | \rho_{\text{phot}} | n \rangle \overbrace{\sum_j \langle j | \rho_{\text{atom}} | j \rangle}^{=1} \ . \tag{C.7}$$

Applying the semiclassical factorization to the first term under the sum in Eq. (C.3) yields

$$\sum_{n=1}^{\infty} n \langle n-1, 3 | \rho | n-1, 3 \rangle = \sum_{n=1}^{\infty} n\, p_{n-1} f_3 + S_3$$
$$= \sum_{n=0}^{\infty} (n+1) p_n f_3 + S_3 = \big(\langle n \rangle + 1 \big) f_3 + S_3 \ , \tag{C.8}$$

where the correlation function S_3 is introduced as the remainder of the subtraction of the factorized part from the full expectation value. Reordering Eq. (C.8) yields the definition of S_3 given in Eq. (5.30). The calculation for the other population-photon correlations S_j runs along the same lines, and we finally obtain for the resonant transition amplitude

$$\frac{\mathrm{d}}{\mathrm{d}t} T_{23} = - \left(\kappa + \frac{\gamma_{12} + \gamma_{23}}{2} \right) T_{23} + g \big[\langle n \rangle (f_3 - f_2) + f_3 + S_3 - S_2 \big] \ , \tag{C.9}$$

which is the equation of motion given in Section 5.3.2. Spontaneous and stimulated emission (first two terms in the square brackets) arise as the factorized part of the sum in Eq. (C.3).

Population-photon correlation dynamics. The time evolution of population-photon correlations is obtained along the same lines. As an example, we consider

$$
\begin{aligned}
\frac{\mathrm{d}}{\mathrm{d}t}S_3 &= \frac{\mathrm{d}}{\mathrm{d}t}\left[\sum_{n=1}^{\infty} n\langle n-1,3|\rho|n-1,3\rangle - \big(\langle n\rangle+1\big)f_3\right] \\
&= \sum_{n=1}^{\infty} n\bigg\{2\kappa\Big(n\langle n,3|\rho|n,3\rangle - (n-1)\langle n-1,3|\rho|n-1,3\rangle\Big) \\
&\qquad\qquad + \gamma_{34}\langle n-1,4|\rho|n-1,4\rangle - \gamma_{23}\langle n-1,3|\rho|n-1,3\rangle \\
&\qquad\qquad - g\sqrt{n}\,\Big(\langle n-1,3|\rho|n,2\rangle + \text{c.c.}\Big)\bigg\} \\
&\quad - [2gT_{23} - 2\kappa\langle n\rangle]f_3 - [\langle n\rangle+1](\gamma_{34}f_4 - \gamma_{23}f_3 - 2gT_{23})\,.
\end{aligned}
\tag{C.10}
$$

The terms under the sum are the contributions from the Liouville equation (5.14)–(5.19), whereas the last line contains the time derivative of the factorized part that is subtracted in order to obtain the correlation S_3. The cavity loss terms can be recast into the following form

$$
\begin{aligned}
\sum_{n=1}^{\infty} &n\Big(n\langle n,3|\rho|n,3\rangle - (n-1)\langle n-1,3|\rho|n-1,3\rangle\Big) \\
&= \sum_{n=1}^{\infty}\langle n-1,3|\rho|n-1,3\rangle\left[(n-1)^2 - n(n-1)\right] \\
&= \sum_{n=1}^{\infty}\langle n-1,3|\rho|n-1,3\rangle(1-n) = -\sum_{n=1}^{\infty} n\,\langle n-1,3|\rho|n-1,3\rangle + f_3\,.
\end{aligned}
\tag{C.11}
$$

Replacing this into Eq. (C.10) yields the equation of motion for S_3 that is given in Eq. (5.31) and that is reprinted here for convenience:

$$
\frac{\mathrm{d}}{\mathrm{d}t}S_3 = -(2\kappa+\gamma_{23})S_3 + \gamma_{34}S_4 + 2gT_{23}\big[\langle n\rangle+1-f_3\big] - 2g\Pi_{23}\,.
\tag{C.12}
$$

Quintuplet level carrier-photon correlations. In the equation of motion for Π_{23} analog correlations $\tilde{S}_2$ and $\tilde{S}_3$ with an additional factor n in the sum occur. According to the classification in Section 5.3.3 these quantities are quintuplet level terms. As our goal is the comparison to the cluster expansion containing correlations up to the quadruplet level, no dynamic equation is derived for $\tilde{S}_2$ and $\tilde{S}_3$, but these quantities

are factorized. After rewriting

$$\tilde{S}_3 = \sum_{n=1}^{\infty} n^2 \Big[\langle n-1, 3 | \rho | n-1, 3 \rangle - \rho_{n-1} f_3 \Big]$$

$$= \sum_{n=0}^{\infty} (n+1)^2 \Big[\langle n, 3 | \rho | n, 3 \rangle - \rho_n f_3 \Big] \qquad \text{(C.13)}$$

$$= \sum_{n=0}^{\infty} \Big[(n^2 + 2n) \langle n, 3 | \rho | n, 3 \rangle \Big] - \Big[\langle n^2 \rangle + 2 \langle n \rangle \Big] f_3 \ .$$

we can identify the following operator averages in the last line in analogy to Eqs. (5.37) and (5.38)

$$\tilde{S}_3 = \langle b^\dagger b b^\dagger b c^\dagger c \rangle + 2 \langle b^\dagger b c^\dagger c \rangle - \Big[\langle b^\dagger b b^\dagger b \rangle + 2 \langle b^\dagger b \rangle \Big] f_3$$

$$= \langle b^\dagger b^\dagger b b c^\dagger c \rangle + 3 \langle b^\dagger b c^\dagger c \rangle - \Big[3 \langle b^\dagger b \rangle + 2 \langle b^\dagger b \rangle^2 + \delta \langle b^\dagger b^\dagger b b \rangle \Big] f_3$$

$$= \delta \langle b^\dagger b^\dagger b b \rangle f_3 + 2 \langle b^\dagger b \rangle \langle b^\dagger b c^\dagger c \rangle + 2 \langle b^\dagger b \rangle^2 f_3 + 3 \langle b^\dagger b \rangle f_3 + 3 \delta \langle b^\dagger b c^\dagger c \rangle + \delta \langle b^\dagger b^\dagger b b c^\dagger c \rangle$$

$$\quad - \Big[3 \langle b^\dagger b \rangle + 2 \langle b^\dagger b \rangle^2 + \delta \langle b^\dagger b^\dagger b b \rangle \Big] f_3$$

$$\approx \Big[2 \langle b^\dagger b \rangle + 3 \Big] \delta \langle b^\dagger b c^\dagger c \rangle \ ,$$

$$\text{(C.14)}$$

where the quintuplet level correlation function $\delta \langle b^\dagger b^\dagger b b c^\dagger c \rangle$ has been dropped. With this, the theory closes on the quadruplet level. Along the very same lines, for $\tilde{S}_2$ one finds

$$\tilde{S}_2 \approx \Big[2 \langle b^\dagger b \rangle + 1 \Big] \delta \langle b^\dagger b v^\dagger v \rangle \ . \qquad \text{(C.15)}$$

D. Obtaining the Rate Equations from the Liouville/von-Neumann Equation

In Section 5.3.2 we have derived a hierarchy of coupled equations of motion from the Liouville/von-Neumann equation. Here we show how the rate equations from Section 5.1 can be recovered for a single atom. For the notation refer to Section 5.3.2. We consider the transition amplitude T_{23} in the semiclassical limit, i.e., where only the factorized contributions are considered. As is explained in Appendix C, this corresponds to Eq. (5.29), where the correlations S_2 and S_3 are omitted. Then the adiabatic solution is given by

$$T_{23} \approx \frac{g}{\kappa + \frac{\gamma_{12}+\gamma_{23}}{2}} \big[\langle n \rangle (f_3 - f_2) + f_3\big] . \tag{D.1}$$

From Eq. (5.26) we obtain for the population in the excited state

$$\frac{\mathrm{d}}{\mathrm{d}t} f_3 = -\frac{2g^2}{\kappa + \frac{\gamma_{12}+\gamma_{23}}{2}} \big[\langle n \rangle (f_3 - f_2) + f_3\big] - \gamma_{23} f_3 + \gamma_{34} f_4 \tag{D.2}$$

First, we identify $\frac{2g^2}{\kappa + \frac{\gamma_{12}+\gamma_{23}}{2}}$ with the emission rate into the laser mode $1/\tau_l$, cf. Eq. (B.2). Furthermore, we assume a fully inverted system due to a rapid clearance of the lower laser level, i.e. $f_2 = 0$, and identify γ_{23} with the spontaneous emission into non-lasing modes $1/\tau_{\mathrm{nl}}$. In the one-electron system that we consider in Chapter 5, the pump rate into the upper level $|4\rangle$ requires the presence of an electron in the lowest level. To recover the atomic rate equations, we must lift the one-electron restriction and replace the scattering term $\gamma_{34} f_4$ by a constant pump rate $\tilde{P}$. With this, we finally obtain

$$\frac{\mathrm{d}}{\mathrm{d}t} f_3 = -\frac{f_3 \big[\langle n \rangle + 1\big]}{\tau_l} - \frac{f_3}{\tau_{\mathrm{nl}}} + \tilde{P} . \tag{D.3}$$

From Eq. (5.35), we get for the photon number $n = \langle n \rangle$

$$\frac{\mathrm{d}}{\mathrm{d}t} n = -2\kappa n + \frac{f_3(n+1)}{\tau_l} . \tag{D.4}$$

By means of Eqs. (3.17) and (3.18) these equations are cast into the familiar form

$$\frac{\mathrm{d}}{\mathrm{d}t} f_3 = -\frac{\beta}{\tau_{\mathrm{sp}}} f_3(n+1) - \frac{1-\beta}{\tau_{\mathrm{sp}}} f_3 + \tilde{P} , \tag{D.5}$$

$$\frac{\mathrm{d}}{\mathrm{d}t} n = -2\kappa n + \frac{\beta}{\tau_{\mathrm{sp}}} f_3(n+1) . \tag{D.6}$$

D. Obtaining the Rate Equations from the Liouville/von-Neumann Equation

The only remaining difference to Eqs. (5.1) and (5.2) is the scaling of f_3 with the total number of emitters, which is here naturally unity for the derivation from a single-atom model.

E. Numerical Methods

The numerical implementation of the theory presented in this thesis is straightforward in principle, as it always involves the time integration of coupled non-linear differential equations. Due to the large number of equations and/or required time steps, the efficiency of the implementation must be given some consideration. This appendix is meant as an aid for reproducing the presented results or transferring the utilized methods to other applications, rather than being a description of the used numerical algorithms, which can be found in textbooks and publications.

E.1. Solving the SLE in Time

The results presented in Chapter 2 have been obtained by solving the semiconductor luminescence equations in time. They constitute a set of coupled differential equations, the total number depending on the number of single-particle states n (localized QD and wetting layer states) and the number of modes m of the quantized light field. E.g., $\langle b_\xi^\dagger v_\nu^\dagger c_\nu \rangle$ constitutes $n \times m$ coupled equations. To cope with the oscillating free contribution, cf. for example Eq. (2.18), a constant-time step Runge-Kutta algorithm of fourth order has been used with a stepsize of the order of femtoseconds. Due to the nested structure of the equations, in particular beyond the doublet level, a pure implementation in a language optimized for linear matrix operations like Matlab is inefficient.

E.2. Solving the Laser Equations

The calculations of the laser characteristics, on the other hand, were performed in Matlab. In Chapter 3 we have assumed that the QDs are in resonance with the lasing mode. Due to this assumption, rapidly oscillating phase factors do not appear in the equations of motion that describe the laser behavior. At excitation powers high enough to bring the system into the transition region, the time-dynamics may exhibit switch-on oscillations depending on the parameter regime, but then the system evolves towards a stationary solution. At low excitation powers the luminescence is

determined only by the spontaneous emission and the time evolution is monotonic. For the calculation of input/output curves and the second order correlation function, only the stationary values are required, which are sometimes reached after microseconds. In this situation, a variable-step size time-integration algorithm is predestined. Rather than using a Runge-Kutta-like method, we use an algorithm based on a numerical differentiation formula (NDF) [76, 129], namely ode15s.

In Matlab, different algorithms for the solution of stiff[1] and non-stiff ordinary differential equations are conveniently provided by the ode-(ordinary differential equations) suite, which is documented in the Matlab manual and in Ref. [129]. For a typical calculation of a single point on the input/output curve, as is shown in Fig. 3.5, the numerical expenses are summarized in Table E.1. Compared are three different algorithms: ode45 corresponds to an adaptive-step size Runge-Kutta method of $4^{th}/5^{th}$ order and is often the standard method for solving odes. ode23 is a lower-order Runge-Kutta algorithm of $2^{nd}/3^{rd}$ order and is faster than ode45 at cruder tolerances. ode15s is a NDF-based solver designed to work efficiently for stiff problems. For each iteration the Jacobian matrix is required. However, this is calculated only if the required convergence rate is not achieved. In fact, this results in very few calculations of the Jacobian matrix, and, thus, of numerical partial derivatives at all. This makes the ode15s algorithm very fast also for non-stiff problems. It is astonishing how much more efficient it is than the Runge-Kutta-based algorithms for the integration of the laser model. The same efficiency is achieved in similar situations, like the atomic rate equations discussed in Chapter 5.

It should be noted that the coupled laser equations are sensitive to the choice of parameters of the physical system and of the ode integration algorithm. Thus, the choice of initial step sizes and correct tolerances are important.

For the calculation of the laser emission after an excitation pulse, discussed in Section 3.5, photons need to be integrated over a long time window to obtain the total number of emitted photons. Appropriate abort criteria can be incorporated with Matlab's ode-suite by means of so-called event functions. The event function checks if an abort criteria is fulfilled, and if this is the case, it causes the ode solver to abort the integration. This method allows for the upper time limit to be determined during the time integration.

---

[1] Stiff differential equations contain variables that evolve on significantly different time scales [57, 129].

	ode45	ode23	ode15s
evaluation time	9 s	11 s	0.9 s
# function calls	93,000	122,000	2,785
# time steps	60,500	40,800	1,500

(a)

	ode45	ode23	ode15s
evaluation time	2.3 s	2.1 s	0.7 s
# function calls	24,000	21,500	1,700
# time steps	15,300	7,100	870

(b)

Table E.1.: Comparison between the numerical expenses of three different ode-solvers contained in Matlab's ode-suite. The calculation was performed for one point on the input/output curve, as it is shown in Fig. 3.5. Table (a) corresponds to a situation below threshold where the evolution is slow. In (b) the evolution into the stationary state is faster due to additional stimulated processes on a faster timescale. Listed are the evaluation time, number of function calls and required number of timesteps. All calculations were performed with the same accuracy. The numbers should only be considered in relation to each other, as absolute values depend on the choice of parameters and computational resources.

Bibliography

[1] URL `http://www.phog.physik.uni-muenchen.de/people/rogach_andrey/`.

[2] K. J. Ahn, J. Förstner, and A. Knorr. "Resonance fluorescence of semiconductor quantum dots: Signatures of the electron-phonon interaction". *Phys. Rev. B* **71**, 153309 (2005).

[3] N. Akopian, N. H. Lindner, E. Poem, Y. Berlatzky, J. Avron, D. Gershoni, B. D. Gerardot, and P. M. Petroff. "Entangled Photon Pairs from Semiconductor Quantum Dots". *Phys. Rev. Lett.* **96**, 130501 (2006).

[4] Z. I. Alferov. "Nobel Lecture: The double heterostructure concept and its applications in physics, electronics, and technology". *Rev. Mod. Phys.* **73**, 767 (2001).

[5] M. H. Anderson, J. R. Ensher, M. R. Matthews, C. E. Wieman, and E. A. Cornell. "Observation of Bose-Einstein Condensation in a Dilute Atomic Vapor". *Science* **269**, 198 (1995).

[6] T. Aschenbrenner. *Lumineszenz und Ladungsträgerdynamik in Halbleiter-Quantenfilmen und Halbleiter-Quantenpunkten*. Master's thesis, Universität Bremen, Germany (2004).

[7] S. Ates, C. Gies, S. M. Ulrich, J. Wiersig, S. Reitzenstein, A. Löffler, A. Forchel, F. Jahnke, and P. Michler. "Coherence Length of High-β Semiconductor Microcavity Lasers". *submitted for publication* (2007).

[8] S. Ates, S. Ulrich, P. Michler, S. Reitzenstein, A. Löffler, and A. Forchel. "Coherence properties of high-β elliptical semiconductor micropillar lasers". *Appl. Phys. Lett.* **90**, 161111 (2007).

[9] A. Badolato, K. Hennessy, M. Atatüre, J. Dreiser, E. Hu, P. M. Petroff, and A. Imamoğlu. "Deterministic coupling of single quantum dots in single nanocavity modes". *Science* **308**, 1158 (2005).

[10] N. Baer, P. Gartner, and F. Jahnke. "Coulomb effects in semiconductor quantum dots". *Eur. Phys. J. B* **42**, 231 (2004).

[11] N. Baer, C. Gies, J. Wiersig, and F. Jahnke. "Luminescence of a Semiconductor Quantum Dot System". *Eur. Phys. J. B* **50**, 411 (2006).

Bibliography

[12] N. Baer, S. Schulz, S. Schumacher, P. Gartner, G.Czycholl, and F. Jahnke. "Optical properties of self-organized wurtzite InN/GaNquantum dots: A combined atomistic tight-binding and full configuration interaction calculation". *Appl. Phys. Lett.* **87**, 231114 (2005).

[13] A. Barenco and M. A. Dupertuis. "Quantum many-body states of excitons in a small quantum dot". *Phys. Rev. B* **52**, 2766 (July 1995).

[14] M. Bayer, A. Forchel, T. L. Reinecke, P. A. Knipp, and S. Rudin. "Confinement of Light in Microresonators for Controlling Light-Matter Interaction". *Phys. Stat. Sol. (a)* **191**, 3 (2002).

[15] M. Bayer, P. Hawrylak, K. Hinzer, S. Fafard, M. Korkusinski, Z. R. Wasilewski, O. Stern, and A. Forchel. "Coupling and Entangling of Quantum States in Quantum Dot Molecules". *Science* **291**, 451 (2001).

[16] M. Bayer, G. Ortner, O. Stern, A. Kuther, A. F. A.A. Gorbunov, P. Hawrylak, S. Fafard, K. Hinzer, T. L. Reinecke, S. N. Walck, J. Reithmaier, F. Klopf, F. Schäfer, and G. W. Bryant. "Fine structure of neutral and charged excitons in self-assembled In(Ga)As/(Al)GaAs quantum dots". *Phys. Rev. B* **65**, 195315 (2002).

[17] G. J. Beirne, M. Reischle, R. Roï£¡ach, W.-M. Schulz, M. Jetter, J. Seebeck, P. Gartner, C. Gies, F. Jahnke, and P. Michler. "Electronic shell structure and carrier dynamics of high aspect ratio InP single quantum dots". *Phys. Rev. B* **75**, 195302 (2007).

[18] O. Benson and Y. Yamamoto. "Master-equation model of a single-quantum-dot microsphere laser". *Phys. Rev. A* **59**, 4756 (1999).

[19] T. Berstermann, T. Auer, H. Kurtze, M. Schwab, M. Bayer, J. Wiersig, C. Gies, F. Jahnke, D. Reuter, and A. Wieck. "Systematic study of carrier correlations in the electron-hole recombination dynamics of quantum dots". *Phys. Rev. B* **76**, 165318 (2007).

[20] D. Bimberg, M. Grundmann, and N. N. Ledentsov. *Quantum Dot Heterostructures*. John Wiley and Sons, 1999.

[21] G. Björk and Y. Yamamoto. "Analysis of Semiconductor Microcavity Lasers using Rate Equations". *IEEE Journal of Quant. Electr.* **27**, 2386 (1991).

[22] R. Bonifacio and L. A. Lugiato. "Cooperative radiation processes in two-level systems: Superfluorescence". *Phys. Rev. A* **11**, 1507 (1975).

[23] R. Bonifacio, P. Schwendimann, and F. Haake. "Quantum Statistical Theory of Superradiance. I". *Phys. Rev. A* **4**, 302 (1971).

[24] R. Bonifacio, P. Schwendimann, and F. Haake. "Quantum Statistical Theory of Superradiance. II". *Phys. Rev. A* **4**, 854 (1971).

[25] P. Borri, W. Langbein, S. Schneider, U. Woggon, R. L. Sellin, D. Ouyang, and D. Bimberg. "Ultralong Dephasing Time in InGaAs Quantum Dots". *Phys. Rev. Lett.* **87**, 157401 (2001).

[26] P. Borri, W. Langbein, S. Schneider, U. Woggon, R. L. Sellin, D. Ouyang, and D. Bimberg. "Exciton Relaxation and Dephasing in Quantum-Dot Amplifiers From Room to Cryogenic Temperatures". *IEEE Jour. of selected Topics in Quant. Electrodynamics* **8**, 984 (2002).

[27] M. Braskén, M. Lindberg, D. Sundholm, and J. Olsen. "Spatial carrier-carrier correlations in strain-induced quantum dots". *Phys. Rev. B* **64**, 035312 (2001).

[28] R. H. Brown and R. Q. Twiss. "Correlation between Photons in two Coherent Beams of Light". *Nature* **177**, 27 (1956).

[29] H. J. Carmichael. *Statistical Methods in Quantum Optics 1*. Springer, Berlin Heidelberg New York, 1999.

[30] J. R. Chelikowsky and M. L. Cohen. "Nonlocal pseudopotential calculations for the electronic structure of eleven diamond and zinc-blende semiconductors". *Phys. Rev. B* **14**, 556 (1976).

[31] Y.-S. Choi, M. T. Rakher, K. Hennessy, S. Strauf, A. Badolato, P. M. Petroff, D. Bouwmeester, and E. L. Hu. "Evolution of the onset of coherence in a family of photonic crystal nanolasers". *Appl. Phys. Lett.* **91**, 031108 (2007).

[32] W. W. Chow, S. W. Koch, and M. Sargent. *Semiconductor Laser Physics*. Springer-Verlag, Berlin, 1994.

[33] C. Cohen-Tannoudji, J. Dupot-Roc, and G. Grynberg. *Photons and Atoms*. Wiley and Sons, 1989.

[34] S. Coleman. "There are no Goldstone bosons in two dimensions". *Commun. Math. Phys.* **31**, 259 (1973).

[35] C. Cornet, A. Schliwa, J. Even, F. D. C. Celebi, A. Lï£¡oublon, E. M. C. Paranthoï£¡, A. Simon, P. M. Koenraad, N. Bertru, D. Bimberg, and S. Loualiche. "Electronic and optical properties of InAs/InP quantum dots on InP(100) and InP(311)B substrates: Theory and experiment". *Phys. Rev. B* **74**, 035312 (2006).

[36] K. B. Davis, M.-O. Mewes, M. R. Andrews, N. J. van Druten, D. S. Durfee, D. M. Kurn, and W. Ketterle. "Bose-Einstein Condensation in a Gas of Sodium Atoms". *Phys. Rev. Lett.* **75**, 3969 (1995).

[37] E. Dekel, D. Gershoni, E. Ehrenfreund, J. M. Garcia, and P. M. Petroffand. "Carrier-Carrier correlations in an optically excited single semiconductor quantum dot". *Phys. Rev. B* **61**, 11009 (April 2000).

[38] F. DeMartini and G. R. Jacobovitz. "Anomalous Spontaneous-Stimulated-Decay Phase Transition and Zero-Threshold Laser Action in a Microscopic Cavity". *Phys. Rev. Lett.* **60**, 1711 (1988).

[39] H. Deng, G. Weihs, C. Santori, J. Bloch, and Y. Yamamoto. "Condensation of Semiconductor Microcavity Exciton Polaritons". *Science* **298**, 199 (2002).

[40] R. H. Dicke. "Coherence in Spontaneous Radiation Processes". *Phys. Rev.* **93**, 99 (1954).

[41] N. J. van Druten, Y. Lien, C. Serrat, S. S. R. Oemrawsingh, M. P. van Exter, and J. P. Woerdman. "Laser with thresholdless intensity fluctuations". *Phys. Rev. A* **62**, 053808 (2000).

[42] J. H. Eberly and K. Wódkiewicz. "The time-dependent physical spectrum of light". *J. Opt. Soc. Am.* **67**, 1252 (1977).

[43] A. Einstein. "Quantentheorie des einatomigen idealen Gases. Zweite Abhandlung". *Sitzungberichte der königlich preussischen Akadademie der Wissenschaften* **XVII-I–XXV**, 3 (1925).

[44] T. Feldtmann, L. Schneebeli, M. Kira, and S. W. Koch. "Quantum theory of light emission from a semiconductor quantum dot". *Phys. Rev. B* **73**, 155319 (2006).

[45] J. Fricke. "Transport equations including many-particle correlations for an arbitrary quantum system: A general formalism". *Ann. Phys.* **252**, 479 (1996).

[46] J. Fricke, V. Meden, C. Woehler, and K. Schoenhammer. "Improved transport equations including correlations for electron-phonon systems: Comparison with exact solutions in one dimension". *Ann. Phys.* **253**, 177 (1997).

[47] S. S. G. Pistone, O. D. Stefano, and R. Girlanda. "Microscopic quantum theory of spatially resolved photoluminescence in semiconductor quantum structures". *Appl. Phys. Lett.* **84**, 2971 (2004).

[48] E. J. Gansen, M. A. Rowe, M. B. Greene, D. Rosenberg, T. E. Harvey, M. Y. Su, R. H. Hadfield, S. W. Nam, and R. P. Mirin. "Photon-number-discriminating detection using a quantum dot, optically gated, field-effect transistor". *Nature Photonics* **1**, 585 (2007).

[49] B. Gayral, J. M. Gï£¡ard, B. Legrand, E. Costard, and V. Thierry-Mieg. "Optical study of GaAs/AlAs pillar microcavities with elliptical cross section". *Appl. Phys. Lett* **72**, 1421 (1998).

[50] J. M. Gérard and B. Gayral. "Strong Purcell effect for InAs quantum boxes in three--dimensional solid-state microcavities". *J. Lightwave Technol.* **17**, 2089 (1999).

[51] J. M. Gérard, B. Sermage, B. Gayral, B. Legrand, E. Costard, and V. Thierry-Mieg. "Enhanced Spontaneous Emission by Quantum Boxes in a Monolithic Optical Microcavity". *Phys. Rev. Lett.* **81**, 1110 (1998).

[52] C. Gies, J. Wiersig, and F. Jahnke. "Output characteristics of pulsed and cw-excited quantum-dot microcavity lasers". *submitted for publication* (2008).

[53] C. Gies, J. Wiersig, M. Lorke, and F. Jahnke. "Semiconductor model for quantum dot-based microcavity lasers". *Phys. Rev. A* **75**, 013803 (2007).

[54] R. J. Glauber. "The Quantum Theory of Optical Coherence". *Phys. Rev.* **130**, 2529 (1963).

[55] L. A. Graham, D. L. Huffaker, and D. G. Deppe. "Spontaneous lifetime control in a native-oxide-apertured microcavity". *Appl. Phys. Lett.* **74**, 2048 (1999).

[56] M. Grundmann, O. Stier, and D. Bimberg. "InAs/GaAs pyramidal quantum dots: Strain distribution, optical phonons, and electronic structure". *Phys. Rev. B* **52**, 11969 (1995).

[57] W. Hackbusch, H. R. Schwarz, and E. Zeidler. *Taschenbuch der Mathematik*. 2nd edition. Teubner, 2003.

[58] H. Haug and S. W. Koch. *Quantum Theory of the Optical and Electronic Properties of Semiconductors*. World Scientific, Singapore, 1993.

[59] P. Hawrylak. "Excitonic artificial atoms: Engineering optical properties of quantum dots". *Phys. Rev. B* **60**, 5597 (August 1999).

[60] P. C. Hohenberg. "Existence of Long-Range Order in One and Two Dimensions". *Phys. Rev.* **158**, 383 (June 1967).

[61] W. Hoyer. *Quantentheorie zu Exzitonbildung und Photolumineszenz in Halbleitern*. Ph.D. thesis, Universität Marburg, Germany (2002).

[62] W. Hoyer, M. Kira, and S. W. Koch. "Influence of Coulomb and phonon interaction on the exciton formation dynamics in semiconductor heterostructures". *Phys. Rev. B* **67**, 155113 (2003).

[63] W. Hoyer, M. Kira, and S. W. Koch. "Cluster expansion in semiconductor quantum optics" in Morawetz, Klaus (Ed.), *Nonequilibrium Physics at Short Time Scales*. Springer, Berlin, 2004.

[64] J. D. Jackson. *Classical Electrodynamics*. John Wiley and Sons Inc., New York, London, Sydney, 1962.

[65] F. Jahnke, M. Kira, W. Hoyer, and S. W. Koch. "Influence of Correlation Effects on the Excitonic Semiconductor Photoluminescence". *phys. stat. sol (b)* **221**, 189 (2000).

[66] F. Jahnke and S. W. Koch. "Many-body theory for semiconductor microcavity lasers". *Phys. Rev. A* **52**, 1712 (1995).

[67] R. Jin, D. Boggavarapu, M. Sargent III, P. Meystre, H. M. Gibbs, and G. Khitrova. "Photon-number correlations near the threshold of microcavity lasers in the weak-coupling regime". *Phys. Rev. A* **49**, 4038 (1994).

[68] J. Kasprzak, M. Richard, S. Kundermann, A. Baas, P. Jeambrun, J. M. J. Keeling, F. M. Marchetti, M. H. Szymaska, R. AndrÃľ, J. L. Staehli, V. Savona, P. B. Littlewood, B. Deveaud, and L. S. Dang. "Bose-Einstein condensation of exciton polaritons". *Nature* **443**, 409 (2006).

[69] G. Khitrova, H. M. Gibbs, F. Jahnke, M. Kira, and S. W. Koch. "Nonlinear Optics of Normal–Mode–Coupling Semiconductor Microcavities". *Rev. Mod. Phys.* **71**, 1591 (1999).

[70] M. Kira, F. Jahnke, W. Hoyer, and S. W. Koch. "Quantum Theory of Spontaneous Emission and Coherent Effects in Semiconductor Microstructures". *Prog. in Quant. Electr.* **23**, 189 (1999).

[71] M. Kira, F. Jahnke, and S. W. Koch. "Microscopic Theory of Excitonic Signatures in Semiconductor Photoluminescence". *Phys. Rev. Lett.* **81**, 3263 (1998).

[72] M. Kira, F. Jahnke, and S. W. Koch. "Quantum Theory of Secondary Emission in Optically Excited Semiconductor Quantum Wells". *Phys. Rev. Lett.* **82**, 3544 (1999).

[73] A. Kiraz, M. Atatüre, and A. Imamoğlu. "Erratum: Quantum-dot single-photon sources: Prospects for applications in linear optics quantum-information processing [Phys. Rev. A **69**, 032305 (2004)]". *Phys. Rev. A* **70**, 059904 (2004).

[74] A. Kiraz, M. Atatüre, and A. Imamoğlu. "Quantum-dot single-photon sources: Prospects for applications in linear optics quantum-information processing". *Phys. Rev. A* **69**, 032305 (2004).

[75] K. v. Klitzing, G. Dorda, and M. Pepper. "New Method for High-Accuracy Determination of the Fine-Structure Constant Based on Quantized Hall Resistance". *Phys. Rev. Lett.* **45**, 494 (1980).

[76] R. W. Klopfenstein. "Numerical differentiation formulas for stiff systems of ordinary differential equations". *RCA Rev.* **32**, 447 (1971).

[77] I. L. Krestnikov, N. N. Ledentsov, A. Hoffmann, D. Bimberg, A. V. Sakharnov, W. V. Lundin, A. S. Tsatsul'nikov, A.F. Usikov, Z. I. Alferov, Y. G. Musikhin, and D. Gerthsen. "Quantum dot origin of luminescence in InGaN-GaN structures". *Phys. Rev. B* **66**, 155310 (2002).

[78] B. Krummheuer, V. M. Axt, and T. Kuhn. "Theory of pure dephasing and the resulting absorption lineshape in semiconductor quantum dots". *Phys. Rev. B* **65**, 195313 (2002).

[79] W. Langbein, P. Borri, U. Woggon, V. Stavarache, D. Reuter, and A. D. Wieck. "Radiatively limited dpehasing in InAs quantum dots". *Phys. Rev. B* **70**, 033301 (2004).

[80] R. B. Laughlin. "Anomalous Quantum Hall Effect: An Incompressible Quantum Fluid with Fractionally Charged Excitations". *Phys. Rev. Lett.* **50**, 1395 (1983).

[81] G. Lindblad. "On the generators of quantum dynamical semigroups". *Commun. Math. Phys.* **48**, 119 (1976).

[82] P. Lodahl, A. Floris van Driel, I. S. Nikolaev, A. Irman, K. Overgaag, D. Vanmaekelbergh, and W. L. Vos. "Controlling the dynamics of spontaneous emission from quantum dots by photonic crystals". *Nature* **430**, 654 (2004).

[83] A. Löffler, J. P. Reithmaier, G. Sek, C. Hofmann, S. Reitzenstein, M. Kamp, and A. Forchel. "Semiconductor quantum dot microcavity pillars with high-quality factors and enlarged dot dimensions". *Appl. Phys. Lett* **86**, 111105 (2005).

[84] H. Lohmeyer. *Optischer Einschluss, Lasing und Purcell-Effekt in Mikrosäulen auf Basis breitlückiger Halbleiter*. Dissertation, Universität Bremen (2007).

[85] H. Lohmeyer, C. Kruse, K. Sebald, J. Gutowski, and D. Hommel. "Enhanced spontaneous emission of CdSe quantum dots in monolithic II-VI pillar microcavities". *Appl. Phys. Lett.* **89**, 091107 (2006).

[86] M. Lorke, T. R. Nielsen, J. Seebeck, P. Gartner, and F. Jahnke. "Influence of carrier-carrier and carrier-phonon correlations on optical absorption and gain in quantum-dot systems". *Phys. Rev. B* **73**, 085324 (2006).

[87] R. Loudon. *The quantum theory of light*. 2nd edition. Clarendon Press, Oxford, 1983.

[88] E. Malić, K. J. Ahn, M. J. P. Bormann, P. Hövel, E. Schöll, A. Knorr, M. Kuntz, and D. Bimberg. "Theory of relaxation oscillations in semiconductor quantum dot lasers". *Appl. Phys. Lett.* **89**, 101107 (2006).

[89] L. Mandel and E. Wolf. *Optical coherence and quantum optics*. Cambridge University Press, Cambridge, 1995.

[90] N. D. Mermin. "Crystalline Order in Two Dimensions". *Phys. Rev.* **176**, 250 (1968).

[91] N. D. Mermin and H. Wagner. "Absence of Ferromagnetism or Antiferromagnetism in One- or Two-Dimensional Isotropic Heisenberg Models". *Phys. Rev. Lett.* **17**, 1133 (Nov 1966).

Bibliography

[92] P. Meystre and M. Sargent III. *Elements of Quantum Optics*. Springer, Berlin, 1999.

[93] P. Michler, editor. *Single Quantum Dots: Fundamentals, Applications, and New Concepts*. Topics in Applied Physics. Springer, Berlin, 2003.

[94] P. Michler, A. Kiraz, C. Becher, W. V. Schoenfeld, P. M. Petroff, L. Zhang, E. Hu, and A. Imamoğlu. "A Quantum Dot Single-Photon Turnstile Device". *Science* **290**, 2282 (2000).

[95] P. Michler, A. Kiraz, L. Zhang, C. Becher, E. Hu, and A. Imamoğlu. "Laser emission from quantum dots in microdisk structures". *Appl. Phys. Lett* **77**, 184 (2000).

[96] E. Moreau, I. Robert, J. M. Gérard, I. Abram, L. Manin, and V. Thierry-Mieg. "Single-mode solid-state single photon source based on isolated quantum dots in pillar microcavities". *Appl. Phys. Lett.* **79**, 2865 (2001).

[97] D. Morris, N. Perret, and S. Fafard. "Carrier energy relaxation by means of Auger processes in InAs/GaAs self-assembled quantum dots". *Appl. Phys. Lett.* **75**, 3593 (1999).

[98] Y. Mu and C. M. Savage. "One-atom lasers". *Phys. Rev. A* **46**, 5944 (1992).

[99] E. A. Muljarov and R. Zimmermann. "Dephasing in Quantum Dots: Quadratic Coupling to Acoustic Phonons". *Phys. Rev. Lett.* **85**, 1516 (2000).

[100] T. R. Nielsen, P. Gartner, and F. Jahnke. "Many-body theory of carrier capture and relaxation in semiconductor quantum-dot lasers". *Phys. Rev. B* **69**, 235314 (2004).

[101] R. A. Oliver, G. A. D. Briggs, M. J. Kappers, C. J. Humphreys, S. Yasin, J. H. Rice, J. D. Smith, and R. A. Taylor. "InGaN quantum dots grown by metalorganic vapor phase epitaxy employing a post-growth nitrogen anneal". *Appl. Phys. Lett.* **83**, 755 (2003).

[102] O. Painter, R. K. Lee, A. Scherer, A. Yariv, J. O'Brien, P. Dapkus, and I. Kim. "Two-Dimensional Photonic Band-Gap Defect Mode Laser". *Science* **284**, 1819 (1999).

[103] G. Parascandolo and V. Savona. "Long-range radiative interaction between semiconductor quantum dots". *Phys. Rev. B* **71**, 045335 (2005).

[104] H.-G. Park, S.-H. Kim, S.-H. Kwon, Y.-G. Ju, J.-K. Yang, J.-H. Baek, S.-B. Kim, and Y.-H. Lee. "Electrically Driven Single-Cell Photonic Crystal Laser". *Science* **305**, 1444 (2004).

[105] M. Pelton, C. Santori, J. Vucković, B. Zhang, G. S. Solomon, J. Plant, and Y. Yamamoto. "Efficient Source of Single Photons: A Single Quantum Dot in a Micropost Microcavity". *Phys. Rev. Lett.* **89**, 233602 (2002).

[106] E. Peter, P. Senellart, D. Martrou, A. Lemaitre, J. Hours, J. M. Gérard, and J. Bloch. "Exciton-Photon strong-coupling regime for a single quantum dot in a microcavity". *Phys. Rev. Lett.* **95**, 067401 (2005).

[107] R. E. Prange and S. M. Girvin, editors. *The Quantum Hall Effect*. 2nd edition. Springer Verlag, 1990.

[108] I. Protsenko, P. Domokos, V. Lefèvre-Seguin, J. Hare, J. M. Raimond, and L. Davidovich. "Quantum theory of a thresholdless laser". *Phys. Rev. A* **59**, 1667 (1999).

[109] I. E. Protsenko and M. Travagnin. "Microscopic model of semiconductor laser without inversion". *Phys. Rev. A* **65**, 013801 (2001).

[110] E. M. Purcell, H. C. Torrey, and R. V. Pound. "Resonance Absorption by Nuclear Magnetic Moments in a Solid". *Phys. Rev.* **69**, 37 (1946).

[111] A. Puzder, A. J. Williamson, F. Gygi, and G. Galli. "Self-Healing of CdSe Nanocrystals: First-Principles Calculations". *Phys. Rev. Lett.* **92**, 217401 (2004).

[112] L. Quiroga and N. F. Johnson. "Entangled Bell and Greenberger-Horne-Zeilinger States of Excitons in Coupled Quantum Dots". *Phys. Rev. Lett.* **83**, 2270 (1999).

[113] J. P. Reithmaier, G. Sek, A. Löffler, C. Hofmann, S. Kuhn, S. Reitzenstein, L. V. Keldysh, V. D. Kulakovskii, T. L. Reinecke, and A. Forchel. "Strong coupling in a single quantum dot-semiconductor microcavity system". *Nature* **432**, 197 (2004).

[114] S. Reitzenstein, A. Bazhenov, A. Gorbunov, C. Hofmann, S. Münch, A. Löffler, M. Kamp, J. P. Reithmaier, V. D. Kulakovskii, and A. Forchel. "Lasing in high-Q quantum-dot micropillar cavities". *Appl. Phys. Lett.* **89**, 051107 (2006).

[115] S. Reitzenstein, C. Böckler, A. Bazhenov, A. Gorbunov, A. Löffler, M. Kamp, V. D. Kulakovskii, and A. Forchel. "Single quantum dot controlled lasing effects in high-Q micropillar cavities". *Optics Express* **16**, 4848 (2008).

[116] S. Reitzenstein, C. Hofmann, A. Gorbunov, M. Strauß, S. H. Kwon, C. Schneider, A. Löffler, S. Hoefling, M. Kamp, and A. Forchel. "AlAs/GaAs micropillar cavities with quality factors exceeding 150,000". *Appl. Phys. Lett.* **90**, 251109 (2007).

[117] J. Renner, L. Worschech, A. Forchel, S. Mahapatra, and K. Brunner. "CdSe quantum dot microdisk laser". *Appl. Phys. Lett.* **89**, 231104 (2006).

[118] P. R. Rice and H. J. Carmichael. "Photon statistics of a cavity-QED laser: A comment on the laser-phase-transition analogy". *Phys. Rev. A* **50**, 4318 (1994).

[119] C. Santori, M. Pelton, G. Solomon, Y. Dale, and Y. Yamamoto. "Triggered Single Photons from a Quantum Dot". *Phys. Rev. Lett.* **86**, 1502 (2001).

Bibliography

[120] P. Sarkar and M. Springborg. "Density-functional study of size-dependent properties of Cd_mSe_n clusters". *Phys. Rev. B* **68**, 235409 (2003).

[121] S. Schulz. *Electronic and Optical Properties of Quantum Dots: A Tight-Binding Approach*. Ph.D. thesis, Universität Bremen, Germany (2007).

[122] S. Schulz and G. Czycholl. "Tight-binding model for semiconductor nanostructures". *Phys. Rev. B* **72**, 165317 (2005).

[123] S. Schulz, S. Schumacher, and G. Czycholl. "Tight-binding model for semiconductor quantum dots with a wurtzite crystal structure: From one-particle properties to Coulomb correlations and optical spectra". *Phys. Rev. B* **73**, 245327 (2006).

[124] M. Schwab, H. Kurtze, T. Auer, T. Berstermann, M. Bayer, J. Wiersig, N. Baer, C. Gies, F. Jahnke, J. P. Reithmaier, A. Forchel, M. Benyoucef, and P. Michler. "Radiative emission dynamics of quantum dots in a single cavity micropillar". *Phys. Rev. B* **74**, 045323 (2006).

[125] M. O. Scully and M. S. Zubairy. *Quantum Optics*. Cambridge Univerisity Press, Cambridge, 1997.

[126] K. Sebald, P. Michler, T. Passow, D. Hommel, G. Bacher, and A. Forchel. "Single-photon emission of CdSe quantum dots at temperatures up to 200 K". *Appl. Phys. Lett.* **81**, 2920 (2002).

[127] J. Seebeck, P. Gartner, and F. Jahnke. "Carrier-LO-phonon quantum kinetics in semiconductor quantum dots at low temperatures". *submitted for publication* (2007).

[128] J. Seebeck, T. R. Nielsen, P. Gartner, and F. Jahnke. "Polarons in semiconductor quantum dots and their role in the quantum kinetics of carrier relaxation". *Phys. Rev. B* **71**, 125327 (2005).

[129] L. F. Shampine and M. W. Reichelt. "The Matlab ode suite". *SIAM J. Sci. Comput.* **18**, 1 (1997).

[130] W. Sheng, S.-J. Cheng, and P. Hawrylak. "Multiband theory of multi-exciton complexes in self-assembled quantum dots". *Phys. Rev. B* **71**, 035316 (2005).

[131] A. J. Shields, M. P. OSullivan, I. Farrer, D. A. Ritchie, R. A. Hogg, M. L. Leadbeater, C. E. Norman, and M. Pepper. "Detection of single photons using a field-effect transistor gated by a layer of quantum dots". *Appl. Phys. Lett.* **76**, 3673 (2000).

[132] A. J. Shields, M. P. OSullivan, I. Farrer, D. A. Ritchie, M. L. Leadbeater, N. K. Patel, R. A. Hogg, C. E. Norman, N. J. Curson, and M. Pepper. "Single Photon Detection with a Quantum Dot Transistor". *Jpn. J. Appl. Phys.* **40**, 2058 (2001).

[133] D. Snoke. "Spontaneous Bose Coherence of Excitons and Polaritons". *Science* **298**, 1368 (2002).

[134] G. S. Solomon, M. Pelton, and Y. Yamamoto. "Single-mode Spontaneous Emission from a Single Quantum Dot in a Three-Dimensional Microcavity". *Phys. Rev. Lett.* **86**, 3903 (2001).

[135] M. J. Stevens, R. H. Hadfield, E. Schwall, S. W. Nam, and R. P. Mirin. "Quantum Dot Single Photon Sources Studied with Superconducting Single Photon Detectors". *IEEE Journal of Selected Topics in Quantum Electronics* **12**, 1255 (2006).

[136] O. Stier. *Electronic and Optical Properties of Quantum Dots and Wires*. Ph.D. thesis, Technische Universität Berlin, Germany (2000).

[137] I. N. Stranski and L. Krastanow. "Theory of orientation separation of ionic crystals". *Ber. Akad. Wiss. Wien, Math.-Naturwiss. Kl., Abt. IIb* **146**, 797 (1938).

[138] S. Strauf, K. Hennessy, M. T. Rakher, Y.-S. Choi, A. Badolato, L. C. Andreani, E. L. Hu, P. M. Petroff, and D. Bouwmeester. "Self-Tuned Quantum Dot Gain in Photonic Crystal Lasers". *Phys. Rev. Lett.* **96**, 127404 (2006).

[139] V. V. Temnov. "Superradiance and subradiance in the overdamped many-atom micro-maser". *Phys. Rev. A* **71**, 053818 (2005).

[140] V. V. Temnov and U. Woggon. "Superradiance and Subradiance in an Inhomogeneously Broadened Ensemble of Two-Level Systems Coupled to a Low-Q Cavity". *Phys. Rev. Lett.* **95**, 243602 (2005).

[141] J. Tignon, T. Hasche, D. S. Chemla, H. C. Schneider, F. Jahnke, and S. W. Koch. "Unified Picture of Polariton Propagation in Bulk GaAs Semiconductors". *Phys. Rev. Lett.* **84**, 3382 (2000).

[142] M. Travagnin. "Effects of Pauli blocking on semiconductor laser intensity and phase noise spectra". *Phys. Rev. A* **64**, 013818 (2001).

[143] S. M. Ulrich. *Non-Classical and Stimulated Photon Emission Processes from Self--Assembled Semiconductor Quantum Dots*. Ph.D. thesis, Universität Stuttgart, Germany (2007).

[144] S. M. Ulrich, C. Gies, S. Ates, J. Wiersig, S. Reitzenstein, C. Hofmann, A. Löffler, A. Forchel, F. Jahnke, and P. Michler. "Photon statistics of semiconductor microcavity lasers". *Phys. Rev. Lett.* **98**, 043906 (2007).

[145] A. V. Uskov, A.-P. Jauho, B. Tromborg, J. Mørk, and R. Lang. "Dephasing times in Quantum Dots due to elastic LO Phonon-Carrier Collisions". *Phys. Rev. Lett.* **85**, 1516 (2000).

Bibliography

[146] K. J. Vahala. "Optical Microcavities". *Nature* **424**, 839 (2003).

[147] E. del Valle, F. P. Laussy, F. Troiani, and C. Tejedor. "Entanglement and lasing with two quantum dots in a microcavity". *Phys. Rev. B* **76**, 235317 (2007).

[148] C. Wiele, F. Haake, and Y. M. Golubev. "Quantum-dot laser with periodic pumping". *Phys. Rev. A* **60**, 4986 (1999).

[149] J. Wiersig, C. Gies, N. Baer, and F. Jahnke. "Intrinsic Non-Exponential Decay of Time-Resolved Photoluminescence from Semiconductor Quantum Dots". *to appear in Adv. in Solid State Phys.* (2006).

[150] J. Wiersig, C. Gies, F. Jahnke, M. Aßmann, T. Berstermann, M. Bayer, J. P. Reithmaier, and A. Forchel. "Non-classical light emission of low-threshold quantum dot microcavity lasers". *submitted for publication* (2008).

[151] C. W. Wilmsen, H. Temkin, and L. A. Coldren, editors. *Vertical Cavity Surface Emitting Lasers*. Cambridge University Press, 2001.

[152] J. P. Woerdman, M. P. Van Exter, and N. J. Van Druten. "Quantum Noise of Small Lasers". *Advances in Atomic, Molecular and Optical Physics* **47**, 205 (2001).

[153] A. Wojs, P. Hawrylak, S. Fafard, and L. Jacak. "Electronic structure and magneto-optics of self-assembled quantum dots". *Phys. Rev. B* **54**, 5604 (1996).

[154] Y. Yamamoto and A. Imamoğlu. *Mesoscopic Quantum Optics*. John Wiley & Sons, Inc., 1999.

[155] Y. Yamamoto, S. Machida, and G. Björk. "Microcavity semiconductor laser with enhanced spontaneous emission". *Phys. Rev. A* **44**, 657 (1991).

[156] H. Yokoyama and S. D. Brorson. "Rate equation analysis of microcavity lasers". *J. Appl. Phys.* **66**, 4801 (1989).

[157] T. Yoshi, A. Scherer, J. Hendrickson, G. Khitrova, H. M. Gibbs, G. Ruper, C. Ell, O. B. Shchekin, and D. G. Deppe. "Vaccum Rabi splitting with a single quantum dot in a photonic crystal nanocavity". *Nature* **432**, 200 (2004).

[158] Z. Yuan, B. E. Kardynal, R. M. Stevenson, A. J. Shields, C. J. Lobo, K. Cooper, N. S. Beattie, D. A. Ritchie, and M. Pepper. "Electrically Driven Single-Photon Source". *Science* **295**, 102 (2002).

List Of Publications

1. *Finite-temperature theory of the trapped two-dimensional Bose gas*, C. Gies, B. P. van Zyl, S. A. Morgan, and D. A. W. Hutchinson, Phys. Rev. A **69**, 023616 (2004).

2. *Coherence properties of the two-dimensional Bose-Einstein condensate*, C. Gies and D. A. W. Hutchinson, Phys. Rev. A **70**, 043606 (2004).

3. *Many-body T-matrix of a two-dimensional Bose-Einstein condensate within the Hartree-Fock-Bogoliubov formalism*, C. Gies, M. D. Lee, and D. A. W. Hutchinson, J. Phys. B: At. Mol. Opt. Phys. **38**, 1797-1809 (2005).

4. *Ultracold Two-Dimensional Trapped Bose Gases*, D. A. W. Hutchinson, C. Gies, S. A. Morgan, M. D. Lee, and B. P. van Zyl, Laser Physics **15**, 1091-1095 (2005).

5. *Radiative emission dynamics of quantum dots in a single cavity micropillar*, M. Schwab, H. Kurtze, T. Auer, T. Berstermann, M. Bayer, J. Wiersig, N. Baer, C. Gies, F. Jahnke, J. P. Reithmaier, A. Forchel, M. Benyoucef, and P. Michler, Phy. Rev. B **74**, 045323 (2006).

6. *Luminescence of a semiconductor quantum dot system*, Norman Baer, Christopher Gies, Jan Wiersig, and Frank Jahnke, Eur. Phys. J. B **50**, 411 (2006).

7. *Microscopic Theory of Quantum Dot Luminescence Spectra*, Christopher Gies, Norman Baer, Jan Wiersig, and Frank Jahnke, phys. stat. sol. c **3**, 2385 (2006).

8. *Semiconductor model for quantum-dot-based microcavity lasers*, Christopher Gies, Jan Wiersig, Michael Lorke, and Frank Jahnke, Phys. Rev. A **75**, 013803 (2007).

9. *Photon Statistics of Semiconductor Microcavity Lasers*, S. M. Ulrich, C. Gies, S. Ates, J. Wiersig, S. Reitzenstein, C. Hofmann, A. Löffler, A. Forchel, F. Jahnke, and P. Michler, Phys. Rev. Lett. **98**, 043906 (2007).

10. *Electronic shell structure and carrier dynamics of high aspect ratio InP single quantum dots*, Gareth J. Beirne, Matthias Reischle, Robert Rossbach, Wolfgang-Michael Schulz, Michael Jetter, Jan Seebeck, Paul Gartner, Christopher Gies, Frank Jahnke, and Peter Michler, Phys. Rev. B **75**, 195302 (2007).

Bibliography

11. *Laser theory for semiconductor quantum dots in microcavities*, Christopher Gies, Jan Wiersig and Frank Jahnke, Supperlattices and Microstructures (2007), doi:10.1016/j.spmi.2007.06.026.

12. *Systematic study of carrier correlations in the electron-hole recombination dynamics of quantum dots*, T. Berstermann, T. Auer, H. Kurtze, M. Schwab, D. R. Yakovlev, and M. Bayer; J. Wiersig, C. Gies, and F. Jahnke; D. Reuter and A. D. Wieck, Phys. Rev. B **76**, 165318 (2007).

13. *Influence of the Spontaneous Emission Factor β on the First-Order Coherence of Semiconductor Microcavity Lasers*, S. Ates, C. Gies, S. M. Ulrich, J. Wiersig, S. Reitzenstein, A. Löffler, A. Forchel, F. Jahnke, and P. Michler, submitted for publication (2007).

14. *Output characteristics of pulsed and cw-excited quantum-dot microcavity lasers*, C. Gies, J. Wiersig, and F. Jahnke, accepted for publication in Phys. Rev. Lett. (2008).

15. *Non-classical light emission of low-threshold quantum dot microcavity lasers*, J. Wiersig, C. Gies, F. Jahnke, M. Aßmann, T. Berstermann, M. Bayer, C. Kistner, S. Reitzenstein, and A. Forchel, submitted for publication (2008).